

AD \_\_\_\_\_

AWARD NUMBER DAMD17-94-J-4041

TITLE: Cloning and Characterizing Genes Involved in Monoterpene  
Induced Mammary Tumor Regression

PRINCIPAL INVESTIGATOR: Michael N. Gould, Ph.D.  
Eric Ariazi, Ph.D.

CONTRACTING ORGANIZATION: University of Wisconsin - Madison  
Madison, Wisconsin 53706

REPORT DATE: May 1998

TYPE OF REPORT: Final

PREPARED FOR: Commander  
U.S. Army Medical Research and Materiel Command  
Fort Detrick, Maryland 21702-5012

DISTRIBUTION STATEMENT: Approved for public release;  
distribution unlimited

The views, opinions and/or findings contained in this report are  
those of the author(s) and should not be construed as an official  
Department of the Army position, policy or decision unless so  
designated by other documentation.

**DTIC QUALITY INSPECTED 1**

# REPORT DOCUMENTATION PAGE

Form Approved  
OMB No. 0704-0188

Public reporting burden for this collection of information is estimated to average 1 hour per response, including the time for reviewing instructions, searching existing data sources, gathering and maintaining the data needed, and completing and reviewing the collection of information. Send comments regarding this burden estimate or any other aspect of this collection of information, including suggestions for reducing this burden, to Washington Headquarters Services, Directorate for Information Operations and Reports, 1215 Jefferson Davis Highway, Suite 1204, Arlington, VA 22202-4302, and to the Office of Management and Budget, Paperwork Reduction Project (0704-0188), Washington, DC 20503.

1. AGENCY USE ONLY (Leave blank)		2. REPORT DATE May 1998		3. REPORT TYPE AND DATES COVERED Final (1 Sep 94 - 31 May 98)	
4. TITLE AND SUBTITLE Cloning and Characterizing Genes Involved in Monoterpene Induced Mammary Tumor Regression				5. FUNDING NUMBERS DAMD17-94-J-4041	
6. AUTHOR(S) Michael N. Gould, Ph.D. Eric Ariazi, Ph.D.					
7. PERFORMING ORGANIZATION NAME(S) AND ADDRESS(ES) University of Wisconsin - Madison Madison, Wisconsin 53706				8. PERFORMING ORGANIZATION REPORT NUMBER	
9. SPONSORING / MONITORING AGENCY NAME(S) AND ADDRESS(ES)  U.S. Army Medical Research and Materiel Command Fort Detrick, MD 21702-5012				10. SPONSORING / MONITORING AGENCY REPORT NUMBER	
11. SUPPLEMENTARY NOTES					
12a. DISTRIBUTION / AVAILABILITY STATEMENT Distribution unlimited; approved for public release				12b. DISTRIBUTION CODE	
13. ABSTRACT (Maximum 200 words) Monoterpene-induced/repressed genes were identified in regressing rat mammary carcinomas treated with dietary limonene using a newly developed method termed subtractive display. The subtractive display screen identified 42 monoterpene-induced genes comprising 9 known genes and 33 unidentified genes, as well as 58 monoterpene-repressed genes comprising 1 known gene and 57 unidentified genes. Several of the identified differentially expressed genes are involved in the TGFβ signal transduction pathway, as demonstrated by isolation of M6P/IGF2R and TGFβIR. TGFβ signaling and its downstream effects were investigated in perillyl alcohol-treated rat mammary carcinomas. RNA expression studies showed TGFβ-related genes were induced and temporally regulated: first: c-jun and c-fos (transient); second: TGFβ1; third: M6P/IGF2R, TGFβIR, and TGFβIR; and fourth: smad3. <i>In situ</i> protein expression studies confirmed upregulation and demonstrated colocalization of these genes in epithelial cells. Smad2/Smad3 exhibited nuclear localization. A subpopulation of Smad2/Smad3 nuclei colocalized with a subpopulation of apoptotic nuclei. RNA expression studies demonstrated the cell cycle and apoptosis related genes p21cip1/WAF1, p27Kip1, bax, bad, and annexin I were induced; cyclin E and cdk2 were repressed; and bcl-2 and p53 were unchanged. Characterization of cell growth and death parameters revealed apoptosis was induced prior to induction of cytostasis.					
14. SUBJECT TERMS Breast Cancer Monoterpene, Limonene, Perillyl Alcohol, Mammary, Therapy, Carcinoma Regression, Subtractive Display, Differentially Expressed Genes, TGF-beta, Signal Transduction, Confocal Microscopy				15. NUMBER OF PAGES 143	
				16. PRICE CODE	
17. SECURITY CLASSIFICATION OF REPORT Unclassified	18. SECURITY CLASSIFICATION OF THIS PAGE Unclassified	19. SECURITY CLASSIFICATION OF ABSTRACT Unclassified	20. LIMITATION OF ABSTRACT Unlimited		

## FOREWORD

Opinions, interpretations, conclusions and recommendations are those of the author and are not necessarily endorsed by the U.S. Army.

\_\_\_\_ Where copyrighted material is quoted, permission has been obtained to use such material.

\_\_\_\_ Where material from documents designated for limited distribution is quoted, permission has been obtained to use the material.

\_\_\_\_ Citations of commercial organizations and trade names in this report do not constitute an official Department of Army endorsement or approval of the products or services of these organizations.


X In conducting research using animals, the investigator(s) adhered to the "Guide for the Care and Use of Laboratory Animals," prepared by the Committee on Care and use of Laboratory Animals of the Institute of Laboratory Resources, national Research Council (NIH Publication No. 86-23, Revised 1985).

NA For the protection of human subjects, the investigator(s) adhered to policies of applicable Federal Law 45 CFR 46.

X In conducting research utilizing recombinant DNA technology, the investigator(s) adhered to current guidelines promulgated by the National Institutes of Health.

X In the conduct of research utilizing recombinant DNA, the investigator(s) adhered to the NIH Guidelines for Research Involving Recombinant DNA Molecules.

X In the conduct of research involving hazardous organisms, the investigator(s) adhered to the CDC-NIH Guide for Biosafety in Microbiological and Biomedical Laboratories.

 5/31/98  
PI - Signature Date

# **Cloning and Characterizing Genes Involved in Monoterpene Induced Mammary Tumor Regression**

Final Report for Grant DAMD17-94-J-4041

by

ERIC ANTHONY ARIAZI

Programs in

Cellular and Molecular Biology

and

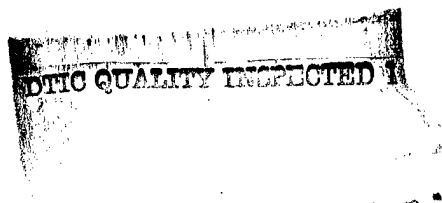
Human Cancer Biology

at the

UNIVERSITY OF WISCONSIN-MADISON

May, 1998

DTIC QUALITY INSPECTED 1



19980904 023

## TABLE OF CONTENTS

### PAGE

<b>a</b>	<b>FRONT COVER</b>
<b>b</b>	<b>STANDARD FORM 298, REPORT DOCUMENTATION PAGE</b>
<b>c</b>	<b>FOREWORD</b>
<b>1</b>	<b>TITLE PAGE</b>  Cloning and Characterizing Genes Involved in Monoterpene Induced Mammary Tumor Regression
<b>2</b>	<b>TABLE OF CONTENTS</b>
<b>8</b>	<b>CHAPTER I</b>  Identifying Differential Gene Expression in Monoterpene-Treated Mammary Carcinomas Using Subtractive Display
<b>9</b>	<b>SUMMARY</b>
<b>10</b>	<b>INTRODUCTION</b>
<b>14</b>	<b>EXPERIMENTAL PROCEDURES</b> <ul style="list-style-type: none"><li>• Summary of Subtractive Display Methodology</li><li>• Preparation of cDNA from Mammary Carcinomas</li><li>• Subtraction</li><li>• Trimming Cycles</li><li>• PCR</li></ul>

- Subtractive Display
- Sequence Analysis
- Competitive Reverse Transcriptase-PCR

## 22 RESULTS

- SD Methodology
- Subtraction of cDNA Libraries
- Reconfiguration and Display of the Subtracted Libraries
- Characterization of Differentially Expressed Clones

## 28 DISCUSSION

- The Subtractive Display Gene Expression Screen
- The Process of Monoterpene-Mediated Mammary Carcinoma Regression

## 33 ACKNOWLEDGEMENTS

## 34 REFERENCES

## 41 TABLES AND FIGURES

- **Table I.** Competitive RT-PCR Primers and Product Sizes
- **Table II.** Isolated MIG/MRG Clones
- **Table III.** Confirmed MIG/MRG Differential Expression
- **Figure 1.** Flowchart of the Subtractive Display Methodology
- **Figure 2.** PCR Product Display During the Subtractive Hybridization Process
- **Figure 3.** Schematic of a cDNA Fragment and Primers Used in Subtractive Display
- **Figure 4** Optimization of Subtractive Display

- **Figure 5.** Subtractive Display Using All 16 Subpopulation Primer Sets
- **Figure 6.** LC1 (MIG-12) RNA Expression Using Competitive RT-PCR

## **58 CHAPTER II**

Consecutive Cycles of Precise Unidirectional 14 bp Deletions Using a Bse RI/Bsg I  
Trimming Plasmid

### **59 SUMMARY**

### **60 INTRODUCTION**

### **62 EXPERIMENTAL PROCEDURES**

- pTRIM14 Construction
- pTRIM14 Testing
- BsgI and BseRI Reaction Conditions
- Plasmid DNA Preparation, Trimming, Ligation, and Subcloning
- Deletion Characterization

### **65 RESULTS AND DISCUSSION**

- Deletion Size
- Trimming Efficiency
- Variations on the Deletion Size
- Variations on the Trimming Plasmid

**70        ACKNOWLEDGEMENTS**

**71        REFERENCES**

**72        FIGURES**

- **Figure 1.** Schematic of pTRIM14, the BseRI/BsgI 14 bp trimming plasmid, as it is processed through one trimming cycle
- **Figure 2.** Analysis of trimming cycle PCR products
- **Figure 3.** Sequence analysis and schematic of precise 14 bp deletions

**78        CHAPTER III**

Characterization and Downstream Effects of the TGF $\beta$  Signal Transduction Pathway in Mammary Carcinomas Treated with the Anticancer Agent Perillyl Alcohol

**79        SUMMARY**

**80        INTRODUCTION**

**83        EXPERIMENTAL PROCEDURES**

- Generation of Advanced Mammary Carcinomas
- Acute Treatment Protocol
- Chronic Treatment Protocol
- Circulating POH Metabolite Analysis
- Tissue Section Preparation and Gross Morphology
- Ultrastructural Morphology
- Nuclease Protection Assay
- Confocal Microscopy
- Fluorescence IHC



- Cellular Proliferation and Apoptosis Staining

98

## RESULTS

- Chronic and Acute POH Treatment Protocols
- Gross and Ultrastructural Morphology
- RNA Expression Analysis of TGF $\beta$  Signaling Components
- In situ Protein Expression Analysis of TGF $\beta$  Signaling Components
- RNA Expression Analysis of Cell Cycle and Apoptosis Genes
- Quantification of Cytostasis and Apoptosis

108

## DISCUSSION

111

## REFERENCES

115

## FIGURES

- **Figure 1.** Percentage of Actively Regressing Advanced Mammary Carcinomas
- **Figure 2.** Analysis of Plasma POH Metabolite Concentrations During the Acute and Chronic Treatment Protocol
- **Figure 3.** Morphology of Advanced Mammary Carcinoma Regression
- **Figure 4.** Induction and Temporal Regulation of TGF $\beta$  Signal Transduction Genes' RNA Expression During the Acute and Chronic POH Treatment Protocols
- **Figure 5.** Nuclease Protection Assay of TGF $\beta$  Signal Transduction Genes in Chronic POH-treated Regressing and Non-Responsive Mammary Carcinomas
- **Figure 6.** LAP-TGF $\beta$ 1, TGF $\beta$ 1, and M6P/IGF2R IHC of Chronic POH-treated Mammary Carcinomas

- **Figure 7.** TGF $\beta$ IIR and TGF $\beta$ 1 IHC of Chronic POH-treated Mammary Carcinomas
- **Figure 8.** TGF $\beta$ IIR and TGF $\beta$ 1 IHC of Chronic POH-treated Mammary Carcinomas
- **Figure 9.** TUNEL, TGF $\beta$ 1, and Smad2/Smad3 IHC of Chronic POH-treated Mammary Carcinomas
- **Figure 10.** Differential RNA Expression of Cell Cycle and Apoptosis Genes During the Acute and Chronic POH Treatment Protocols
- **Figure 11.** Nuclease Protection Assay of Cell Cycle and Apoptosis-Related Genes in Chronic POH-treated Regressing and Non-Responsive Mammary Carcinomas
- **Figure 12.** Induction of Cytostasis and Apoptosis

139

#### **PUBLICATIONS SUPPORTED BY GRANT DAMD17-94-J-4041**

- Journal Articles
- Meeting Abstracts

140

#### **LIST OF PERSONNEL RECIEVING PAY FROM THIS EFFORT**

## **CHAPTER I**

Identifying Differential Gene Expression in Monoterpene-Treated Mammary Carcinomas Using Subtractive Display

## SUMMARY

Monoterpene-induced/repressed genes were identified in regressing rat mammary carcinomas treated with dietary limonene using a newly developed method termed subtractive display. The subtractive display screen identified 42 monoterpene-induced genes comprising 9 known genes and 33 unidentified genes, as well as 58 monoterpene-repressed genes comprising 1 known gene and 57 unidentified genes. Several of the identified differentially expressed genes are involved in the mitoinhibitory transforming growth factor  $\beta$  signal transduction pathway, as demonstrated by isolation of the mannose 6-phosphate/insulin-like growth factor II receptor and the transforming growth factor  $\beta$  type II receptor. The monoterpene induced/repressed genes indicate that apoptosis and differentiation act in concert to effect carcinoma regression. Apoptosis is suggested by the cloning of a marker of programmed cell death, lipocortin 1. Consistent with a differentiation/remodeling process occurring during tumor regression, subtractive display identified YWK-II and neuroligin 1. Thus far, of the cDNAs putatively identified as differentially expressed in this complex *in situ* carcinoma model, 5 were tested, and each one has been confirmed to be differentially expressed. Additionally, many of the identified known genes are expressed as rare transcripts and exhibit small but significant changes in abundance. Together, these points demonstrate the unique utility of this new gene expression screen to identify altered gene expression in a complex *in vivo* environment.

## INTRODUCTION

The monoterpenes limonene and perillyl alcohol, an emerging class of naturally occurring anti-cancer compounds, are highly effective against a variety of rodent organ-specific cancer models (reviewed in (1,2). Dietary administration of monoterpenes is effective for chemoprevention and chemotherapy of both 7,12-dimethylbenz[*a*]anthracene (DMBA)-induced and *N*-methyl-*N*-nitrosourea (NMU)-induced rat mammary carcinomas (3-10). As a chemotherapeutic agent, dietary 10% limonene caused ~66% of advanced DMBA- or NMU-induced carcinomas to completely regress and an additional ~23% to partially regress (6). Moreover, a 2% perillyl alcohol diet resulted in 50% complete and an additional 25% partial regression of advanced DMBA-induced mammary carcinomas (7). Treatment with both monoterpenes at these anti-cancer doses did not cause systemic toxicity. Monoterpenes are currently being tested in Phase I clinical trials on advanced cancer patients in England (11) and the United States.

Several observations suggest that monoterpene-mediated mammary carcinoma regression may involve a differentiation/remodeling process. Histopathology of monoterpene-treated, actively regressing tumors displays regions of dense anaplastic epithelium characteristic of mammary carcinomas and regions of a remodeled epithelial compartment. Regressing carcinomas do not show increased levels of lymphocyte infiltration, inflammation, or necrosis (6). Furthermore, monoterpene-treatment of neuro2A neuroblastoma cells causes morphologic differentiation within 4 h as characterized by neurite outgrowths (12).

Monoterpenes inhibit enzymes in the mevalonate-lipid metabolism pathway, including a selective inhibition of isoprenylation of 21-26 kDa small G proteins (13-15) and inhibition of ubiquinone (CoQ) and cholesterol synthesis (16). Inhibition of isoprenylation may affect signal

transduction pathways because unprocessed or non-prenylated small G proteins are not properly localized within the cell and are thus non-functional (17). Furthermore, investigations into gene expression and protein level alterations associated with monoterpene-mediated tumor regression revealed a large increase of the mitoinhibitory transforming growth factor  $\beta$ 1 (TGF $\beta$ 1) and the mannose 6-phosphate/insulin-like growth factor II receptor (M6P/IGF2R), which both facilitates latent-TGF $\beta$ 1 activation and degrades the mammary mitogen insulin-like growth factor II (IGF2; 18). Interestingly, while M6P/IGF2R RNA expression was significantly induced 2-fold in 10% limonene-treated carcinomas, the induced RNA expression of M6P/IGF2R was not observed in the non-responsive 10% limonene-treated carcinomas (19).

We hypothesized that biochemical events in the cytoplasm modify signal transduction leading to altered gene expression. Thus, in order to further elucidate the monoterpenes' mechanism of cancer chemoprevention and chemotherapy, we screened for differentially expressed genes in 10% limonene-treated, DMBA-induced, advanced mammary carcinomas resected at mid-regression.

Complex tissues, such as mammary carcinomas, are composed of large heterogeneous cell populations and hence require sensitive gene expression screening methods. This is because a particular gene may be induced or repressed only in a specific cell type, which would be diluted by all the other cell types. In order to achieve the required level of sensitivity, the subtraction method of Wang and Brown (20) was initially chosen because this approach uses polymerase chain reaction (PCR) amplification to generate a renewable source of cDNA for multiple rounds of subtraction, and the method efficiently removes commonly expressed cDNA from the experimental and control cDNA pools to allow for enrichment of differentially expressed genes. However, cloning the differentially expressed cDNAs involves cycles of classical probe hybridization experiments to isolate only a few clones at a time, followed by subtraction of the newly cloned cDNAs from the library. The cloning cycle is repeated until the

library is completely screened, which may take 20-30 or more cloning cycles and thus renders this methodology inefficient.

A possible alternative method considered was Liang and Pardee's differential display (21), since it is also a PCR-based technique that selectively amplifies subsets of cDNAs based on primer design applied to two matched but non-subtracted cDNA populations. This technique clones genes quickly but only ~10% of the genes are differentially expressed when tested (22-24). Problems with reproducibility are probably due to the low stringency in annealing of primers, though recent modifications in primer design and experimental protocol have somewhat improved reproducibility (25-28). In addition, because the primers effectively anneal as 6- or 7-base oligomers of arbitrary sequence, a statistical argument is needed to determine when the libraries are sufficiently screened (21). Furthermore, there exists a high level of background noise in differential display due to the vast majority of competing heterologous RNA. Differential display shows a strong bias toward identifying abundant mRNAs (29). An efficient gene expression screen should identify rare transcripts, which account for ~90% of mRNA species in most cells (29).

In order to more efficiently identify differentially expressed monoterpene target genes, we developed and characterized an alternative approach, termed subtractive display (SD), which incorporates the strengths and minimizes the weaknesses of subtractive hybridization and differential display. In brief, SD removes common cDNAs from two cDNA populations and enriches for differentially expressed cDNAs by subtractive hybridization. Subpopulations of subtracted cDNAs are consecutively PCR-amplified, displayed on a sequencing gel, subcloned and characterized to confirm their differential expression. We have applied SD to identify differentially expressed genes in 10% limonene-treated advanced rat mammary carcinomas. The SD gene expression screen effectively identified differential gene expression patterns in this complex model. All 5 putatively identified known genes thus far tested were confirmed as

differentially expressed genes, hence demonstrating the high reproducibility of SD.

Additionally, many of the identified known genes were expressed as rare mRNAs and exhibited significant yet modest differential expression, demonstrating the high sensitivity of SD.



## EXPERIMENTAL PROCEDURES

### Summary of Subtractive Display (SD) Methodology

A flowchart of the SD methodology is given in Fig. 1. cDNA was generated from two matched tissue sources, or for this set of experiments, monoterpene-treated, regressing, mammary carcinomas (+cDNA) and control, non-treated carcinomas (-cDNA). +/- cDNA was fragmented with restriction endonucleases followed by ligation of symmetrical linkers which subsequently serves as PCR-primer sites. The sequence at the cDNA fragment ends reflect the methods used to generate the cDNA libraries and restriction endonuclease recognition sites, and hence, are non-random sequences. The subtractive process involves multiple rounds of hybridization and PCR amplification, which renews the cDNA source. +cDNA was subtracted from -cDNA, and concurrently, -cDNA was subtracted from +cDNA, to derive induced and repressed genes, respectively. Subtracted cDNA was subcloned into a trimming plasmid and subjected to three cycles of precise, unidirectional deletions. The trimming procedure serves to reconfigure the subtracted libraries such that one end of the cDNA is composed of randomized sequence and both ends of the cDNA fragment are flanked by different or asymmetric primers, derived from the trimming plasmid sequence. The subtracted, reconfigured cDNA libraries were PCR-displayed using 16 sets of primers consisting of 1 fixed primer and 1 of 16 subpopulation primers. The subpopulation primers are designed to anneal with a 2-base overlap (3' end of primer) to the randomized sequence end of the reconfigured cDNA. The penultimate 2-bases of the 3' end of the subpopulation primers were a specific combination of 1 of 16 possible ( $2^4$ ) 2-base combinations, thus selecting for PCR-amplification of a subpopulation of subtracted, reconfigured cDNA. Individual cDNA bands were isolated and characterized to confirm differential expression.

### Preparation of cDNA from Mammary Carcinomas

Regressing (monoterpene-treated) and non-regressing (control, not treated) carcinomas for all studies were generated by the following protocol. Virgin female Wistar-Furth inbred rats at 50-55 days of age were given a single dose of DMBA (50 mg/kg body weight) by gastric intubation. Developing carcinomas were followed by palpation until they grew to  $\geq 10$  mm in diameter, at which time rats were randomized to either a monoterpene diet of 10% (w/w) *d*-limonene or a control diet and pair-fed. Carcinomas from rats on monoterpene diet that regressed to 50% of their maximum diameter were resected. All remaining carcinomas were collected by 15 weeks after diet randomization. All animal use was in compliance with NIH guidelines for humane care and was approved by the University of Wisconsin-Madison Medical Center Animal Use Committee.

Total tumor RNA was isolated using RNazol B Reagent (Tel-Test, Friendswood, Texas, USA) and poly(A)+ RNA was isolated using the PolyATtract System 1000 (Promega, Madison, WI, USA) following the manufacturer's directions. The Superscript Plasmid System (Gibco BRL Life Technologies, Gaithersburg, MD, USA) was used for double-stranded cDNA synthesis from poly(A)+ RNA. 5  $\mu$ g of cDNA synthesized from 7 regressing and 7 non-regressing carcinomas were pooled and termed +cDNA and -cDNA, respectively. A portion of the +cDNA and -cDNA was reserved for construction of non-fragmented cDNA plasmid libraries with the vector pSport1 and transformed by electroporation into Electromax Efficiency DH12S *E. coli* host cells (Gibco BRL Life Technologies).

### Subtraction

We used the PCR-based subtractive hybridization method of Wang and Brown described in detail elsewhere (20). In brief, the subtraction protocol operates by fragmenting the

cDNA with restriction endonucleases (i. e. *AluI* and *AluI* plus *RsaI*) and ligating onto their termini 21 bp oligodeoxynucleotide linkers having a 5' blunt end and a 4-base 3' overhang. The flush end contained an *EcoRI* site. Following linker ligation, the fragmented cDNAs are subjected to PCR amplification using the 21-bp linkers as primers (sequences given in 20). It is assumed that cDNA fragments common to both +cDNA and -cDNA populations were amplified equally, while different cDNA fragments within a population may be differentially amplified. Dependent on the direction of subtraction, whether up- or down-regulated cDNAs were being enriched, either +cDNA or -cDNA and their derived populations were tracer or driver cDNA. Thus in the following, driver or tracer cDNA is specified but not if +cDNA or -cDNA was used. 50 µg of driver cDNA was completely digested with *EcoRI* to suppress contaminating driver cDNA from being amplified. Driver cDNA was then photobiotinylated and combined with 2.5 µg non-biotinylated tracer cDNA. The mixture was completely denatured by boiling and then cooled for a long hybridization (20 hours). Addition of streptavidin led to formation of streptavidin-biotin-DNA complexes that were removed by several phenol-chloroform extractions. Subtracted tracer cDNA (termed 1cDNA) was again subtracted from 25 µg biotinylated driver cDNA, this time for a short hybridization of 2 hours to yield 2cDNA. +2cDNA and -2cDNA were PCR amplified. 2.5 µg non-biotinylated tracer 2cDNA was subtracted against 50 µg *EcoRI* treated-biotinylated driver 2cDNA for a long hybridization followed by 25 µg driver 1cDNA for a short hybridization, resulting in 4cDNA, which was then PCR amplified. Another similar cycle was performed giving 6cDNA.

The subtractive hybridization process was monitored by displaying the cDNA libraries after each round of subtraction on a sequencing gel. The cDNA libraries were amplified using a primer derived from the original linker sequence ligated onto the cDNA fragment ends but modified by deletion of the two 5' bases and the addition of the 2 mixed bases A/T and G/C on the 3' end that overlaps the cDNA insert [5'-CTTGCTTGAATTCGGACTA(A/T)(C/G)-3'],

giving 4 possible primers and 16 possible primer pairs. This mixed primer anneals at both ends of the cDNA fragments and because of the two mixed bases at the 3' end that overlap the cDNA insert, the sequence selectively amplifies a representative cDNA subpopulation such that individual bands are visualized (Fig. 2). The PCR temperature profile used was 94° C - 5 min hot start followed by 94° C - 1 min, 50° C - 1 min, 72° C - 2 min for 30 cycles. The PCR products were resolved on a 5% polyacrylamide gel and visualized by exposure to X-OMAT AR film (Kodak, Rochester, New York, USA).

### Trimming Cycles

The subtracted cDNA libraries were next reconfigured such that unique primer sites flank the cDNA insert. This was accomplished by cloning the libraries into the trimming plasmid pTRIM14 using the *EcoRI* site within the libraries' linkers and the *EcoRI* site located 2 bp downstream of pTRIM14's trimming cassette (30). This procedure resulted in deletion of 9 bp of the cDNA libraries' linker ends, allowing 12 bp to remain. Precise unidirectional deletions were then generated on one end of the subtracted cDNA libraries by three trimming cycles of 14 bp each. We followed the trimming cycle protocol as detailed elsewhere (30). In brief, pTRIM14's trimming cassette contains *BseRI* and *BsgI* recognition sites configured such that stepwise digestion first with *BsgI* and then *BseRI* produces cleavage of DNA 16/14 nt distal and 4/2 nt proximal, respectively, relative to the 3' end of the cassette, thus conserving the trimming cassette but cutting into the 5' end of the cDNA fragment. The trimming cycle continues by treatment with Mung Bean nuclease to remove single-stranded ends of the linearized DNA and finally re-circularization of the plasmids with T4 DNA ligase. Noteworthy, cDNA fragments that may contain *BsgI* or *BseRI* are not lost from the library since a portion of the cDNA fragment is retained. Additionally, this trimming procedure was shown to produce deletions with very high efficiency on a population of plasmids (30).

## PCR

All PCR reactions were carried out using the following conditions unless otherwise stated. In a final reaction volume of 50  $\mu$ l, PCR was performed using 200  $\mu$ M of each dNTP, 400 nM of each primer, and 2.5 units of AmpliTaq DNA polymerase (Perkin Elmer, Foster City, CA, USA). The 1X PCR buffer was composed of 50 mM KCl, 10 mM Tris-HCl (pH 8.3), 1.5 mM  $MgCl_2$ , and 0.001% (w/v) gelatin. All primers were synthesized at the Wisconsin Biotechnology Center (Madison, WI, USA) unless otherwise stated.

## Subtractive Display (SD)

The subtracted and reconfigured cDNA libraries were displayed using sets of a fixed primer (5'-ATTACGAATTCGGACTA-3') and 1 of 16 possible subpopulation primers (5'-GAGGAGGTGCAGTANN-3'), as determined by the specific combination of the two variable penultimate 3' bases designated by NN (Fig. 1 and 3). An explanation of these primer sequences is given under Results. The nucleotide concentration for PCR used was 20  $\mu$ M of each dNTP plus 10  $\mu$ Ci of [ $\alpha$ - $^{35}$ S] dATP, and the PCR temperature profile used was 94° C - 5 min hot start followed with 94° C - 1 min, 59° C - 1 min, 72° C - 1 min for 30 cycles and lastly 72° C - 10 min to ensure double stranded cDNA. Labelled PCR products were resolved on a 5% polyacrylamide sequencing gel and visualized by a PhosphorImager (Molecular Dynamics, Sunnyvale, CA, USA). These experiments were also performed in parallel by omitting the radiolabel and instead silver staining the gel (31) to visualize the bands directly, which greatly improves efficiency of band isolation. Unique bands were excised, eluted from the gel and reamplified using the same fixed PCR primer and a modified subpopulation primer, or pan primer, that amplifies the entire cDNA population. The pan primer has two C bases and an *Eco*RI site (underlined) added to the 5' end and the two terminal variable 3' bases removed from

the subpopulation primer (5'-CCGAATTCGAGGAGGTGCAGTA-3). Isolated cDNA fragments were digested with *Eco*RI, subcloned into the multiple cloning site of the pSport1 plasmid (Gibco BRL Life Technologies), and transformed by electroporation into Electromax Efficiency DH12S *E. coli* host cells (Gibco BRL Life Technologies).

### Sequence Analysis

All subcloned cDNA fragments were sequenced using the M13/pUC forward primer and the PRISM Ready Reaction Dye Deoxy Terminator Cycle Sequencing Kit (Perkin Elmer), following the manufacturer's protocol. The sequencing reaction products were resolved on an ABI PRISM Automated DNA Sequencer (Advanced Biotechnologies Inc., Columbia, MD, USA) at the Wisconsin Biotechnology Center. The monoterpene-induced gene (MIG) and monoterpene-repressed gene (MRG) sequences were compared to a non-redundant nucleotide sequence database that includes sequences from the Brookhaven Protein Data Bank, Genbank, Genbank updates, EMBL and EMBL updates using the BLAST algorithm at the National Center for Biotechnology Information (NCBI) (32).

### Competitive Reverse Transcriptase-PCR (RT-PCR)

Relative RNA expression levels between regressing (10% limonene-treated) and non-regressing (control, not treated) mammary carcinomas were determined by competitive RT-PCR (33-38). The competitive RT-PCR assay involved PCR of a target gene (*i. e.*, a MIG/MRG cDNA,) competing for amplification with its exogenously added MIMIC, and amplification of an internal standard [*i.e.*, glyceraldehyde 3-phosphate dehydrogenase (G3PDH)] competing for amplification with its exogenously added MIMIC, for a total of 4 PCR products per sample. A MIMIC is a piece of heterologous DNA with flanking sequences identical to the primer sequences used for the target gene, such that a known amount of MIMIC is exogenously added

for to enable simultaneous co-amplification with a target gene. In essence, the competitive RT-PCR assay normalizes the MIG/MRG cDNA to an external control (MIG/MRG MIMIC) and to an internal G3PDH control, which itself was normalized to an external control (G3PDH MIMIC). After the target MIG/MRG expression for each sample was normalized, its expression level in each sample of the control and regressing carcinoma groups was averaged and compared in order to determine fold-induction or fold-repression. Statistical significance was calculated using the two-tailed Student's *t* test.

Relative RNA expression levels for lipocortin 1 (LC1), transforming growth factor  $\beta$  type II receptor (TGF $\beta$ IIIR), and neuroligin 1 were determined by competitive RT-PCR. RNA was prepared from 5 individual regressing (10% limonene-treated) and 5 individual non-regressing (control, not treated) mammary carcinomas as described above. cDNA was generated using the 1st-Strand cDNA Synthesis Kit (Clontech Laboratories, Palo Alto, CA, USA). Primers were designed using Oligo 5.0 Primer Analysis software (National Biosciences, Plymouth, MN, USA), with the exception of the G3PDH primers (Clontech Laboratories). MIMICs were generated using the PCR MIMIC Construction kit (Clontech Laboratories). Generation of MIMICs involves a 1° PCR reaction using a composite primer, consisting of target gene or gene-specific primer sequence at the 5' end and heterologous DNA primer sequence on the 3' end. Next, an aliquot of the 1° PCR reaction was used as template in a 2° PCR reaction using only target gene or gene-specific primers. Primers and dNTPs were removed by passing the 2° PCR reaction over a Chromaspin-100 column (Clontech Laboratories) and the MIMIC was quantified by spectrophotometric analysis. Primer sequences and product sizes are given in Table 1. In a reaction volume of 50  $\mu$ l, the final concentration of exogenously added PCR MIMICs were  $4.0 \times 10^{-2}$  amol/ $\mu$ l of LC1 MIMIC,  $8.0 \times 10^{-5}$  amol/ $\mu$ l of TGF $\beta$ IIIR MIMIC,  $4.0 \times 10^{-6}$  amol/ $\mu$ l of neuroligin 1 MIMIC, and  $4.0 \times 10^{-5}$  amol/ $\mu$ l G3PDH MIMIC 1 or G3PDH MIMIC 2. The PCR temperature profile used for all competitive

RT-PCR experiments was 94° C - 5 min hot start followed by 94° C - 1 min, 60° C - 1 min, 72° C - 2 min for 30 cycles, with the exception of LC1, which required an annealing temperature of 58° C. PCR products were resolved on a 2% NuSieve GTG agarose gel (FMC BioProducts, Rockland, ME, USA). Primers were 5' end-labelled with fluorescein during their synthesis, thereby allowing PCR product quantitation using a FluorImager (Molecular Dynamics).



## RESULTS

### SD Methodology

A concise description of the SD methodology is given under Experimental Procedures and depicted in Fig. 1.

### Subtraction of cDNA Libraries

The subtractive hybridization procedure developed by Wang and Brown (20) served to remove commonly expressed cDNA fragments and enrich for those that are differentially expressed. The subtraction process involved initial fragmentation of the cDNA libraries with restriction endonucleases and ligation of 21 bp oligodeoxynucleotide linkers onto the cDNA fragment ends, thus allowing for a renewable source of cDNA by PCR. The monoterpene-treated derived cDNA (+cDNA) was subtracted against control, non-treated derived cDNA (-cDNA) to enrich for monoterpene-induced genes (MIG). The inverse subtraction, control, non-treated cDNA subtracted against monoterpene-treated cDNA, was also performed to enrich for monoterpene-repressed genes (MRG). The cDNA libraries were subjected to cycles of alternating long (20 hrs) and short (2 hrs) hybridizations for a total of 6 hybridizations. We monitored the subtractive process by PCR amplification of the cDNA libraries after each round of subtraction, before the libraries were reconfigured using pTRIM14, and displayed them on a sequencing gel. A representative cDNA subpopulation was PCR amplified by modifying the 21 bp primer, which anneals to the linkers initially ligated onto the fragment ends, such that the two 5' bases were removed and two mixed bases were added to the 3' end, thus overlapping the cDNA insert, as described in detail under Experimental Procedures. Fig. 2 demonstrates the efficiency of the subtractions. The unsubtracted +cDNA and -cDNA lanes showed smears, while with each additional cycle of subtraction, individual bands became increasingly

prominent. Furthermore, the banding patterns between the subtracted +cDNA and the subtracted -cDNA lanes were reproducible, indicating that specific cDNA fragments were increasingly enriched while others were driven out of the population. Efficiency of subtraction was further tested by isolating 2 prominent bands from both the +6cDNA and -6cDNA lanes, followed by subcloning and sequencing the cDNAs by similar methods of clone characterization discussed below. One of the derived +6cDNA fragments was identified by a nucleotide database search using the BLAST algorithm (32) as the YWK-II gene, which was again identified at the end of the SD process (indicated by an arrow; compare Fig. 2 and 5) and shown to be differentially expressed as discussed below.

### **Reconfiguration and Display of the Subtracted Libraries**

The subtracted cDNA libraries were next reconfigured for the display step. The libraries were reconfigured because during their construction both ends of the cDNA fragments were ligated to the same linker, *i. e.* the ends are symmetrical, and the first few bases at both ends of the cDNA fragments are not random but reflect both the methods used to make the cDNA (priming the poly(A) tail with a sequence containing a *NotI* site) and that used to fragment the cDNA (restriction digestion with two 4-base cutters). One end of each cDNA fragment needs to be random sequence, such that a subpopulation primer will selectively amplify a small number of distinct bands during the subtractive display step, as discussed below. Reconfiguration of the subtracted cDNA libraries was accomplished by cloning the subtracted libraries into pTRIM14 (30) and processing the cDNA libraries through 3 cycles of precise, unidirectional, 14 bp trimming, as discussed under Experimental Procedures. pTRIM14 was constructed with a trimming cassette composed of *BsgI* and *BseRI* recognition sites. A trimming cycle operates by sequential digestion with *BsgI* and then *BseRI* to produce cuts 16/14 nt distal and 4/2 nt proximal, respectively, relative to the 3' end of the trimming cassette, thereby producing a

deletion onto the 5' end of the cDNA fragment but retaining the trimming cassette. Single-stranded DNA ends are removed by digestion with Mung Bean nuclease followed by ligation with T4 DNA ligase. The subtracted cDNA libraries were subjected to three trimming cycles, generating +6 $\Delta$ 3 and -6 $\Delta$ 3 cDNA (6 rounds of subtraction and 3 cycles of trimming). Accounting for subcloning the subtracted libraries into pTRIM14 (deletion of 9 bp) and 3 trimming cycles, the entire 21 bp linker plus an additional 30 bp on the left end of the cDNA libraries was completely removed, leaving one cDNA end with randomized sequence, as described in greater detail under Experimental Procedures.

The reconfigured, subtracted cDNA libraries were displayed by consecutive amplification of cDNA subpopulations using 16 sets of PCR primers (Fig. 3 and 5). In each primer set, one primer is always the same or fixed and anneals at the unmodified or right (3') end of the cDNA fragment. This fixed primer is a 17-mer with a sequence of 5'-ATTACGAATTCGGACTA-3', and comprised in the 5'-3' direction of pTRIM14 sequence, an *Eco*RI site (underlined), and original linker sequence. The second primer in each primer set anneals on the randomized or left (5') end of the cDNA fragment and is termed the subpopulation primer. The 5' end of the subpopulation primer anneals to 14 bp of pTRIM14 sequence, and its 3' end overlaps the cDNA fragment by 2 bp. These two 3' bases in each individual subpopulation primer will consist of 1 of the 16 possible 2-base combinations, resulting in a subpopulation primer sequence of 5'-GAGGAGGTGCAGTANN-3' (Fig. 2). Therefore, 1 of a total of 16 sets of PCR primers results in selective annealing and amplification of a subpopulation of the cDNA, and consecutive amplification with each of the sixteen sets of primers allows complete screening of the libraries.

In order to maximize subpopulation selective amplification and minimize redundancy of clone isolation, the dNTP concentration and annealing temperature of the SD reactions were optimized. Optimization of dNTP concentration and annealing temperature increases the number

of unique bands in one subpopulation and reduces the number of bands that appear multiple times across various subpopulations due to mispriming of the two terminal 3' bases of the subpopulation primer. Initial SD optimization experiments used representative sets of SD primers including the fixed primer and the subpopulation primers CC, AC, AG, and GA, as specified by the variable bases of the subpopulation primer (or the two 3' penultimate bases of the sequence 5'-GAGGAGGTGCAGTANN-3'), at dNTP concentrations of 200  $\mu$ M, 20  $\mu$ M, 10  $\mu$ M and 2  $\mu$ M, all at an annealing temperature of 59° C (data not shown). Details of the method are given under Experimental procedures. The 20  $\mu$ M SD reaction amplified the cDNA fragments efficiently with moderate band redundancy, while the 10  $\mu$ M SD reaction amplified the cDNA fragments with lower efficiency but less band redundancy. SD conditions were further refined using the subpopulation primer sets AC, AG, and GA because of their similar sequence. These three primer sets were used in SD experiments under annealing conditions of 57° C, 59° C, 61° C, and 63° C using 10  $\mu$ M and 20  $\mu$ M dNTP (Fig. 3). SD reaction conditions of 20  $\mu$ M dNTP and an annealing temperature of 59° resulted in reproducible efficient amplification with relatively low redundancy of bands.

SD reactions were performed with all 16 sets of subpopulation primers using both 10  $\mu$ M dNTP (data not shown) and 20  $\mu$ M dNTP (Fig. 5). Both experiments were performed in parallel, with radiolabel and without radiolabel in order to isolate bands by silver staining (31). Unique bands were excised, eluted from the gel, reamplified using the same fixed PCR primer and a pan primer that amplifies all cDNA fragments (sequence given under Experimental Procedures), and PCR products were subcloned into pSport1. Individual subcloned cDNAs were designated as a monoterpene-induced gene (MIG) or monoterpene-repressed gene (MRG) by virtue of the cloning process (*i.e.*, whether the cDNA originated from the monoterpene-treated +cDNA or the untreated control -cDNA, respectively).

## Characterization of Differentially Expressed Clones

We isolated 42 MIG cDNAs and 58 MRG cDNAs (Table 2), all of which were sequenced using an automated sequencer and compared against sequence databases using the BLAST algorithm for possible identification. A MIG/MRG clone was defined to be a known gene if it shows  $\geq 95\%$  sequence identity over the entire cDNA fragment with a known gene from the sequence data base. The cDNA insert sizes ranged from 45 to 312 bp due to the methods used for library generation, modification, and cloning. Considering the MIG cDNAs as one group, 9 were known, of which 3 were identified by more than 1 MIG cDNA. Additionally, 33 MIG cDNAs were not identified in the sequence database. Considering the MRG cDNAs as one group, 1 was a known gene and 57 MRG cDNAs were not identified in the sequence database.

More than 1 cDNA fragment, varying in molecular weight, identified cytochrome c oxidase subunit II (COX II), sperm membrane protein YWK-II (39), and Y89 (5' end similar to YWK-II) (Table 2). The multiple cDNA fragments that identified each of these genes had common sequences but differed in the size of the cDNA fragment; for example, of the 6 cDNAs that identified COX II, all the clones shared 70 bp while the largest clone (MIG-27) had an additional 32 bp not found in the smallest clone (MIG-3).

The potential of the SD screen to identify differentially expressed genes was suggested by the isolation of M6P/IGF2R as MIG-42. We have previously shown that the M6P/IGF2R was induced 2.0-fold ( $P \leq 0.002$ ) at the RNA level in 10% limonene-treated, regressing mammary carcinomas using an RNase Protection Assay (RPA) (Table 3; (19).

We next tested the differential expression of other identified MIG/MRG clones. We initially confirmed that YWK-II, a gene identified by 7 separate MIG clones (Table 2), was induced 2.9-fold ( $P \leq 0.00006$ ) in a panel of 10% limonene-treated regressing carcinomas relative to control non-regressing carcinomas (Table 3). Expression was quantitated by

Northern blot analysis and a PhosphorImager (Molecular Dynamics). YWK-II was also found to be most highly expressed in rat brain, moderately expressed in normal mammary gland, liver, and kidney, and at low levels in the spleen (data not shown).

However, Northern blots and RPAs use ~1 µg of polyA<sup>+</sup> RNA or 10 µg of total RNA per sample. In order to conserve regressing tumor RNA, which is quite limited, we used competitive RT-PCR (48-53) to determine relative fold-induction or fold-repression of the remaining MIG/MRG cDNAs.

We tested the differential expression of MIG-12, identified as lipocortin 1 (LC1; (40)), using the competitive RT-PCR assay described under Experimental Procedures (Fig. 6A). LC1 was induced 2.9-fold ( $P \leq 0.00003$ ) in 10% limonene-treated regressing carcinomas relative to control non-regressing carcinomas (Fig. 6B, Table 3). We then examined LC1 RNA expression in the normal rat mammary gland by the same assay and found that LC1 was induced 3.1-fold ( $P < 0.0005$ ) in the involuting mammary gland relative to the virgin mammary gland (data not shown). LC1 has been shown to be a marker for apoptosis in the involuting rat mammary gland (40).

The transforming growth factor  $\beta$  type II receptor (TGF $\beta$ IIIR; (41-44)) was identified by MIG-33 and was induced 3.1-fold ( $P < 0.0002$ ) in 10% limonene-treated regressing carcinomas relative to control non-regressing carcinomas (Table 3) by the competitive RT-PCR assay.

The SD screen identified neuroligin 1 as the clone MRG-31 (45). The competitive RT-PCR assay demonstrated neuroligin 1 expression to be repressed 8.8-fold in 1/5 or not detectable in 4/5 10% limonene-treated regressing carcinomas as compared to control carcinomas (Table 3).

## DISCUSSION

### The Subtractive Display Gene Expression Screen

In order to better understand the mechanism by which monoterpenes mediate tumor regression, we sought to identify differential gene expression patterns of actively regressing, advanced DMBA-induced rat mammary carcinomas treated with limonene relative to control (not treated) carcinomas. Due to the complexity of regressing tumor tissue, we required a very sensitive gene expression screening method that could detect relatively small alterations in gene expression levels and/or genes which may be expressed in low abundance. Because of these concerns, we integrated the strengths of subtractive hybridization and differential display into a new methodology termed subtractive display (SD).

Wang and Brown's subtractive hybridization method (20) generates cDNA for subtraction using PCR; however, clones are isolated by classical probe-hybridization techniques that require an undefined number of probing cycles. In contrast, SD cloning of enriched cDNAs is PCR-based and is therefore faster, more efficient and more sensitive. Unlike Liang and Pardee's differential display (21) where the 5' primer preferentially anneals somewhere upstream on the cDNA at a low temperature, the SD method uses a 16-base subpopulation primer and a 17-base fixed primer, each annealing at defined left and right linkers, respectively, on the cDNA fragment ends. In addition, annealing is performed at the highest temperature that still permits PCR to proceed (59° C). The combination of larger primers annealing at defined sites and a very high annealing temperature both contribute to high specificity and stringency, leading to high reproducibility between identical reactions. In addition, by primer design, the libraries are completely screened in 16 sets of reactions. Furthermore, because the cDNA libraries are subtracted before the display step, background noise is significantly reduced,

thereby increasing reproducibility and detection of rare cDNAs. Moreover, there exists a potential for noise with differential display because differential display depends on precise registry of cDNA fragments in paired lanes such that unique bands are isolated; yet identical cDNA fragments in treated and non-treated populations may both be amplified but differ in size by a few base pairs. Alternatively, with SD, since all cDNA fragments are putatively differentially expressed because of the subtraction step, the precise registry of cDNA fragments in paired gel lanes is not necessary to identify the differentially expressed genes.

The SD screen identified the M6P/IGF2R, which was already known to be induced 2-fold at an RNA level in the epithelium of regressing carcinomas (19). This initially suggested that SD had high sensitivity. Additionally, every MIG/MRG clone tested for differential gene expression exhibited consistent differential expression across a panel of regressing carcinomas relative to non-regressing carcinomas, thus demonstrating the ability of SD to identify a high percentage of true differentially expressed clones. It should be noted that identification of a single gene by multiple clones versus one clone does not indicate the degree of differential expression; YWK-II was identified by 7 separate bands varying in molecular weight but showed a degree of induction similar to M6P/IGF2R, TGF $\beta$ IIIR, and LC1, all of which were identified by one clone (Table 2). However, YWK-II may be more abundantly expressed. The multiple isolation of cDNA fragments that identify the same gene may have resulted from restriction digestion of the original cDNA before subtraction with *AluI* and *AluI* plus *RsaI*, and/or cloning artifacts. Furthermore, band intensity does not indicate degree of differential expression, as there was no discernible difference in band intensity which identified neuroligin 1 and bands that identified the other known clones.



## **The Process of Monoterpene-Mediated Mammary Carcinoma Regression**

Based upon histopathological analysis of monoterpene-treated regressing mammary carcinomas, the phenomenon of tumor regression was postulated to involve a differentiation/remodeling process (6). The identified MIG/MRG cDNAs are consistent with such a mechanism of regression. The present study supports involvement of the TGF $\beta$  signalling pathway with tumor regression, since the M6P/IGF2R was again identified, and importantly the next link of the pathway, the TGF $\beta$ IIR, was also identified as upregulated. The M6P/IGF2R facilitates TGF $\beta$ 1 activation (18,46) and trafficks IGF2, a potent mammary cell growth factor, into lysosomes for degradation (reviewed in (47)). Also the M6P/IGF2R may function as a tumor suppressor (48,49). Interestingly, the SD screen identified the TGF $\beta$ IIR, since it is postulated that breast tumors may not respond to TGF $\beta$  because the tumors express low levels TGF $\beta$  II receptors (50), reviewed in (51).

Two downstream effects of TGF $\beta$  signalling relevant to tumor regression are apoptosis and differentiation (reviewed in (52-56)). The SD screen isolated LC1, which is a marker for apoptosis during mammary gland involution. At the protein level, LC1 was induced 10-fold only in the alveolar epithelium, but remained at basal levels in ductal epithelium and stroma during involution, as determined by immunohistochemistry (40). Because RNA expression of LC1 in the context of the entire involuting mammary gland was not reported, we determined LC1 RNA expression during involution relative to the virgin mammary gland and found LC1 was induced 3.1-fold. Therefore, the degree of LC1 induction (2.9-fold, Table 3) during tumor regression and mammary gland involution was very similar, indicating that the observed LC1 induction during tumor regression was biologically meaningful.

Both the induced YWK-II expression and repressed neuroligin 1 expression are consistent with a differentiation process facilitating monoterpene-mediated tumor regression. YWK-II, a transmembrane protein, is expressed in the mammary gland (data not shown) and

has been shown to be a marker for differentiation of spermatogonia (57). It modulates cell-cell adhesion, as in sperm-egg adhesion during fertilization (58). Also, the polypeptide sequences of the YWK-II transmembrane and cytoplasmic domains are 70.6% homologous to the same domains of the human A4 amyloid protein found in brain plaques of Alzheimer disease patients (39). Differential gene expression of the A4 amyloid gene is associated with retinoic acid-induced morphologic differentiation of neurite processes in two model systems; the A4 amyloid mRNA is induced 34-fold in P19 embryonal carcinoma cells (59) and 10-fold in SH-SY5Y neuroblastoma cells (60). Neuroligin 1 is a neuronal cell surface protein found enriched in synaptic plasma membranes and binds to brain specific  $\beta$ -neurexins as a ligand. Expression of neuroligin 1 was tested in various tissues, but was restricted to brain tissue (45). Therefore, neuroligin 1 expression in mammary carcinomas may reflect deregulated gene expression associated with this neoplastic process. Interestingly as carcinomas regressed, neuroligin 1 expression was repressed or turned off, which is consistent with regulated gene expression in most normal tissue.

The SD screen was applied to monoterpene-treated mammary carcinomas resected at mid-regression. Therefore, the identified MIG/MRG cDNAs reflect differential gene expression patterns consistent with apoptosis and differentiation of actively regressing carcinomas. In order to better understand the process by which monoterpenes first initiate tumor regression, we are currently identifying early MIG/MRG cDNAs using SD on mammary carcinomas treated with monoterpenes for 24 hours.

In summary, the observed alterations in gene expression help to better define the process associated with monoterpene-mediated tumor regression. Although the data presented correlates monoterpene-treatment, induction of TGF $\beta$  signaling components, and tumor regression, the data does not show that TGF $\beta$  signalling is a causal event in monoterpene-mediated tumor regression and thus requires more experimentation. However, our working hypothesis is that

monoterpenes promote the upregulation of the M6P/IGF2R, thereby causing increased levels of activated TGF $\beta$ 1 available for ligand binding to the upregulated TGF $\beta$ IIIR and initiating a mitoinhibitory signal transduction pathway. The TGF $\beta$  signal blocks proliferation of the anaplastic epithelium, thereby invoking both apoptosis, as indicated by LC1, and differentiation, as suggested by both YWK-II and neuroligin 1. Alternatively or in addition, upregulation of the M6P/IGF2R degrades IGF2, whereby removal of a mitogen could cause inhibition of cellular proliferation and apoptosis.. Thus, the integration of apoptosis and differentiation culminates in mammary carcinoma regression.

## ACKNOWLEDGEMENTS

The authors would like to thank Wendy S. Kennan and Jill D. Haag for assistance with generation and collection of tissue, Dr. Laurie A. Shepel for advice during the course of this investigation and for critical review of this manuscript, and Jennifer L. Ariazi for critical review of this manuscript.

## REFERENCES

1. Crowell, P. L., and Gould, M. N. (1994) *Crit Rev Oncog* **5**(1), 1-22
2. Gould, M. N. (1995) *J Cell Biochem Suppl* **22**, 139-44
3. Crowell, P. L., Kennan, W. S., Haag, J. D., Ahmad, S., Vedejs, E., and Gould, M. N. (1992) *Carcinogenesis* **13**(7), 1261-4
4. Elegbede, J. A., Elson, C. E., Qureshi, A., Tanner, M. A., and Gould, M. N. (1984) *Carcinogenesis* **5**(5), 661-4
5. Elson, C. E., Maltzman, T. H., Boston, J. L., Tanner, M. A., and Gould, M. N. (1988) *Carcinogenesis* **9**(2), 331-2
6. Haag, J. D., Lindstrom, M. J., and Gould, M. N. (1992) *Cancer Res* **52**(14), 4021-6
7. Haag, J. D., and Gould, M. N. (1994) *Cancer Chemother Pharmacol* **34**(6), 477-83
8. Maltzman, T. H., Hurt, L. M., Elson, C. E., Tanner, M. A., and Gould, M. N. (1989) *Carcinogenesis* **10**(4), 781-3
9. Gould, M. N., Moore, C. J., Zhang, R., Wang, B., Kennan, W. S., and Haag, J. D. (1994) *Cancer Res* **54**(13), 3540-3

10. Russin, W. A., Hoesly, J. D., Elson, C. E., Tanner, M. A., and Gould, M. N. (1989) *Carcinogenesis* **10**(11), 2161-4
11. McNamee, D. (1993) *Lancet* **342**, 801
12. Shi, W., and Gould, M. N. (1995) *Cancer Lett* **95**(1-2), 1-6
13. Crowell, P. L., Chang, R. R., Ren, Z. B., Elson, C. E., and Gould, M. N. (1991) *J Biol Chem* **266**(26), 17679-85
14. Crowell, P. L., Ren, Z., Lin, S., Vedejs, E., and Gould, M. N. (1994) *Biochem Pharmacol* **47**(8), 1405-15
15. Gelb, M. H., Tamanoi, F., Yokoyama, K., Ghomashchi, F., Esson, K., and Gould, M. N. (1995) *Cancer Lett* **91**(2), 169-75
16. Ren, Z., and Gould, M. N. (1994) *Cancer Lett* **76**(2-3), 185-90
17. Kato, K., Cox, A. D., Hisaka, M. M., Graham, S. M., Buss, J. E., and Der, C. J. (1992) *Proc Natl Acad Sci USA* **89**, 6403
18. Dennis, P. A., and Rifkin, D. B. (1991) *Proc Natl Acad Sci USA* **88**(2), 580-4

19. Jirtle, R. L., Haag, J. D., Ariazi, E. A., and Gould, M. N. (1993) *Cancer Res* **53**(17), 3849-52
20. Wang, Z., and Brown, D. D. (1991) *Proc Natl Acad Sci USA* **88**(24), 11505-9
21. Liang, P., and Pardee, A. B. (1992) *Science* **257**(5072), 967-71
22. Mou, L., Miller, H., Li, J., Wang, E., and Chalifour, L. (1994) *Biochemical & Biophysical Research Communications* **199**(2), 564-9
23. Hadman, M., Adam, B. L., Wright, G. L., Jr., and Bos, T. J. (1995) *Analytical Biochemistry* **226**(2), 383-6
24. Callard, D., Lescure, B., and Mazzolini, L. (1994) *Biotechniques* **16**(6), 1096-7, 1100-3
25. Liang, P., Averboukh, L., and Pardee, A. B. (1993) *Nucleic Acids Res* **21**(14), 3269-75
26. Liang, P., Bauer, D., Averboukh, L., Warthoe, P., Rohrwild, M., Muller, H., Strauss, M., and Pardee, A. B. (1995) *Methods Enzymol* **254**, 304-21
27. Liang, P., and Pardee, A. B. (1995) *Curr Opin Immunol* **7**(2), 274-80
28. Zhao, S., Ooi, S. L., and Pardee, A. B. (1995) *Biotechniques* **18**(5), 842-6, 848, 850

29. Bertoli, D. J., Schlichter, U. H., Adams, M. J., Burrows, P. R., Steinbiss, H. H., and Antoniow, J. F. (1995) *Nucleic Acids Research* **23**(21), 4520-3
30. Ariazi, E. A., and Gould, M. N. (1996) *BioTechniques* **20**, 446-51
31. Sanguinetti, C. J., Dias Neto, E., and Simpson, A. J. (1994) *Biotechniques* **17**(5), 914-21
32. Altschul, S. F., Gish, W., Miller, W., Myers, E. W., and Lipman, D. J. (1990) *Journal of Molecular Biology* **215**(3), 403-10
33. Araki, N., Robinson, F. D., and Nishimoto, S. K. (1993) *Journal of Bone & Mineral Research* **8**(3), 313-22
34. Debuire, B., Sol, O., Lemoine, A., and May, E. (1995) *Clinical Chemistry* **41**(6 Pt 1), 819-25
35. Gebhardt, A., Peters, A., Gerding, D., and Niendorf, A. (1994) *Journal of Lipid Research* **35**(6), 976-81
36. Kawaguchi, H., Yavari, R., Stover, M. L., Rowe, D. W., Raisz, L. G., and Pilbeam, C. C. (1994) *Endocrine Research* **20**(3), 219-33
37. Mularoni, A., Beck, L., Sadir, R., Adessi, G. L., and Nicollier, M. (1995) *Biochemical & Biophysical Research Communications* **217**(3), 1105-11



38. Zhao, J., Araki, N., and Nishimoto, S. K. (1995) *Gene* **155**(2), 159-65
39. Yan, Y. C., Bai, Y., Wang, L. F., Miao, S. Y., and Koide, S. S. (1990) *Proc Natl Acad Sci USA* **87**(7), 2405-8
40. McKanna, J. A. (1995) *Anatomical Record* **242**(1), 1-10
41. Wrana, J. L., Attisano, L., Carcamo, J., Zentella, A., Doody, J., Laiho, M., Wang, X. F., and Massague, J. (1992) *Cell* **71**(6), 1003-14
42. Wrana, J. L., Attisano, L., Wieser, R., Ventura, F., and Massague, J. (1994) *Nature* **370**(6488), 341-7
43. Carcamo, J., Zentella, A., and Massague, J. (1995) *Mol Cell Biol* **15**(3), 1573-81
44. Chen, R. H., Moses, H. L., Maruoka, E. M., Derynck, R., and Kawabata, M. (1995) *J Biol Chem* **270**(20), 12235-41
45. Ichtchenko, K., Hata, Y., Nguyen, T., Ullrich, B., Missler, M., Moomaw, C., and Sudhof, T. C. (1995) *Cell* **81**(3), 435-43
46. Kovacina, K. S., Steele-Perkins, G., Purchio, A. F., Lioubin, M., Miyazono, K., Heldin, C. H., and Roth, R. A. (1989) *Biochemical & Biophysical Research Communications* **160**(1), 393-403

47. Kornfeld, S. (1992) *Annual Review of Biochemistry* **61**, 307-30
48. De Souza, A. T., Hankins, G. R., Washington, M. K., Fine, R. L., Orton, T. C., and Jirtle, R. L. (1995) *Oncogene* **10**(9), 1725-9
49. De Souza, A. T., Hankins, G. R., Washington, M. K., Orton, T. C., and Jirtle, R. L. (1995) *Nat Genet* **11**(4), 447-9
50. Sue, S. R., Chari, R. S., Kong, F. M., Mills, J. J., Fine, R. L., Jirtle, R. L., and Meyers, W. C. (1995) *Ann Surg* **222**(2), 171-8
51. Filmus, J., and Kerbel, R. S. (1993) *Curr Opin Oncol* **5**(1), 123-9
52. Lin, H. Y., and Moustakas, A. (1994) *Cell Mol Biol (Noisy-le-grand)* **40**(3), 337-49
53. Massague, J., Andres, J., Attisano, L., Cheifetz, S., Lopez-Casillas, F., Ohtsuki, M., and Wrana, J. L. (1992) *Mol Reprod Dev* **32**(2), 99-104
54. Derynck, R. (1994) *Trends Biochem Sci* **19**(12), 548-53
55. Bassing, C. H., Yingling, J. M., and Wang, X. F. (1994) *Vitamins & Hormones* **48**, 111-56

56. Yingling, J. M., Wang, X. F., and Bassing, C. H. (1995) *Biochimica et Biophysica Acta* **1242**(2), 115-36
57. Yan, Y. C., Miao, S. Y., Zong, C., Li, Y. H., Wang, L. F., and Koide, S. S. (1992) *Archives of Andrology* **28**(1), 1-6
58. Vanage, G., Lu, Y. A., Tam, J. P., and Koide, S. S. (1992) *Biochemical & Biophysical Research Communications* **183**(2), 538-43
59. Fukuchi, K., Deeb, S. S., Kamino, K., Ogburn, C. E., Snow, A. D., Sekiguchi, R. T., Wight, T. N., Piussan, H., and Martin, G. M. (1992) *Journal of Neurochemistry* **58**(5), 1863-73
60. Konig, G., Masters, C. L., and Beyreuther, K. (1990) *FEBS Letters* **269**(2), 305-10

**Table I. Competitive RT-PCR Primers and Product Sizes**

Primer sequences for competitive RT-PCR and respective product sizes are shown. In order to achieve sufficient agarose gel resolution of all 4 PCR products for each competitive RT-PCR experiment, G3PDH MIMIC 1 was used in the LC1 competitive RT-PCR reactions while G3PDH MIMIC 2 was used in the TGF $\beta$ IIIR and neuroligin 1 competitive RT-PCR reactions. MIMIC sequences reflect only the 3' end of the composite primer used in the 1 $^{\circ}$  PCR reactions during MIMIC construction to amplify from the heterologous DNA, and the 5' end of the composite primers are given by each respective target gene primer sequence.

<u>Target DNA</u>	<u>Primers (5'-3')</u>	<u>Product Size (bp)</u>
LC1	5' CCCTACCCTTCCTTCAATC 3' TGGCTTCATACAGTTTCTCAG	745
LC1 MIMIC	5' TGTTATACAGGGAGATGAAA 3' TTGAGTCCATGGGGAGCTTT	414
TGF $\beta$ IIIR	5' GCCAACAACATCAACCACAAT 3' GGGGCTCATAATCTTTCACTTCTC	724
TGF $\beta$ IIIR MIMIC	5' CGCAAGTGAAATCTCCTCCG 3' TTTCATCTCCCTGTATAACA	245

neuroligin 1	5' GAATAACGAGGGAGGGGGAGGTGGAT 3' CCGCTGGAGAAAGATGGAATGGTGGTA	526
neuroligin 1 MIMIC	5' CGCAAGTGAAATCTCCTCCG 3' CAATCAGCTCACGAAACTTG	193
G3PDH	5' TGAAGGTCGGTGTCAACGGATTTGGC 3' CATGTAGGCCATGAGGTCCACCAC	983
G3PDH MIMIC 1	5' CGCAAGTGAAATCTCCTCCG 3' TTGAGTCCATGGGGAGCTTT	604
G3PDH MIMIC 2	5' CGCAAGTGAAATCTCCTCCG 3' TCTGTCAATGCAGTTTGTAG	450

**Table II. Isolated MIG/MRG Clones**Identified Monoterpene-Induced Genes (MIG)

<u>Clone</u>	<u>Gene Identity</u>
MIG-3 / MIG-9 / MIG-21	cytochrome c oxidase subunit II (COX II)
MIG-23 / MIG-24 / MIG-27	
MIG-12	lipocortin 1 (LC1)
MIG-19	calmodulin (RCM3)
MIG-30 / MIG-32 / MIG-34	sperm membrane protein (YWK-II)
MIG-35/ MIG-53 / MIG-54 /	
MIG-55	
MIG-33	transforming growth factor- $\beta$ type II receptor (TGF $\beta$ IIR)
MIG-38	calcium transporting ATPase (SERCA I)
MIG-42	mannose 6-phosphate/ insulin-like growth factor receptor (M6P/IGF2R)
II	

MIG-51 fast myosin alkali light chains MLC1-f and  
MLC3-f

MIG-59 / MIG-60 cDNA clone Y89 5' end similar to YWK-II

33 MIG clones are unidentified

Identified Monoterpene-Repressed Genes (MRG)

<u>Clone</u>	<u>Gene Identity</u>
--------------	----------------------

MRG-31	neuroligin 1
--------	--------------

57 MRG clones are unidentified

**Table III. Confirmed MIG/MRG Differential Expression**

The differential expression of selected MIG/MRG known cDNAs was confirmed by the indicated method. RPA indicates an RNA Protection Assay was used to quantitate expression. Neuroligin 1 was repressed in 1/5 or not detected (ND) in 4/5 monoterpene-treated regressing carcinomas. P values were calculated by Student's *t* test.

<u>Gene</u>	<u>Fold Induction/Repression</u>	<u>Quantitation Method</u>
M6P/IGF2R	2.0-Fold Induced ( $P \leq 0.002$ )	RPA (Data from (19))
YWK-II	2.9-Fold Induced ( $P \leq 0.00006$ )	Northern blot
LC1	2.9-Fold Induced ( $P \leq 0.00003$ )	Competitive RT-PCR
TGF $\beta$ IIR	3.1-Fold Induced ( $P \leq 0.0002$ )	Competitive RT-PCR
neuroligin 1	8.8-Fold Repressed (1/5); ND (4/5)	Competitive RT-PCR



**Figure 1. Flowchart of the Subtractive Display Methodology.**

cDNA libraries are generated from matched tissues and designated +cDNA (monoterpene-treated) and -cDNA (control, non-treated). cDNA (solid box) is fragmented with restriction endonucleases and ligated to linkers (hatched boxes) for PCR amplification. Non-random sequence at cDNA fragment ends resulting from cDNA library construction methods and restriction digestion are shown as stipled boxes. +cDNA and -cDNA are subjected to multiple rounds of subtractive hybridization and PCR amplification to enrich for both induced and repressed genes. Subtracted libraries are reconfigured by subcloning into a trimming vector and subjected to 3 cycles of precise, unidirectional trimming which serves to randomize DNA sequence and provide a different linker on one end of the cDNA fragments (cross-hatched box) or asymmetric linkers. Subtracted, reconfigured cDNA libraries are PCR-display using 16 sets of primers including 1 fixed primer and 1 of 16 subpopulation primers. The subpopulation primer overlaps the cDNA insert by 2-bases, which selects for amplification of a subset of cDNAs.

# Subtractive Display

## +/- cDNA Libraries

- Fragment with Restriction Endonucleases
- Ligate Symmetrical Linkers



- Multiple Rounds of Subtractive Hybridization and PCR Amplification



**Libraries Enriched for Either Induced/Repressed Genes**

- Subclone into Trimming Vector and Process Through 3 Cycles: Produces Precise, Unidirectional Deletions



**Subtracted, Reconfigured cDNA Libraries with Asymmetric Linker and Randomized cDNA Sequence on One End**

**Subpopulation Primer**

- PCR-Display with 16 Sets of Primers

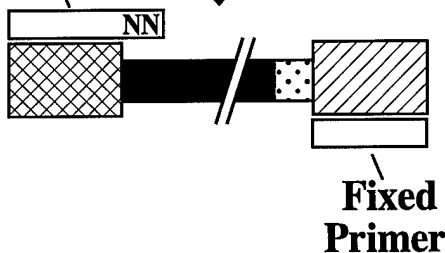


**Figure 2. PCR Product Display During the Subtractive Hybridization Process.**

A subpopulation of the cDNA libraries was selectively amplified using a primer of sequence 5'-CTTGCTTGAATTCGGACTA(A/T)(G/C)-3', which anneals at both ends of the cDNA fragments and overlaps two bases of the cDNA insert. Lanes alternate monoterpene-treated regressing (+) and control non-regressing (-) carcinoma derived cDNA. Beginning on the left, lanes labelled + and - are cDNAs before subtraction, and the numbered lanes toward the right are cDNAs after each consecutive round of subtraction. The arrow indicates the band identified as the YWK-II gene. PCR products were labelled with [ $\alpha$ - $^{35}$ S] dATP and resolved on a 5% polyacrylamide sequencing gel and visualized on X-ray film.

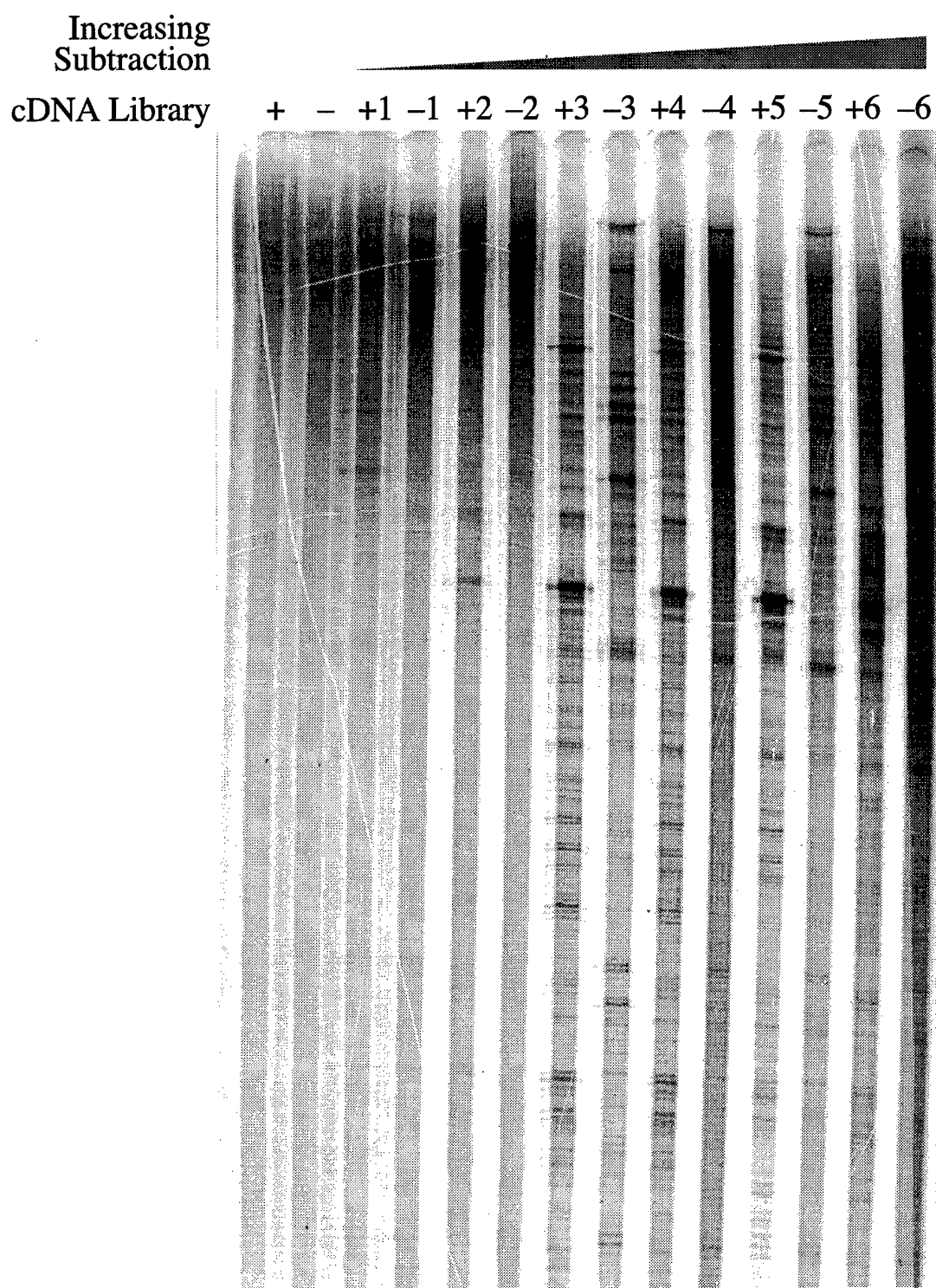


**Figure 3. Schematic of a cDNA Fragment and Primers Used in Subtractive Display.**

The schematic represents a cDNA fragment processed through 6 rounds of subtractive hybridization and 3 cycles of trimming ( $\pm 6\Delta 3$  cDNA). The unique linker sequences at each end of the cDNA fragment are boxed; the bold sequence in the right linker is an *Eco*RI recognition site. The shaded region of the cDNA insert represents 2 randomized base pairs, after trimming, which overlap the 2 bases (NN) at the 3' end of the subpopulation primer.

# Subtracted, Reconfigured cDNA Library + Subpopulation PCR Primer Set

Subpopulation (Upper)  
PCR Primer

GAGGAGGTGCAGTA NN

GAGGAGGTGCAGTA  
CTCC'TCCACGTCAT'

TAGTCC GAATTC GTAAT  
ATCAGG CTTAAG CATTAA

ATCAGGCTTAAGCATTAA

cDNA Insert

Fixed (Lower)  
PCR Primer

**Figure 4 Optimization of Subtractive Display.**

cDNA libraries processed through 6 rounds of subtraction and 3 cycles of trimming (6Δ3 subtracted cDNA) were PCR-amplified in the presence of [ $\alpha$ -<sup>35</sup>S] dATP using the fixed primer along with the AC, AG, or GA (sequence specifies the 2 bases at the 3' end) subpopulation primers, as indicated. Lanes alternate monoterpene-treated regressing (+) and control non-regressing (-) carcinoma derived cDNA. Annealing of primers was carried out at 63° C, 61° C, 59° C, and 57° C using dNTP concentrations of either 10  $\mu$ M or 20  $\mu$ M, as indicated. Labelled PCR products were resolved on a 5 % polyacrylamide sequencing gel and visualized on a PhosphorImager.

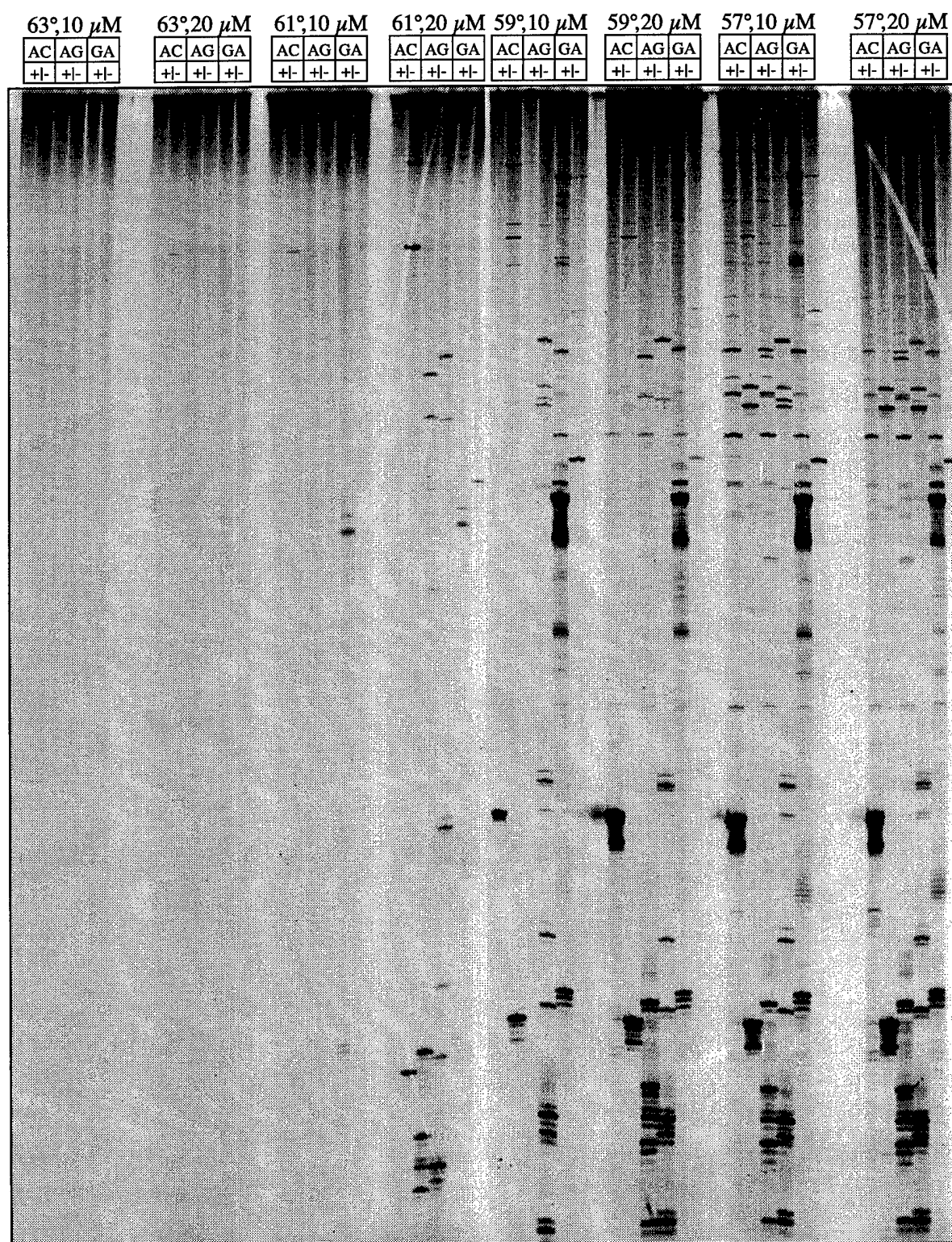
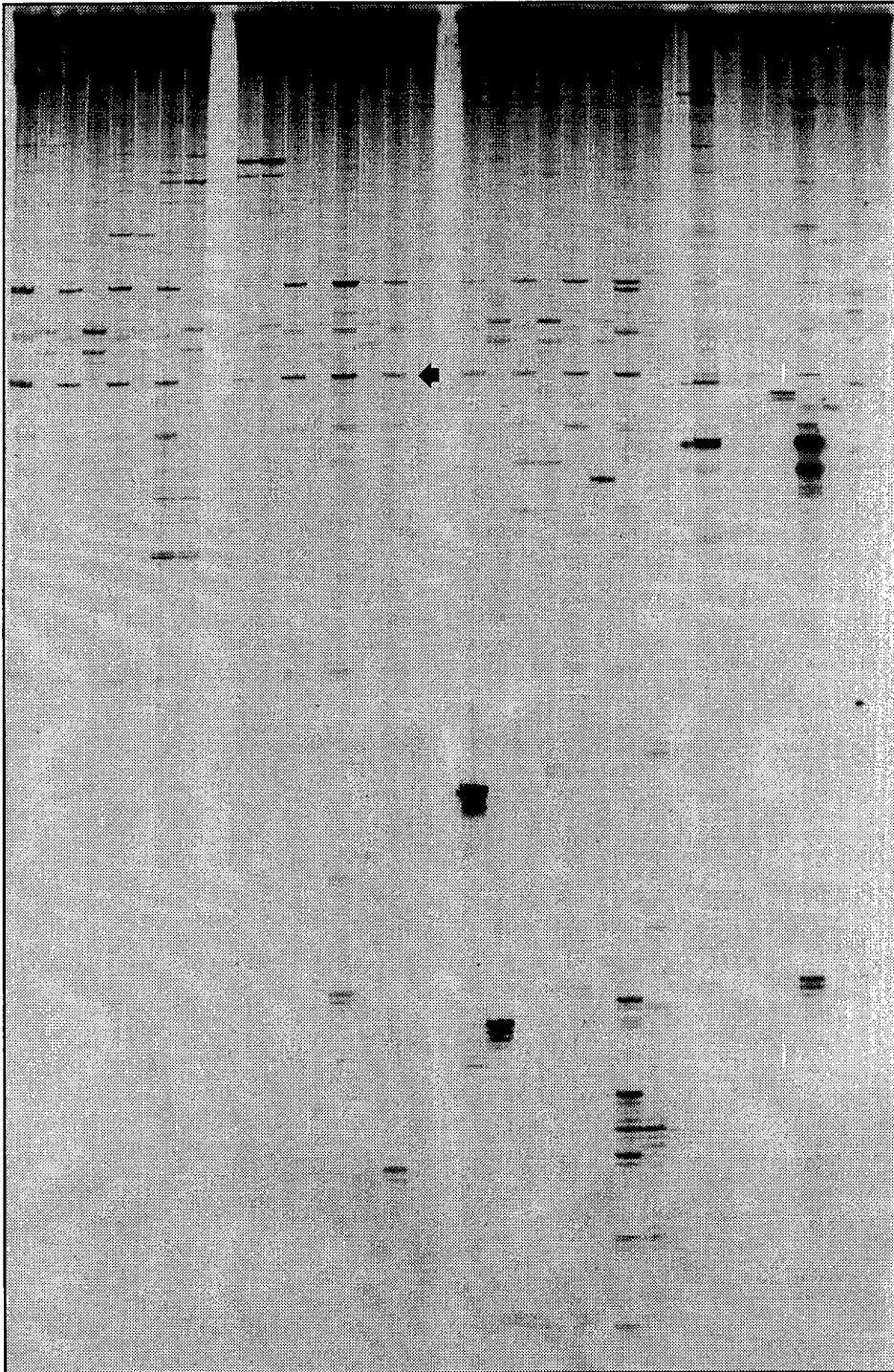




**Figure 5. Subtractive Display Using All 16 Subpopulation Primer Sets.**

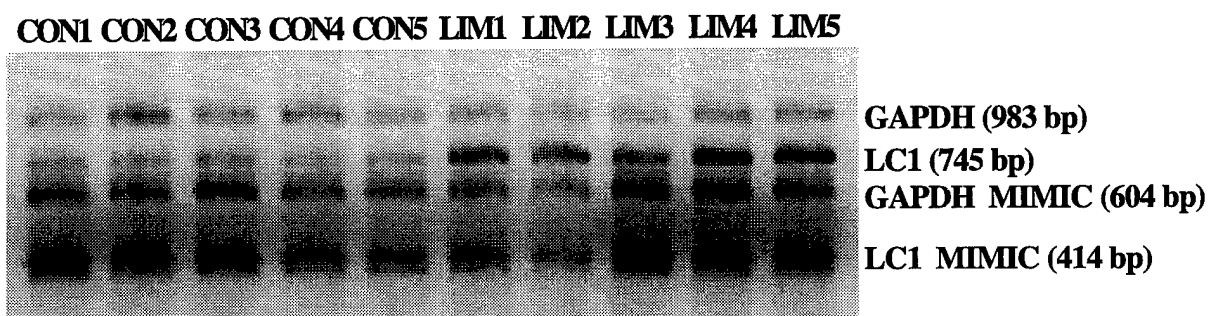
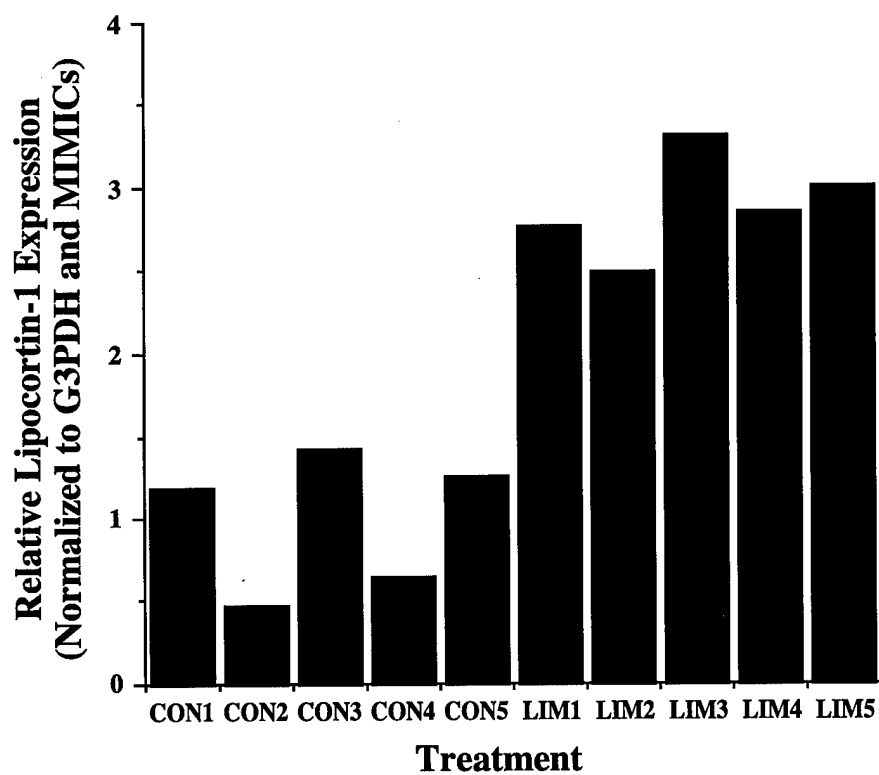
cDNA libraries processed through 6 rounds of subtraction and 3 cycles of trimming (6Δ3 subtracted cDNA) were PCR-amplified in the presence of [ $\alpha$ -<sup>35</sup>S] dATP using the fixed primer along with each of the 16 subpopulation primers; the subpopulation primer used, specified by the 2-base sequence at the 3' end of the primer, is indicated above each lane. Lanes alternate monoterpene-treated regressing (+) and control non-regressing (-) carcinoma derived cDNA. Annealing of primers was carried out at 59° C using 20  $\mu$ M dNTP. The arrow indicates one of the bands that identified the YWK-II gene. Labelled PCR products were resolved on a 5 % polyacrylamide sequencing gel and visualized on a PhosphorImager.

CC	CT	CA	CG	TC	TT	TA	TG	AC	AT	AA	AG	GC	GT	GA	GG
+ -	+ -	+ -	+ -	+ -	+ -	+ -	+ -	+ -	+ -	+ -	+ -	+ -	+ -	+ -	+ -



**Figure 6. LC1 (MIG-12) RNA Expression Using Competitive RT-PCR.**

*A*, The differential expression of LC1 between a panel of control non-regressing (lanes labelled CON1-CON5) and 10% limonene-treated regressing (lanes labelled LIM1-LIM5) carcinomas was demonstrated by competitive RT-PCR. PCR products corresponding to G3PDH, LC1, G3PDH MIMIC, and LC1 MIMIC and their respective sizes (in bp) are indicated. PCR primers were 5'-labelled with fluorescein; products were resolved on a 2% agarose gel and visualized on a FluorImager. *B*, LC1 was induced 2.9-fold in 10% limonene-treated regressing carcinomas compared to control non-regressing carcinomas. The LC1 expression was quantified from the gel in panel *A*. by first normalizing the LC1 and G3PDH bands to their respective MIMICs and second by normalizing LC1 to G3PDH.

**A****B**

## CHAPTER II

### Consecutive Cycles of Precise Unidirectional 14 bp Deletions Using a *Bse* RI/*Bsg* I Trimming Plasmid

## SUMMARY

A straightforward method for generating precise, consecutive, unidirectional 14 bp deletions into cloned DNA, adopted from the trimming principle developed by Szybalski and his colleagues, is presented. The method utilizes pTRIM14, a plasmid constructed with the class-IIS restriction enzyme recognition sites for *Bse*RI and *Bsg*I arranged in the form of a cassette, just upstream from the cloned DNA. Class-IIS restriction enzymes cleave DNA downstream of their recognition sites. pTRIM14, containing the cloned DNA, is processed through a trimming cycle which involves sequential restriction digestions with *Bsg*I and then *Bse*RI, followed by treatment with Mung Bean nuclease and then with ligase. One trimming cycle results in a net 14 bp deletion. We demonstrate precise, consecutive deletions at very high efficiency.

## INTRODUCTION

Trimming plasmids, as developed by Szybalski and his colleagues (1-3), can be used to produce small, precise, consecutive, unidirectional deletions into cloned DNA and thus lend themselves well to various projects requiring the generation of such consecutive deletions, such as removal of unwanted restriction sites problematic for a particular biotechnological purpose or fine-mapping of promoter regions. Trimming plasmids are based on class-IIS restriction endonucleases that cleave DNA at a precise distance 3' of their recognition sites (reviewed in 3). A plasmid containing one or a combination of class-IIS restriction enzyme recognition sites, in the form of a cassette, digested with the proper class-IIS enzyme(s), followed by removal of the single-stranded DNA staggered ends and religation results in a net deletion of DNA 3' of the cassette. Trimming plasmids have been constructed using *Bsp*MI (1) or a cassette of *Mbo*II and *Fok*I (2) recognition sites to generate deletions up to 4 bp or 12 bp, respectively. However, the *Mbo*II/*Fok*I 12 bp trimming plasmid is based on 5 bp recognition sites which are likely to be present at fairly high frequency in cloned DNA and uses a dihydrofolate reductase gene as a selectable marker against the antibiotic trimethoprim, an uncommon procedure in many laboratories.

We have constructed a new trimming plasmid, termed pTRIM14, that contains a cassette designed with *Bse* RI and *Bsg* I 6 bp recognition sites to facilitate 14 bp deletions into cloned DNA and uses ampicillin resistance as a selectable marker. *Bse* RI (recognition site: 5'-GAGGAG-3') and *Bsg* I (recognition site: 5'-GTGCAG-3') are class-IIS restriction enzymes that cleave DNA downstream of their recognition sites to generate staggered ends at 10/8 and 16/14 nucleotides (nt), respectively. These recognition site sequences were arranged into a *Bse* RI/*Bsg* I trimming cassette such that the *Bse* RI site is at the 5' end directly adjacent to the *Bsg* I site at the 3' end (5'-GAGGAG GTGCAG-3') and subcloned between the *Hind*III and *Eco*RI

sites of pUC18's multiple cloning site (MCS), yielding pTRIM14 (Figure 1). Cloned DNA may then be inserted into the *EcoRI* site of pTRIM14 for subsequent processing through deletion or trimming cycles. The trimming cycle begins by stepwise digestion first with *BsgI* and then *Bse RI* to cleave 16/14 nt distal and 4/2 nt proximal, respectively, relative to the 3' end of the cassette, thus conserving the trimming cassette but removing the intervening 6 bp *EcoRI* site and 8 bp at the 5' end of the cloned DNA fragment. The trimming cycle proceeds by treatment with Mung Bean nuclease to generate blunt ends and finally recircularization with T4 DNA ligase back into a plasmid. In the end, the trimming cycle results in a precise 14 bp deletion which may be repeated as often as necessary (Figure 1).



## EXPERIMENTAL PROCEDURES

### pTRIM14 Construction

pTRIM14 was built as follows: the oligodeoxynucleotides TRIM14 $\alpha$  (5'-AGCTTGAGGAGGTGCAGTAG-3') and TRIM14 $\beta$  (5'-AATTCTACTGCACCTCCTCA-3') were synthesized (University of Wisconsin Biotechnology Center, Madison, WI, USA) and annealed at 37° C to form the *Bse* RI/*Bsg* I trimming cassette with 5' *Hind*III and 3' *Eco*RI staggered ends. The intervening sequence between the *Hind*III and *Eco*RI sites in the MCS of pUC18 was removed by restriction digestion and the resulting linearized plasmid was ligated to the *Bse*RI/*Bsg*I cassette to give pTRIM14.

### pTRIM14 Testing

In order to test pTRIM14, it was necessary to insert a cloned DNA into the pTRIM14 *Eco*RI site (Figure 1). For such a purpose, a 313 bp fragment of the rat sperm membrane protein YWK-II cDNA (4) corresponding to nucleotide positions 1074 to 1386 was used. The YWK-II cDNA fragment was isolated during screening of a subtracted cDNA library (unpublished data) and had oligodeoxynucleotide linkers containing *Eco*RI sites ligated onto its termini, which facilitated subcloning of the YWK-II cDNA fragment into the *Eco*RI site of pTRIM14 (Figure 1). However, the YWK-II cDNA fragment contains one *Bse*RI recognition site in reverse orientation centered at nucleotide position 1306. Therefore, the YWK-II fragment was subcloned in reverse orientation into pTRIM14, yielding pT14 $\Delta$ 0. Consequently, when pT14 $\Delta$ 0 is subjected to its first trimming cycle, there is a deletion of 110 bp because of the

internal *Bse*RI site within the subcloned YWK-II cDNA fragment (Figure 3) and this is addressed under Results and Discussion.

### **BsgI and BseRI Reaction Conditions**

Each trimming cycle requires consecutive digestions with Bsg I and Bse RI, which to the best of our knowledge, are only commercially available from New England Biolabs (Beverly, MA, USA). Also, reaction conditions for Bsg I and Bse RI digestions are critical for optimal efficiency of cleavage. The enzymes cleave DNA efficiently only with their supplied reaction buffers as any contaminating salt significantly reduces cleavage efficiency. As a result, before plasmid DNA is used as substrate for Bsg I and BseRI digestions, it is important to first remove contaminating salts by passing the plasmid DNA through a Chroma Spin 400 centrifuge column (Clontech Laboratories, Palo Alto, CA, USA). Bsg I and Bse RI digestions are carried out using 5 U enzyme/  $\mu$ g DNA since star activity may occur at 10 U enzyme/  $\mu$ g DNA. Additionally, Bsg I and Bse RI have a short half-life and are inactive after two hours at 37° C. To ensure complete digestion, an additional aliquot of fresh enzyme is added to the reaction after two hours, and the digestion then proceeds for another two hours. Similarly, an additional aliquot of Mung Bean nuclease is added after its initial one hour digestion, which then proceeds for another hour to insure blunted DNA ends.

### **Plasmid DNA Preparation, Trimming, Ligation, and Subcloning**

Plasmid DNA for each trimming cycle was prepared with Qiagen plasmid preps (Qiagen, Chatsworth, CA, USA). An initial 10  $\mu$ g of plasmid was sufficient to complete one cycle. Before a plasmid was subjected to a trimming cycle and after each of the *Bsg*I, *Bse* RI and Mung Bean nuclease digestions, any contaminating salts and proteins were removed by a Chroma Spin 400 centrifuge column (Clontech Laboratories). Digestions with *Bse* RI, *Bsg* I,

and Mung Bean nuclease (New England Biolabs) were performed according to the manufacturer's protocol with the above modifications. Ligations were completed with the Ligation Express kit (Clontech Laboratories) using 0.5 µg of plasmid DNA in a total ligation volume of 28.4 µl and incubated at 16° C for 30 min. After each trimming cycle, 3 µl of ligation mixture was transformed into subcloning efficiency DH5α bacterial cells (BRL, Gaithersburg, MD, USA) using the manufacturer's protocol. Resulting bacterial colonies were cultured in Luria-Bertani (LB) medium supplemented with 50 µg/ ml ampicillin (Sigma, St. Louis, MO, USA).

### **Deletion Characterization**

Deletions resulting from each trimming cycle were characterized initially by polymerase chain reaction (PCR) and finally by DNA sequencing of the YWK-II fragment. PCR was performed using 2 µl of bacterial culture directly as the DNA template source and M13/pUC forward and reverse primers (BRL) for 30 cycles (94° C 1 min, 55° C 1 min, 72° C 45 sec) of amplification. The M13/pUC primers flank the trimming cassette and cloned DNA (Figure 1), resulting in amplification of the cloned DNA. PCR products generated after each trimming cycle were evaluated by electrophoresis through a 3% Trevigel-500 agarose gel (Trevigen, Gaithersburg, MD, USA). Plasmid DNA was isolated (Qiagen plasmid preps) and sequenced (Sequenase Quick-Denature plasmid sequencing kit; USB, Cleveland, OH, USA) from 5 samples after each trimming cycle. <sup>35</sup>S- labelled sequencing products were resolved on a standard 5% sequencing gel and exposed to X-OMAT AR film (Kodak, Rochester, New York, USA).

## RESULTS AND DISCUSSION

Three sets of experiments were conducted to characterize trimming. The first set of experiments evaluated trimming precision. The second set of experiments determined trimming efficiency for 1 cycle on a single plasmid clone. The third set of experiments determined trimming efficiency for 2 cycles carried out consecutively, that is without isolating an intermediate single plasmid clone between trimming cycles and instead using the entire population of plasmids generated from the first trimming cycle to begin a second trimming cycle. Data from each set of experiments is verified on independent gels, however, in an effort to conserve publication size, data from all three sets of experiments are presented in Figure 2 .

### Deletion Size

Trimming was initially characterized by subjecting pT14 $\Delta$ 0 to three consecutive trimming cycles ( $\Delta$ 1,  $\Delta$ 2, and  $\Delta$ 3) generating pT14 $\Delta$ 1, pT14 $\Delta$ 2, and pT14 $\Delta$ 3, respectively. Trimming cycle  $\Delta$ 1 resulted in the deletion of 110 bp from pT14 $\Delta$ 0, due to the internal *Bse* RI cleavage site in the cloned DNA, generating pT14 $\Delta$ 1 (compare lanes labelled T14 $\Delta$ 0 to T14 $\Delta$ 1, Figure 2). This demonstrates that if a *Bse* RI or *Bsg* I site is present within the cloned DNA, the first trimming cycle will result in a deletion extending 10 or 16 bp 3' of the internal *Bse* RI or *Bsg* I site, respectively, and thus a net deletion of more than 14 bp (Figure 3B). Trimming cycle  $\Delta$ 2 was carried out on pT14 $\Delta$ 1, producing pT14 $\Delta$ 2, which in turn was used for trimming cycle  $\Delta$ 3 to generate pT14 $\Delta$ 3. Trimming cycles  $\Delta$ 2 and  $\Delta$ 3 resulted in two consecutive 14 bp deletions as shown in Figure 2 (compare lanes labelled T14 $\Delta$ 1, T14 $\Delta$ 2, and T14 $\Delta$ 3) and were further demonstrated as precise 14 bp unidirectional deletions by sequence analysis in Figure

3A. Trimming cycles  $\Delta 1$ ,  $\Delta 2$ , and  $\Delta 3$ , and their resultant deletions are schematized in Figure 3B.

### Trimming Efficiency

Trimming efficiency for 1 cycle was determined using PCR to score precise deletions (Figure 2, lanes labelled 1-20 and 1 Cycle). Plasmid was prepared from a single isolated pT14 $\Delta 1$  clone and processed through one trimming cycle. The resulting population of plasmids were transformed into DH5 $\alpha$  cells from which 20 bacterial colonies were isolated. PCR was performed directly from the bacterial clones as the source of DNA template using M13/pUC primers to amplify the cloned DNA (Figure 1). Because the resulting PCR products after each trimming cycle differ by only 14 bp, small anomalies in DNA migration during electrophoresis become significant and may affect data analysis. Therefore, independent PCR products resulting from the trimming efficiency experiments were mixed with a PCR product from the parental pT14 $\Delta 1$  (T14 $\Delta 1$  Mr, Figure 2). T14 $\Delta 1$  Mr serves only as a molecular weight marker or as an internal reference for each lane to determine that a deletion occurred as opposed to an anomaly in DNA migration. Twenty independent PCR products resulting from 1 trimming cycle [T14 $\Delta 2$  (middle bands labelled 1 Cycle, Figure 2)] and from 2 consecutive trimming cycles [T14 $\Delta 3$ , (bottom bands labelled 2 Cycles, Figure 2)] as discussed below, were mixed with T14 $\Delta 1$  Mr, and resolved on a 3% Trevigel-500 agarose gel, thus displaying three bands in one lane if the plasmids were properly trimmed. All 20 T14 $\Delta 2$  PCR products from individual bacterial colonies show a 14 bp deletion as compared to T14 $\Delta 1$  Mr [(Figure 2, lanes 1-20; compare migration of T14 $\Delta 2$  (middle band labelled 1 Cycle) to T14 $\Delta 1$  Mr (top band)]. As stated above, this result was verified on an independent gel using only samples generated from the efficiency of 1 trimming cycle experiment. These results indicate a trimming efficiency up to 100% from a single plasmid clone after 1 trimming cycle.

A similar set of experiments were performed to determine the efficiency of 2 consecutive trimming cycles without isolating a unique plasmid between cycles. Plasmid DNA was prepared from a single pT14 $\Delta$ 1 clone, processed through 1 trimming cycle and the resulting plasmids transformed into DH5 $\alpha$  cells. Plasmid DNA was then prepared from the entire population of transformed cells, processed through a second trimming cycle and again transformed into DH5 $\alpha$  cells. PCR was performed directly on 20 isolated bacterial colonies using M13/pUC primers to amplify the cloned DNA. As above, the 20 independent PCR products derived from 2 consecutive trimming cycles [T14 $\Delta$ 3 (2 Cycles, Figure 2)] were mixed with the reference molecular weight marker T14 $\Delta$ 1 Mr and T14 $\Delta$ 2 PCR products and resolved on a 3% Trevigel-500 agarose gel. T14 $\Delta$ 3 PCR products are scored for a 28 bp deletion or two cycles of 14 bp deletions as compared to T14 $\Delta$ 1 Mr [Figure 2, lanes 1-20; compare migration of T14 $\Delta$ 3 (bottom band labelled 2 Cycles) to T14 $\Delta$ 1 Mr (top band)]. Eighteen of the 20 T14 $\Delta$ 3 PCR products show a 28 bp deletion while the T14 $\Delta$ 3 PCR products in lanes 9 and 14 are absent and instead show a 14 bp deletion since densitometric analysis of the gel indicates that the T14 $\Delta$ 2 PCR product in lanes 9 and 14 are twice the intensity as the other lanes. Again, as stated above, this result was verified on an independent gel using only samples generated from the efficiency of 2 consecutive trimming cycles experiment. These results indicate a trimming efficiency up to 90% for two consecutive cycles without an isolated intermediate.

The trimming efficiencies of 100% for 1 cycle and 90% for 2 consecutive cycles should be considered as estimates because of the limited sample size of 20 colonies. Furthermore, when the *Bsg* I and *Bse* RI digestions are performed for only 2 hours each without adding a fresh aliquot of enzyme for digestion of an additional 2 hours as detailed under Materials and Methods, the trimming efficiency for 1 cycle drops to 65% and for 2 consecutive cycles to 30% (data not shown).

### Variations on the Deletion Size

We did not observe 12 or 13 bp deletions resulting from inefficient digestion of the staggered DNA ends by Mung Bean nuclease after restriction endonuclease treatment. However, Mung Bean nuclease blunting efficiency was maximized by essentially carrying out the reaction twice, that is the addition of a fresh aliquot of the enzyme to the reaction and allowing it digest for another hour, as stated in the Materials and Methods. Therefore, if the Mung Bean step is performed twice, we would not expect to generate a subset of clones with 12 bp, which could occur if the staggered ends were complementary and incompletely removed. But, if T4 DNA polymerase is substituted for Mung Bean nuclease to fill in the staggered ends instead of removing the staggered ends, a net deletion of 10 bp should occur, although we did not characterize this protocol modification.

It should be noted that when a cloned DNA is inserted into pTRIM14, the cloned DNA will be 8 bp 3' of the trimming cassette due to the two nucleotides, TA, and the regeneration of *EcoRI* sites flanking the cloned DNA (Figure 1). As a result, the first trimming cycle will delete 14 bp, 6 bp of which is from the *EcoRI* site plus 8 bp cloned DNA; however, subsequent trimming cycles will delete 14 bp of cloned DNA.

### Variations on the Trimming Plasmid

In like manner to pTRIM14, we have also built the 8 bp precise trimming plasmids pTRIM8B, based on a cassette of the 6 bp recognition site enzymes *Bsg I/Bbs I* (5'-GTGCAG GAAGAC-3'), and pTRIM8S, based on a cassette of the 6 and 7bp recognition site enzymes, respectively, *Bsg I/Sap I* (5'-GTGCAG GCTCTTC-3').

In short, pTRIM14 is a precise trimming plasmid based on a cassette designed with *Bse* RI and *Bsg* I recognition sites and generates consecutive, precise, 14 bp unidirectional deletions in cloned DNA at high efficiency.



## ACKNOWLEDGEMENTS

The authors thank Helen Moinova and Daniel R. McFarlin for technical assistance and Dr. Laurie Shepel for critical evaluation of the manuscript. This work was supported by NIH NCI grant CA38128 and by DOD (Army) grant DAM17-94-J4041 (EAA).

## REFERENCES

1. Hasan, N., Kim, S. C., Podhajska, A. J., and Szybalski, W. (1986) *Gene* **50**, 55-62.
2. Hasan, N., Kur, J., and Szybalski, W. (1989) *Gene* **82**, 305-311.
3. Szybalski, W., Kim, S. C., Hasan, N., and Podhajska, A. J. (1991) Class-II restriction enzymes - a review. *Gene* **100**, 13-26.
4. Yan, Y. C., Bai, Y., Wang, L., Miao, S., and Koide, S. S. (1990) *Proc. Natl. Acad. Sci. USA* **87**, 2405-2408.

**Figure 1. Schematic of pTRIM14, the BseRI/BsgI 14 bp trimming plasmid, as it is processed through one trimming cycle.**

M13/pUC primer binding sites used for PCR to amplify the cloned DNA inserted into pTRIM14 are indicated by empty boxes flanking the trimming cassette (solid box) and the EcoRI site (striped box). The cloned DNA (YWK-II fragment, stippled box) is inserted into pTRIM14 8 bp 3' of the trimming cassette at the EcoRI site with the result of regenerating two EcoRI sites flanking the inserted cloned DNA. Specific DNA sequences and enzymatic reactions are indicated. The 5' nucleotide cleavage coordinates for BseRI and BsgI are indicated in parentheses beneath the trimming cassette and their cleavage sites by arrowheads. The 14 bp sequence demarcated by the dashed box, is comprised of a 6 bp EcoRI site plus 8 bp of cloned DNA sequence and is deleted during the first trimming cycle.

# 14bp Trimming Cycle (Precise Deletion)

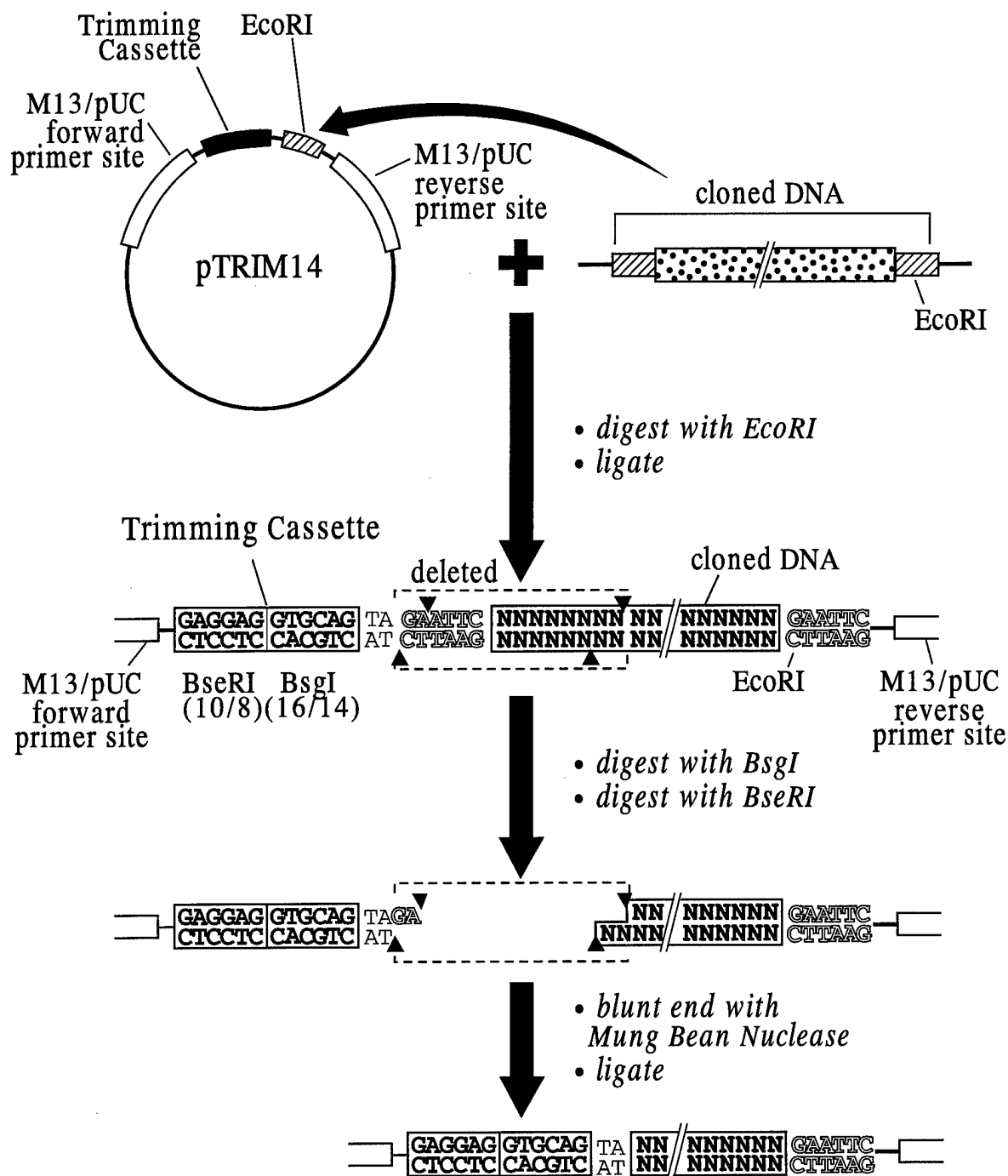


**Figure 2. Analysis of trimming cycle PCR products.**

PCR was performed with M13/pUC forward and reverse primers to amplify the cloned DNA as shown in Figure 1. PCR products were resolved on a 3% Trevigel-500 agarose gel (Trevigen) stained with ethidium bromide. Molecular weight (Mr) marker size in bp is shown. Each PCR product resulting from the corresponding trimming cycle is labelled T14 $\Delta$ 0-T14 $\Delta$ 3. Lanes labelled 1-20 are mixed independent PCR products from 20 independently isolated bacterial clones containing trimming plasmids resultant of trimming cycles. The top band in lanes 1-20 (indicated by T14 $\Delta$ 1 Mr), serves only as a reference molecular weight marker for each lane in order to discern 14 bp and 28 bp deletions as opposed to gel anomalies. The middle bands (T14 $\Delta$ 2 PCR products as indicated by 1 Cycle) and the bottom bands (T14 $\Delta$ 3 PCR products as indicated by 2 Cycles) are the resulting independent PCR products from 1 trimming cycle and 2 consecutive (no isolated plasmid intermediate) trimming cycles, respectively.

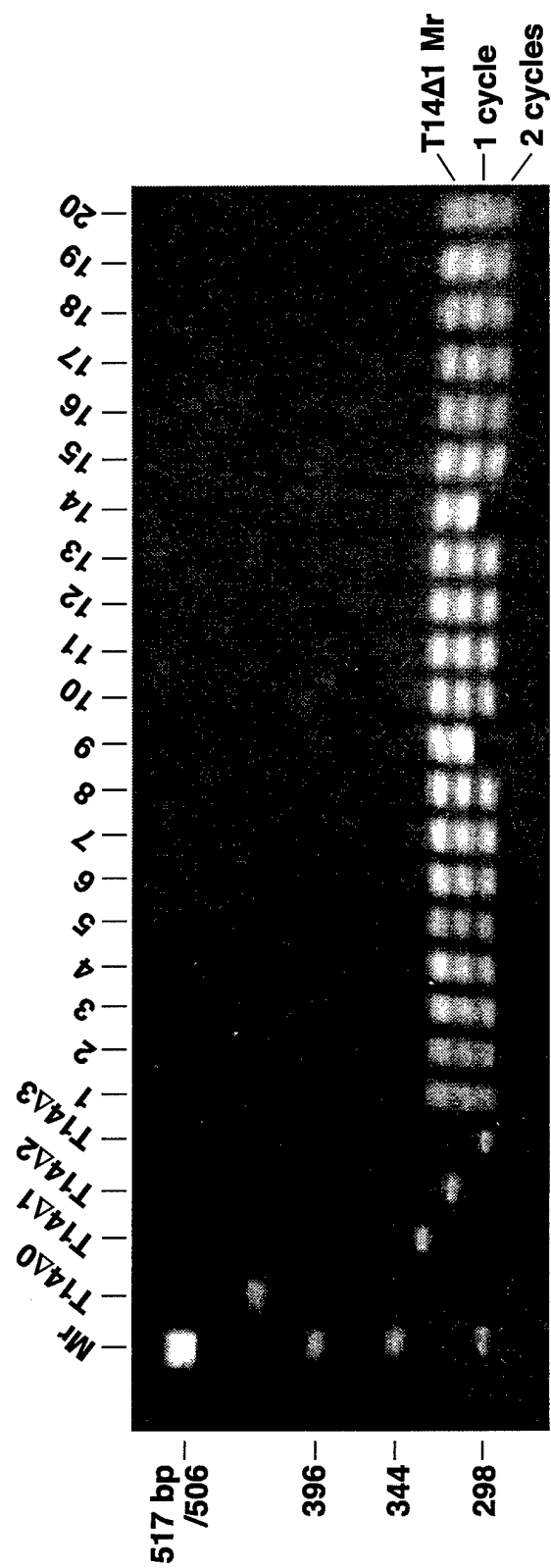
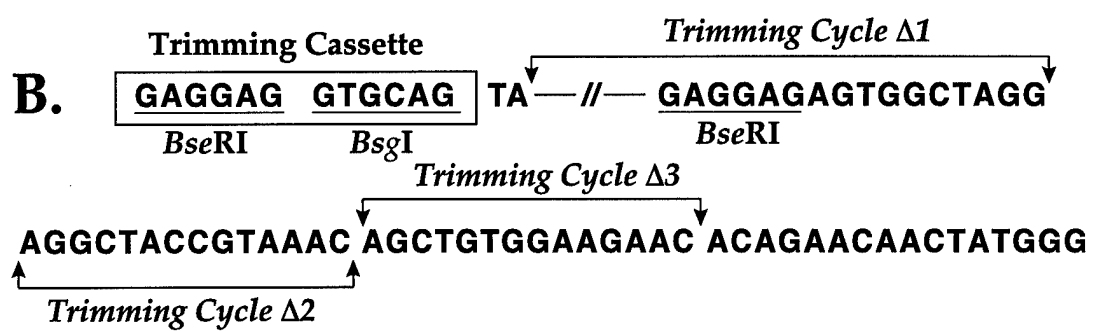
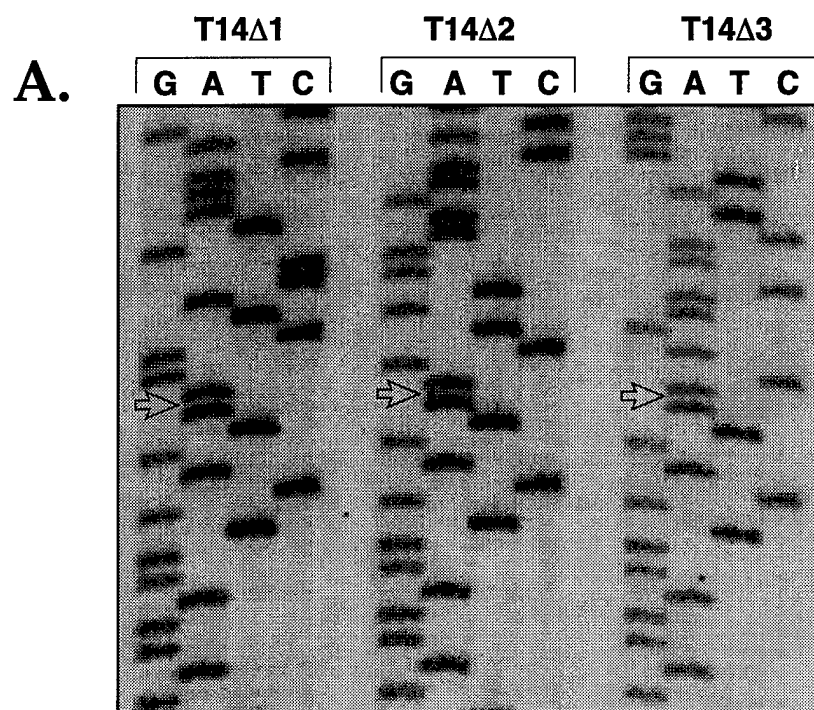


**Figure 3. Sequence analysis and schematic of precise 14 bp deletions.**

A. 5% polyacrylamide sequencing gel of pT14 $\Delta$ 1 (T14 $\Delta$ 1), pT14 $\Delta$ 2 (T14 $\Delta$ 2), and pT14 $\Delta$ 3 (T14 $\Delta$ 3) after trimming cycles  $\Delta$ 1,  $\Delta$ 2, and  $\Delta$ 3, respectively. The sequence reflects the trimming cassette plus the TA nucleotides followed by cloned DNA (YWK-II) sequence. The hollow arrows indicate the juncture between the trimming cassette plus the TA nucleotides and the cloned DNA (YWK-II fragment) or the site of the precise deletion. B. Schematic showing sequence as read in Figure 3A. The sequences indicated by the double arrow bars labelled trimming cycles  $\Delta$ 1,  $\Delta$ 2, and  $\Delta$ 3 are the sequences deleted by each corresponding trimming cycle. The double hatched line below the double arrow bar labelled trimming cycle  $\Delta$ 1 represents the sequence 5' to the internal BseRI site located in the cloned DNA (YWK-II cDNA fragment).





### **CHAPTER III**

#### **Characterization and Downstream Effects of the TGF $\beta$ Signal Transduction Pathway in Mammary Carcinomas Treated with the Anticancer Agent Perillyl Alcohol**

## SUMMARY

TGF $\beta$  signaling and its downstream effects were investigated in perillyl alcohol-treated rat mammary carcinomas. RNA expression studies showed TGF $\beta$ -related genes were induced and temporally regulated: first: c-jun and c-fos (transient); second: TGF $\beta$ 1; third: M6P/IGF2R, TGF $\beta$ IIR, and TGF $\beta$ IR; and fourth: smad3. *In situ* protein expression studies confirmed upregulation and demonstrated colocalization of these genes in epithelial cells. Smad2/Smad3 exhibited nuclear localization. A subpopulation of Smad2/Smad3 nuclei colocalized with a subpopulation of apoptotic nuclei. RNA expression studies demonstrated the cell cycle and apoptosis related genes p21<sup>cip1</sup>/WAF1, p27<sup>Kip1</sup>, bax, bad, and annexin I were induced; cyclin E and cdk2 were repressed; and bcl-2 and p53 were unchanged. Characterization of cell growth and death parameters revealed apoptosis was induced prior to induction of cytostasis.

## INTRODUCTION

Chemotherapeutic agents can be grouped into two broad classes: cytotoxic and cytostatic agents. Generally, the cytotoxic agents affect proliferating cells resident in tumors, but do not discriminate well between proliferating tumor cells and proliferating normal cells, such as those found in bone marrow, intestinal mucosa, hair follicles and gonads, leading to normal tissue toxicity which limits both dose and frequency of drug administration. Whereas the cytotoxic agents kill proliferating cells, the cytostatic agents selectively inhibit tumor cell proliferation and may also selectively cause the tumor cells to differentiate or to apoptose, and thus may not cause such severe toxicity. The naturally-occurring monoterpenes, limonene (LIM) and perillyl alcohol (POH), are potentially cytostatic agents and have been shown to be effective chemopreventive and chemotherapeutic agents in rodent organ-specific tumor models [reviewed in (1-3)]. Our laboratory has extensively characterized the anti-cancer activities of monoterpenes in the chemical carcinogen dimethylbenz-[*a*]-anthracene (DMBA)- and *N*-methyl-*N*-nitrosourea (NMU)-induced rat mammary carcinoma models (4-10). Dietary administration of 10% LIM or 2% POH caused the complete regression of ~66% of advanced DMBA- or NMU-induced rat mammary carcinomas. Furthermore, the only toxicity observed during treatment was initial weight loss due to food aversion (8,9). Because of the high efficacy and low toxicity of monoterpenes during preclinical development, LIM and POH are currently being evaluated in several Phase I and Phase II clinical trials in England (11) and the United States (12,13).

Several biochemical activities are associated with monoterpene-mediated carcinoma regression, including selective inhibition of 21-26 kD small G proteins (14-16) and inhibition of ubiquinone synthesis (17). Investigations into gene expression demonstrated that the mannose 6-phosphate/insulin-like growth factor type II receptor (M6P/IGF2R), which facilitates latent

associated peptide-TGF $\beta$ 1 (LAP-TGF $\beta$ 1) activation and degrades both the mammary mitogen insulin-like growth factor II (IGF2) (18) and the mitoinhibitory transforming growth factor  $\beta$ 1 (TGF $\beta$ 1), was significantly induced in actively regressing carcinomas as shown by immunohistochemistry (IHC) (19). Noteworthy, it has been suggested that the M6P/IGF2R may be a tumor suppressor gene since the locus showed frequent loss of heterozygosity and the second allele was mutated in human breast cancer (20) and hepatocellular carcinomas (21). Investigations into gene expression were further explored by screening 10% LIM-treated, actively regressing advanced rat mammary carcinomas using subtractive display (SD) (22). Identified cDNAs were consistent with a differentiation/remodeling process of tumor regression. The SD screen again identified the M6P/IGF2R, as well as the transforming growth factor  $\beta$  type II receptor (TGF $\beta$ IIR). Induction of the M6P/IGF2R and TGF $\beta$ IIR suggested the TGF $\beta$  signal transduction pathway was involved in carcinoma regression. Downstream events consistent with activation of TGF $\beta$  signaling relevant to carcinoma regression are induction of both cytostasis and apoptosis. Suggestive of an apoptotic process, the SD screen (22) identified a marker of apoptosis for the involuting mammary gland, lipocortin 1, also termed annexin I (23).

TGF $\beta$  initiates its cellular actions by facilitating oligomerization and activation of transmembrane serine/threonine kinase receptors. An activated signaling complex forms by sequential binding of TGF $\beta$ 1 to TGF $\beta$ IIR, followed by recruitment of TGF $\beta$  type I receptor (TGF $\beta$ IR) into a hetero-oligomeric complex with a stoichiometry of dimeric TGF $\beta$ 1 bound with two TGF $\beta$ IIR and two TGF $\beta$ IR molecules. Due to intrinsic kinase activity, the TGF $\beta$ IIR phosphorylates the TGF $\beta$ IR in a region rich in glycine and serine residues termed the GS domain, located in the juxtamembrane region of only Type I receptors [reviewed in (24)]. Smad2 and Smad3 are phosphorylated by activated TGF $\beta$ IR, leading to heteromerization with Smad4. The hetero-oligomeric Smad complex is translocated to the nucleus and regulates

transcription of specific genes through direct or indirect binding to DNA and other transcription factors [(25) and reviewed in (26)].

In addition to TGF $\beta$  signaling through SMADs, TGF $\beta$  has been shown to initiate signaling cascades which activate Ras and several members of the mitogen-activated protein kinase (MAPK) superfamily including extracellular signal-regulated kinases (Erks), and stress-activated protein kinase/c-Jun N-terminal kinase (SAPK/JNK). Importantly, TGF $\beta$ -mediated activation of these signaling components occurred within minutes of treatment and was blocked by a dominant negative Ras [reviewed in (27)]. Activation of the SAPK/JNK pathway by TGF $\beta$  has also been blocked by dominant negative mutants of MAPK kinase kinase 1 (MEKK1), MAPK kinase 4 (MKK4), JNK1, and c-Jun (28). Additionally, c-Jun, a physiologic substrate for SAPK/JKN, along with c-fos have been induced in TGF $\beta$  treated cells, and hence lead to increased AP-1 activity (29)

Thus, we explored the potential for POH-mediated activation of the TGF $\beta$  signal transduction pathway and possible downstream molecular and cellular alterations consistent with activation of this pathway. Characterization of the TGF $\beta$  pathway and downstream effects included a study of morphologic remodeling events during tumor regression, RNA expression and *in situ* protein expression analysis of TGF $\beta$  signaling components, RNA quantification of cell cycle and apoptosis related genes, and determination of cell proliferation and apoptotic indices.

## EXPERIMENTAL PROCEDURES

### Generation of Advanced Mammary Carcinomas

Virgin female Wistar-Furth rats (Harlan Sprague Dawley, Madison, WI USA) at 50-55 days of age were administered a single dose of 50 mg/kg DMBA (Eastman Kodak, Rochester, NY USA) in sesame oil by gastric intubation. The rats were provided with Teklad Lab Blox chow and acidified water *ad libitum*, unless otherwise noted. All rats were palpated weekly until advanced mammary carcinomas (defined as  $\geq 10$  mm in diameter) developed, at which time the rats were randomized to either the acute or chronic treatment protocol. Rats that did not develop advanced mammary carcinomas within 15 weeks after DMBA administration were euthanized with ether. All animal use was in compliance with NIH guidelines for humane care and was approved by the University of Wisconsin-Madison Medical Center Animal Use Committee.

### Acute Treatment Protocol

Rats in the acute treatment group were randomly paired and assigned to POH or CON treatment, and subsequently assigned to a timecourse group of 1 h, 4 h, 12 h, 24 h or 48 h of treatment. Paired rats were initially dosed with 1 g/kg POH (>96% pure by gas-chromatographic analysis; Aldrich, Milwaukee, WI USA) diluted 10-fold in sesame oil or vehicle alone (CON treatment) by gastric intubation. Rats were additionally dosed every 10 h after initial administration until the time of carcinoma resection, dependent on the rat's assigned timecourse grouping. Additionally, rats were administered 1 ml/kg bromodeoxyuridine (BrdU) labeling reagent (Amersham Life Sciences, Arlington Heights, IL USA) via intraperitoneal (IP) injection 1 hr before carcinoma resection.

### **Chronic Treatment Protocol**

Rats in the chronic treatment group were randomly paired and assigned to a 2% POH (w/w) or pair-fed control diet. Diets were prepared by thoroughly mixing POH with Teklad 4% mouse/rat diet and stored at -20°C. Fresh diets were prepared weekly and rats were provided with fresh diet on a daily basis in order to minimize evaporative loss of POH. For pair feeding, the mass of food consumed by the 2% POH-fed rat was measured every 24 h, and the assigned partner was provided with an equal mass of food. Rats were followed by palpation for 10 weeks and scored for active carcinoma regression (defined as greater than 50% reduction of the carcinoma's maximum diameter). Once one rat within a paired group was determined to bear an actively regressing carcinoma, both rats of the paired group were implanted with a BrdU slow release pellet (Amersham Life Sciences, Arlington Heights, IL, USA) in their interscapular fat pads. Carcinomas were resected 2 days later. All remaining rats were euthanized with ether 10 weeks after diet randomization.

In order to address possible POH mediated alterations in non-carcinoma tissues, rats which were not administered DMBA and thus bear normal mammary glands, were also placed into a 4 week chronic POH or pair-fed CON treatment protocol.

### **Circulating POH Metabolite Analysis**

At the time of carcinoma resection, blood was withdrawn from rats via heart puncture using a syringe flushed with 20 mg/ml heparin (Sigma) in 0.9% saline. Blood samples were centrifuged to generate plasma, which was stored at -20°C. Monoterpene metabolites are stable for 1 yr under these conditions. POH metabolite concentrations were determined using organic extracts of plasma by capillary gas chromatography with on-line flame ionization and infrared detection (GC-FID) as previously described (9). Briefly, 5  $\mu$ l of a 10  $\mu$ M perillylaldehyde in

methanol solution was added as an internal control to 50  $\mu$ l of plasma, since the migration peak for perillaldehyde did not overlap with any POH metabolites. Next, 50  $\mu$ l of a 0.2 M phosphoric acid/ 1 M potassium chloride solution was added to the plasma mixture followed by extraction with 100  $\mu$ l of t-butylmethyl ether. Organic extracts were analyzed on a Hewlett-Packard 5891 gas chromatograph equipped with a 30 m, 0.32 mm inside-diameter, 0.25 mm film-thickness Supelco SPB-5 column. The injection volume was 5  $\mu$ l with the injector and detector temperatures at 250°C and 300°C, respectively. The temperature program was 90°C for 8 min, followed by ramping 10°C/min to 275°C and held for 10 min, followed by an active purge for 1 min. Standard curves were generated for the POH metabolites perillic acid (PA) and dihydroperillic acid (DHPA) in rat plasma at concentrations ranging from 0.20 to 1.5 mM, using perillylaldehyde as an internal control. The ratio of the monoterpene peak area to the perillylaldehyde peak area versus the concentration of the monoterpene in the sample was plotted, and the slope of this line was used to determine the plasma concentration of each POH metabolite. The slopes of the standard curves generated for all monoterpenes were linear, with correlation coefficients ( $r$ ) ranging from 0.98 to 1.0. The extraction efficiency was >90% and the limit of detection was 5-10  $\mu$ M for each monoterpene.

### **Tissue Section Preparation and Gross Morphology**

A small portion of each resected carcinoma was fixed with freshly prepared 4% paraformaldehyde (PFA) in phosphate buffered saline (PBS), pH 7.4 for 4 h on ice, dehydrated in a graded series of ethanol and embedded in paraffin. Tissue sections were cut 4  $\mu$ m thick, mounted on poly-L-lysine coated glass slides, deparaffinized with xylenes, rehydrated in a graded series of ethanol, washed in ddH<sub>2</sub>O and again washed in PBS. All washes for staining experiments were carried out for 5 min each at room temperature. Tissue sections from every resected carcinoma were additionally stained with H&E for gross morphologic analysis. Tissue



sections were viewed using an Olympus BX50 Light Microscope (Olympus, Lake Success, NY, USA).

### **Ultrastructural Morphology**

At the time of resection for selected carcinomas in the chronic treatment group, a small portion of tissue was immediately placed in 3% glutaraldehyde on dental wax. The tumors were cut into 1 mm cubes and transferred to vials with 3% glutaraldehyde in 0.1 M cacodylate, pH 7.4 for 2 hr, washed 3 times with 0.1 M cacodylate buffer containing 7.5% sucrose, and postfixed with 1% OsO<sub>4</sub> for 1.5 hr on ice. Following dehydration in a graded series of ethanol, the tissue was first infiltrated with 1:1 propylene oxide:Eponate 12 (Ted Pella, Redding, CA, USA), then infiltrated overnight with Eponate 12 and embedded in fresh Eponate 12. Thin sections were cut with a diamond knife on a Reichert Ultracut E ultramicrotome and stained with uranyl acetate and lead citrate. Electron micrographs were taken with an Hitachi H-7000 electron microscope operated at 75 kV.

### **Nuclease Protection Assay (NPA)**

The NPA allows simultaneous quantitation of multiple genes' RNA expression by hybridization of a panel of labeled probes to the sample RNA, followed by digestion of unhybridized probe and sample RNA with a mixture of single-strand specific nucleic acid nucleases comprised of a mixture of S1 Nuclease, RNase A, and RNase T1. Due to their duplex structure, probes specifically hybridized to the complementary target RNA species are protected from nuclease digestion, and resolved by polyacrylamide gel electrophoresis (PAGE). The NPAs were carried out using Ambion's Multi-NPA kit (Austin, TX, USA).

Total RNA was isolated from frozen tissues using the RNeasy Total RNA Isolation System (Qiagen, Los Angeles, CA USA). Briefly, tissues were lysed and homogenized in a

denaturing solution containing guanidine isothiocyanate and  $\beta$ -mercaptoethanol followed by the addition of ethanol in order to adjust the sample's salt concentration, thus allowing efficient and selective binding of RNA to the silica-gel membrane of the RNeasy column. After passing the tissue lysates over the RNeasy column, samples were washed three times and eluted in water.

NPA oligodeoxynucleotide probes were designed using Oligo 5.0 software (National Biosciences, Plymouth, MN, USA) and the appropriate gene's cDNA sequence (GenBank sequences available from the National Center of Biotechnology Information internet web site at <http://www.ncbi.nlm.gov/>). Because multiplexing of probes was possible in the NPA, genes of interest were grouped into panels, and each gene's probe was designed to a specified size, such that the entire panel of probes would resolve by PAGE. Selection of candidate NPA oligodeoxynucleotide probes was based on specificity as determined by Basic Local Alignment Search Tool (BLAST) sequence similarity searches (56). Candidate NPA probes, which returned BLAST queries showing an exact sequence match only with the appropriate gene and not with other gene family members, were selected. Additional random sequences were attached to the 3'-end of selected NPA probes, such that nucleases would cleave the additional 3' random sequence during the nuclease digestion step of the NPA assay, thereby allowing differentiation between the full-length non-protected probe and protected probe on the gel. NPA oligodeoxynucleotide probes were synthesized and PAGE purified (Genosys Biotechnologies, The Woodlands, Texas, USA).

The NPA oligodeoxynucleotide probe sequences are given below. The designations of the NPA oligodeoxynucleotide probes are underlined; the full-length size of each probe is indicated in parentheses. Lower case indicates the additional random sequences at the 3'-end of the full-length probes.

M6P/IGF2R (111-mer)

Protected Probe Size: 98-mer

Sequence: 5'- CTG TAG GCA CCA CGG AGT CAG ATG TGT AGG AGG TCC TCG TCA  
 CTG TCA TCA TGG AAG GAC ACC AGC TTG GCA GGG GTT GTT GGC TTG CGC  
 TGT CCG Ggg act cga cgt atc -3'

TGF $\beta$ IIIR (98-mer)

Protected Probe Size: 86-mer

Sequence: 5'- GCG AAG CGG CCC TTC CCC ACC AGC GTG TCC AGC TCG ATG GGC  
 AGC AGT TCC GTA TTG TGG TTG ATG TTG TTG GCG CAC GTA GAG CTt gca ctc tca  
 ta -3'

c-jun (86-mer)

Protected Probe Size: 75-mer

Sequence: 5'- CAT CTT TGC AGT CAT AGA ACA GTC GGT CAC TTC ACG CGG GGT  
 TAG CCT GGG CTG TGC GCA GAA GTT TCG GGG CCG tgc tgt aat at -3'

TGF $\beta$ IR (75-mer)

Protected Probe Size: 65-mer

Sequence: 5'- TCG CCG CCG CCA CCA ACA CGA TGA GAA GCA GGC AGC GAC GCA  
 AAG CAG CCG ACG CCG CCT CCA Tga gta tta cta -3'

TGF $\beta$ 1 (65-mer)

Protected Probe Size: 56-mer

Sequence: 5'- GCG TAT CAG TGG GGG TCA GCA GCC GGT TAC CAA GGT AAC GCC  
 AGG AAT TGT TGC TAc gcc gac ta -3'

c-fos (56-mer)

Protected Probe Size: 48-mer

Sequence: 5'- AAC ATC ATG GTC GTG GTT TGG GCA AAG CTC GGC GAG GGG TCC  
 AGG GGT ctg agt ca -3'

18S rRNA (48-mer)

Protected Probe Size: 41-mer

Sequence: 5'- CGG GTC GGG AGT GGG TAA TTT GCG CGC CTG CTG CCT TCC TTA  
tgc agc -3'

smad3 (41-mer)

Protected Probe Size: 35-mer

Sequence: 5'- TGA CCG CCT TCT CGC ACC ACT TCT CCT CCT GCC CGc gac aa -3'

annexin I (111-mer)

Protected Probe Size: 98-mer

Sequence: 5'- GCC TTG CAA TAG GAA GAA AAC AAC GGC TAA GAG ATG TTC TCC  
TCG GAA TCT TAC AGA GCA GTT GGG ATG TTT AGT TTC CTC CAC ACA GAG CCA  
CCA GGc ggc gcg tcg cag -3'

cdk2 (98-mer)

Protected Probe Size: 86-mer

Sequence: 5'- GGC CCA GGA TCA GGT CAG ACC ACA GGT GAA GAG GGC TTT GGG  
AAG GAC ATC AGA GTC GAA GGT GGG GCA CTG GTT TAG TCA CAT CCg atg cac  
gct at -3'

cyclin E (86-mer)

Protected Probe Size: 75-mer

Sequence: 5'- GCT GTG GCT CTG CAT CCC ATG CTT GCT CAC GAC CAC TCG CCG  
TAC CCT ATC AAC AGC AAC CCT GCG ACA CCC AGC etc: ata tct ag -3'

p21<sup>cip1</sup>/WAF1 (75-mer)

Protected Probe Size: 65-mer

Sequence: 5'- CAC AAA TAA TAA TTA AGA CAC ACT GAA TGA AGG CTA AGG CAG  
AAG ATG GGG AAG AGG CCT CCT GAt atg tct act -3'

18S rRNA (65-mer)

Protected Probe Size: 56-mer

Sequence: 5'- CGG GTC GGG AGT GGG TAA TTT GCG CGC CTG CTG CCT TCC TTG  
GAT GTG GTA GCC GTg gag tca ta -3'

bax (56-mer)

Protected Probe Size: 47-mer

Sequence: 5'- CGG AGG AAG TCC AGT GTC CAG CCC ATG ATG GTT CTG ATC AGC  
TCG GGt gag cgc ac-3'

bad (47-mer)

Protected Probe Size: 41-mer

Sequence: 5'- GAA CAT ACT CTG GGC TGC TGG TCT CCA CCG CTT CCT CCC GCa  
gat ag -3'

p27Kip1 (41-mer)

Protected Probe Size: 35-mer

Sequence: 5'-C TGC AGG CGG AAG GCT TGG GGT GCT CGG TTT GTC Tat tac t -3'

p53 (86-mer)

Protected Probe Size: 75-mer

Sequence: 5'- CAT ACG GTA CCA CCA CGC TGT GCC GAA AAG TCT GCC TGT CGT  
CCA GAT ACT CAG CAT ACG GAT TTC CTT CCA CCC ttc ggc tgc ac -3'

bcl-2 (75-mer)

Protected Probe Size: 65-mer

Sequence: 5'- GAT CCA GGT GTG CAG ATG CCG GTT CAG GTA CTC AGT CAT CCA  
CAG AGC GAT GTT GTC CAC CAG GGa ctg tcg aga -3'

The NPA probes were 5'-end radiolabeled using [ $\gamma$ - $^{32}\text{P}$ ] ATP (6,000 Ci/mmol, 150 mCi/ml) and T4 Polynucleotide Kinase (Gibco BRL Life Technologies, Gaithersburg, MD,

USA), followed by repurification using a MicroSpin G-25 sephadex column (Pharmacia Biotech, Piscataway, NJ, USA). Equal amounts of radiolabeled probes were pooled, based on counts per minute (cpm) as determined by scintillation counting, except for the 18S rRNA probe which was pre-diluted with 250-fold excess cold 18S rRNA oligonucleotide in order to lower its specific activity due to the abundance of the endogenous 18S rRNA. Pooled probes were combined with 50 µg of total RNA per sample such that  $1 \times 10^6$  cpm of each probe were present (except for the 18S rRNA probe). The NPA oligodeoxynucleotide probe pool-total RNA mixtures were ethanol precipitated, resuspended in 10 µl of 3:1 Hybridization Buffer: Hybridization Dilution Buffer, and hybridized for 16 h at 37°C. Non-hybridized probes and sample RNA were digested by adding 200 µl of a nuclease digestion mixture and incubating the samples for 30 min at 37°C, followed by stopping the reaction with 40 µl of Inactivation Buffer. The nuclease digestion mixture was prepared by diluting the Nuclease Mix 1:200 with Nuclease Digestion Buffer, both supplied by the Multi-NPA kit, and was supplemented with an additional 6.5 µl of S1 Nuclease (Gibco BRL Life Technologies). NPA pilot control studies were conducted in order to empirically determine the optimal amount of supplemental S1 nuclease by testing each individual probe for complete digestion of non-protected probe, including digestion of the non-hybridized additional random sequence attached to the 3' end of protected probes, without significant degradation of the protected probe. After the nuclease digestion step, samples were ethanol precipitated, resuspended in 10 µl of Gel Loading Buffer, and resolved on an 8 M urea polyacrylamide gel. The polyacrylamide gels were scanned using a PhosphorImager (Molecular Dynamics, Sunnyvale, CA, USA), and protected probe bands quantified using ImageQuant software (Molecular Dynamics) to determine gene expression. Relative expression of each gene was calculated by first normalizing the target gene's expression to the 18S rRNA level, and next by averaging the target gene's expression between all the samples within one treatment group. The normalized and averaged expression of each gene in

each CON-treated timecourse group was defined as 100% expression and used to determine relative differential expression of the target gene in the matched POH-treated group along with a calculation to determine the standard deviation. Statistical significance was determined by analysis of variance (ANOVA).

### **Confocal Microscopy**

Digital image acquisition employed use of a laser-scanning confocal microscope, consisting of a Bio-Rad MRC-1000 laser scan head (Bio-Rad Life Science Research, Hercules, CA, USA) mounted transversely to an inverted Nikon Diaphot 200 microscope (Melville, NY, USA). The laser was a 15 mW krypton/argon mixed gas air-cooled laser, which emitted three strong lines in exact co-alignment at 488 nm (blue), 568 nm (yellow), and 647 nm (red). The three lines were selected using the excitation color wheel containing the 522DF32 (green), 605DF32 (red), and 680DF32 (far red) filter blocks. Using a triple dichroic filter set, it was possible to perform simultaneous triple labeling using the three laser lines, at which time the laser light appears almost white in color. The transmitted green, red, and far red emitted light signals were directed to the respective photomultiplier tubes (PMT). For samples stained with a red emitting fluorochrome such as lissamine rhodamine (LSRC) and/or a far red emitting fluorochrome such as Cy5, there was a fixed short-pass filter which split the red light from far red light such that red light was transmitted into PMT1, but far red light was transmitted into PMT3. Shorter wavelengths, such as fluorescein (FITC), were detected in PMT2. Power output of the laser at the source was adjusted with the motorized neutral density filter wheel driven by the computer software. The software which controlled the microscope and its settings was the BioRad MRC-1024 Laser Sharp (version 2.1T) program, which provided true 24-bit imaging with simultaneous display of green, red and blue (generated by the far red emitted light and psuedocolored) signal channels, and control over fluorescence bleed through by digital

mixing. Digital images were stored as uncompressed TIF files and exported into Photoshop 4.0 software (Adobe Systems, San Jose, CA, USA) for image processing and hard copy presentation. Confocal microscopy was carried out at the Keck Neural Imaging Laboratory in the Center for Neuroscience (University of Wisconsin-Madison Medical School).

### **Fluorescence IHC**

The IHC procedures used to both localize and determine qualitative protein gene expression profiles were based on a standardized protocol which varied depending on the required antibodies for the particular experiment, unless otherwise noted. The fluorescence IHC experiments were visualized using confocal microscopy. Applying the standardized protocol, tissue sections were pretreated with 1 mg/ml trypsin (Trypsin Tablets, Sigma Chemical Co., St. Louis, MO, USA) for 5 min at room temperature and then washed three times in PBS. The tissue sections were blocked with 5% donkey serum (Jackson ImmunoResearch Laboratories, West Grove, PA, USA), prepared in 1% bovine serum albumin (BSA, IgG and protease free; Jackson ImmunoResearch Laboratories) /PBS, for 1 h at 37°C in a humidified chamber; afterwards, the excess serum was blotted off the tissue sections. Dependent on the double or triple labeling experiment, appropriate species-specific polyclonal 1° antibodies were combined and diluted as necessary in 1% BSA/PBS, and incubated with the tissue sections overnight at 4° C in a humidified chamber; afterwards, the slides were washed three times in PBS. Negative controls for each IHC staining experiment were included by not applying the 1° antibody mixture and instead allowing the blocking solution to continue to incubate with the sections overnight at 4° C in a humidified chamber. The 1° antibodies were detected using a mixture of fluorochrome-conjugated 2° antibodies (all available from Jackson ImmunoResearch Laboratories). The mixture of 2° antibodies, diluted as necessary in 1% BSA/PBS, was incubated with the tissue sections for 1 h at 37°C in a humidified chamber; afterwards, the



slides were washed three times in PBS. The choice of each specific 2° antibody present in the mixture depended on the species-specific Ig class of each 1° antibody employed, i.e. whether the 1° antibodies were raised in goat, rabbit, or chicken. The fluorochromes conjugated to the 2° antibodies were chosen so that the fluorescence of each label could be distinguished in separate color channels while acquiring digital images by confocal microscopy. Also, all the 2° antibodies were raised in donkey, because 2° antibodies of differing species-specific Ig class would oligomerize. Following the incubation of 2° antibodies and tissue sections, the slides were mounted with ProLong Antifade medium (Molecular Probes, Eugene, OR, USA) and coverslipped.

The triple-labeling IHC experiment staining for LAP-TGFβ1, TGFβ1, and the M6P/IGF2R, employed the following 1° polyclonal antibodies: goat anti-LAP-TGFβ1 IgG antibody (R&D Systems, Minneapolis, MN, USA) diluted to 20 µg/ml, chicken anti-TGFβ1 IgY antibody (R&D Systems) diluted to 20 µg/ml, and rabbit anti-M6P/IGF2R IgG antibody (Matt Ellis, manuscript in preparation) diluted 1:800. The following 2° antibodies were used to label the 1° antibodies: FITC-conjugated donkey anti-goat IgG antibody diluted 1:200 resulting in detection of LAP-TGFβ1 in the green channel, LSRC-conjugated donkey anti-chicken IgY antibody diluted 1:200 resulting in detection of TGFβ1 in the red channel, and Cy5-conjugated donkey anti-rabbit IgG antibody diluted 1:100 resulting in detection of M6P/IGF2R in the blue channel. It should be noted that since LAP-TGFβ1 can be converted to TGFβ1 in the active form by proteolysis, the trypsin pretreatment step was omitted.

The double-labeling IHC experiment staining for TGFβIR and TGFβ1 employed the following 1° polyclonal antibodies: rabbit anti-TGFβIR (V-22) IgG antibody (Santa Cruz Biotechnology, Santa Cruz, CA, USA) diluted to 2 µg/ml, and chicken anti-TGFβ1 IgY antibody diluted to 20 µg/ml. The following 2° antibodies were used to label the 1° antibodies: FITC-conjugated donkey anti-rabbit IgG antibody diluted 1:200 resulting in detection of

TGF $\beta$ IR in the green channel, and LSRC-conjugated donkey anti-chicken IgY antibody diluted 1:200 resulting in detection of TGF $\beta$ 1 in the red channel.

The double-labeling IHC experiment staining for TGF $\beta$ IR and TGF $\beta$ 1, employed the following 1° polyclonal antibodies: rabbit anti-TGF $\beta$ IR (L-21) IgG antibody (Santa Cruz Biotechnology, Santa Cruz, CA, USA) diluted to 2  $\mu$ g/ml, and chicken anti-TGF $\beta$ 1 IgY antibody diluted to 20  $\mu$ g/ml. The following 2° antibodies were used to label the 1° antibodies: FITC-conjugated donkey anti-rabbit IgG antibody diluted 1:200 resulting in detection of TGF $\beta$ IR in the green channel, and LSRC-conjugated donkey anti-chicken IgY antibody diluted 1:200 resulting in detection of TGF $\beta$ 1 in the red channel.

The triple-labeling IHC experiment staining for TUNEL nuclei, TGF $\beta$ 1, and Smad2/Smad3 was modified from the standard IHC protocol by initially staining tissue sections for TUNEL or apoptotic nuclei, as described below. After TUNEL staining, the following 1° polyclonal antibodies were employed: goat anti-TGF $\beta$ 1 IgG antibody (Santa Cruz) diluted to 20  $\mu$ g/ml, and rabbit anti-Smad2/Smad3 (E-20) IgG antibody (cross reacts with both Smad2 and Smad3; Santa Cruz Biotechnologies). The following 2° antibodies were used to label the 1° antibodies: LSRC-conjugated donkey anti-goat IgG antibody diluted 1:200 resulting in detection of TGF $\beta$ 1 in the red channel, and Cy5-conjugated donkey anti-rabbit IgG diluted 1:100 resulting in detection of both Smad2 and Smad3 in the blue channel. The TUNEL stained nuclei were detected in the green channel due to the incorporated FITC-conjugated dUTP into cellular DNA of apoptotic cells.

### **Cellular Proliferation and Apoptosis Staining**

Tissue sections were simultaneously stained for apoptosis, using a TUNEL kit (In Situ Cell Death Detection Kit-Fluorescein; Boehringer Mannheim, Indianapolis, IN, USA), in concert with cellular proliferation, using a kit that immunolocalizes BrdU incorporation into

newly synthesized cellular DNA (BrdU Labeling and Detection Kit I, Boehringer Mannheim). Intestinal tissue was stained as a positive control for both TUNEL and BrdU labeling. Briefly, tissue sections were pretreated with 1mg/ml Trypsin (Trypsin Tablets; Sigma) for 5 min at room temperature, washed three times in PBS, incubated with TUNEL reaction mixture (containing TdT, dNTPs and FITC-conjugated dUTP) for 60 min at 37° C in a humidified chamber, and again washed three times in PBS. As a negative control, tissue sections were TUNEL stained in the absence of TdT. Tissue sections were then blocked with 5% donkey serum in 1% BSA/PBS at 37°C for 1 h in a humidified chamber. Next, the sections were incubated with anti-BrdU working solution at 37°C for 1 h using a humidified chamber, followed by three washes with PBS. The anti-BrdU working solution was composed of a 1° monoclonal mouse anti-BrdU antibody and nucleases which facilitate exposure of the incorporated BrdU to the antibody. Tissue sections were stained in the absence of the 1° monoclonal mouse anti-BrdU antibody as a negative control. The 2° fluorescein-conjugated sheep anti-mouse IgG1 antibody supplied with the cell proliferation kit was substituted with a 2° Cy5-conjugated donkey anti-mouse IgG1 antibody (Jackson ImmunoResearch Labs), in order to differentiate the BrdU labeled nuclei from the TUNEL-stained nuclei. The 2° Cy5-conjugated donkey-anti-mouse IgG1 antibody was diluted 1:100 in 1% BSA/PBS and incubated on the tissue sections at 37°C for 1 h in a humidified chamber. The slides were washed three times with PBS, counterstained with 1 µg/ml propidium iodide (PI; Molecular Probes) for 30 min at room temperature, washed three times in PBS, mounted with ProLong Antifade medium, and coverslipped. TUNEL-stained nuclei and BrdU-labeled-nuclei were visualized and quantitated using confocal microscopy by capturing 6 randomly chosen images per sample at 400X original magnification for subsequent scoring of the appropriately labeled nuclei. TUNEL-stained nuclei were visualized in the green channel due to the FITC-conjugated dUTP. BrdU labeled nuclei were visualized in the blue channel due to the 2° Cy5-conjugated antibody. Total nuclei were

visualized in the red channel due to the PI stain. Labeled nuclei were scored using the UTHSCSA ImageTool version 1.27 program (University of Texas Health Science Center at San Antonio, San Antonio, Texas; available from the Internet by anonymous FTP at [maxrad6.uthsca.edu](http://maxrad6.uthsca.edu)). TUNEL indices were calculated by normalizing the total TUNEL nuclei to the total PI stained nuclei in all 6 images per sample. BrdU labeling indices were calculated by the same method. TUNEL and BrdU labeling indices for individual carcinomas in each treatment group were averaged and standard deviations calculated. Statistical significance was determined by ANOVA.

\*

## RESULTS

### Chronic and Acute POH Treatment Protocols

Rats bearing advanced DMBA-induced mammary carcinomas, defined as being at least 10 mm in diameter, were treated with POH following a chronic or acute protocol.

Rats placed into the chronic treatment protocol were fed 2% POH in their diets, and the rats' carcinomas were tracked by palpation. Carcinomas which shrank to one-half of the tumors' maximum diameter were defined as actively regressing and resected. Over the course of the 10 week chronic treatment protocol, 83% ( $n = 35$ ) of POH-treated advanced mammary carcinomas underwent active tumor regression as compared to 5.6% ( $n = 18$ ) of control (CON)-treated carcinomas (Figure 1). In the chronic POH treatment group, the average time until active carcinoma regression was  $23 \pm 13$  days (mean  $\pm$  standard deviation; Figure 1).

Rats placed into the acute treatment protocol were serially administered 0.1 g/kg POH or vehicle alone (CON-treatment) via gastric intubation every 10 h over a 48 hr time period. Tissues were collected after 1h, 4 h, 12 h, 24 h, and 48 h of acute treatment. Blood, and hence plasma, was also collected at the time of tissue resection. Since metabolism of POH occurs rapidly and hence cannot be detected in plasma (9), circulating levels of the two primary metabolites of POH, perillylic acid (PA) and dihydroperillylic acid (DHPA), were compared between acute- and chronic-treated rats (Figure 2). The total level of POH metabolites in plasma at 12 h ( $714 \pm 102 \mu\text{M}$  [PA] + [DHPA]), 24 h ( $852 \pm 218 \mu\text{M}$  [PA] + [DHPA]), and 48 h ( $734 \pm 222 \mu\text{M}$  [PA] + [DHPA]) of acute POH treatment was not significantly different from the total level of circulating POH metabolites at the time of active carcinoma regression ( $808 \pm 207 \mu\text{M}$  [PA] + [DHPA];  $p = 0.4$  at 12 h,  $p = 0.7$  at 24 h, and  $p = 0.5$  at 48 h of treatment). Therefore,

the acute POH protocol achieves physiologically relevant levels of POH metabolites by 12 h and maintains physiologic concentrations throughout the acute treatment protocol.

### **Gross and Ultrastructural Morphology**

All collected tissues were stained with H&E to examine gross morphologic alterations associated with tumor regression. The control carcinomas were characterized by dense anaplastic epithelium (Figure 3A) typical of DMBA-induced rat mammary carcinomas (30). The regressing carcinomas also displayed some regions of anaplastic epithelium but predominantly exhibited a shrinking epithelial compartment partially replaced with extracellular matrix (ECM) (Figure 3B). The remaining epithelial cells showed marked compaction and initially remodeled into pseudolumen structures reminiscent of normal mammary gland (Figure 3B).

Examination of of chronic POH and CON-treated normal mammary gland (never exposed to DMBA) on therapy for 4 weeks did not indicate any gross morphological changes (data not shown).

The ultrastructural morphology of regression was investigated using electron microscopy (EM). The CON-treated carcinomas exhibited dense cords of anaplastic epithelium. The carcinoma cells were relatively well differentiated as suggested by numerous microvilli (Figure 3C). A large increase in apoptotic cells was found in POH-treated regressing carcinomas compared to the control carcinomas. Cells were determined to be apoptotic using morphologic criteria of chromatin margination, cytoplasmic condensation, presence of lucent vacuoles, loss of microvilli, nuclear compaction and fragmentation, and presence of residual bodies [(31); reviewed in (32)]. Apoptotic cells generally resided at the periphery of epithelial cords (Fig. 3D) and newly formed pseudolumen structures (Fig. 3E), or were sloughed off into the newly formed pseudolumen structures (Fig. 3E and 3F). The regions once occupied by apoptotic cells were partially replaced with ECM (Fig. 3D and 3E).

## RNA Expression Analysis of TGF $\beta$ Signaling Components

RNA expression of many genes involved with TGF $\beta$  signal transduction, specifically, c-jun, c-fos, TGF $\beta$ 1, M6P/IGF2R, TGF $\beta$ IIR, TGF $\beta$ IR, and smad3, were quantified using a multiplexed-nuclease protection assay (NPA) and a panel of antisense oligodeoxynucleotide probes (sequences are given under the Experimental Procedures section).

Briefly, the multiplexed-NPA procedure involved 5'-end radiolabeling of the probes using [ $\gamma$ - $^{32}\text{P}$ ] ATP, followed by pooling and hybridization of the probes to 50  $\mu\text{g}$  of total RNA per sample. Next, the excess unhybridized probe, or non-protected probe, was digested away from the hybridized, or protected, probe using a mixture of single-strand specific nucleases comprised of S1 nuclease, Rnase A and Rnase T1. Each probe was designed with additional random, non-complementary bases at the 3'-end, so that the non-complementary sequence would be digested away from the hybridized, complementary, portion of each probe, resulting in an increase in electrophoretic mobility of protected probe over non-protected probe. The NPA probes were resolved on a 12 % polyacrylamide/ 8M urea gel and quantitated using phosphor-imaging technology. Expression of each gene was normalized to 18S rRNA expression. Included in every experiment was a control for complete digestion of non-protected probe whereby pooled probe was hybridized to 50  $\mu\text{g}$  of yeast RNA and digested in the absence or presence of the nuclease mix.

Using the panel of probes for TGF $\beta$  related genes, the NPAs revealed that the tested genes were induced and temporally regulated by POH-treatment relative to CON treatment, as plotted in Figure 4. Both c-jun and c-fos were transiently induced 2.0-fold ( $p = 0.0003$ ) and 1.9-fold ( $p = 0.0005$ ), respectively, at 12 h of POH treatment. TGF $\beta$ 1 RNA expression was first significantly induced at 24 h of POH treatment (1.8-fold,  $p = 0.004$ ), and was further potentiated at 48 h of POH treatment (3.3-fold,  $p = 0.0002$ ) and during active carcinoma

regression (3.3-fold,  $p = 0.0001$ ). The M6P/IGF2R RNA expression was first induced to a statistically significant level by 48 h of POH treatment (2.2-fold,  $p = 0.0003$ ) and was maintained during active regression (2.3-fold,  $p = 0.0001$ ). The RNA expression of both TGF $\beta$ IIIR and TGF $\beta$ IR followed a pattern similar to the M6P/IGF2R. TGF $\beta$ IIIR and TGF $\beta$ IR were induced at 48 h of POH treatment [3.2-fold ( $p = 0.0001$ ) and 2.4-fold ( $p = 0.00008$ ), respectively] and maintained the induction during active carcinoma regression [3.2-fold ( $p = 0.0004$ ) and 2.5-fold ( $p = 0.001$ ), respectively]. Smad3 was induced only during active carcinoma regression (3.5-fold,  $p = 0.0007$ ).

Figure 5 shows the expression profile of the TGF $\beta$  related gene panel during active regression of chronically treated mammary carcinomas as determined by the NPA. Carcinomas treated chronically with POH, but which did not regress, were included in the analysis. These POH-treated non-responsive carcinomas showed no significant differences in expression of the TGF $\beta$  related genes compared to CON-treated carcinomas.

NPAs of chronic POH and CON-treated normal mammary gland (never exposed to DMBA) on therapy for 4 weeks showed no induction in RNA expression of the tested TGF $\beta$ -related genes (data not shown).

Thus, the above data indicated that POH treatment initiated a series of RNA upregulation events involved in TGF $\beta$  signaling, only in those carcinomas which responded to therapy, and specifically in carcinoma tissue over normal tissue. The series of RNA events was characterized by a relatively early transient induction of both c-jun and c-fos, followed by the continuous inductions of TGF $\beta$ 1, next the three receptors M6P/IGF2R, TGF $\beta$ IIIR and TGF $\beta$ IR, and lastly smad3.



### ***In situ* Protein Expression Analysis of TGF $\beta$ Signaling Components**

The protein expression profiles of many of the genes involved in TGF $\beta$  signaling were characterized *in situ* using fluorescence-IHC in concert with confocal microscopy. The investigated signaling components included LAP-TGF $\beta$ 1, activated TGF $\beta$ 1, M6P/IGF2R, TGF $\beta$ IIIR, TGF $\beta$ IR, and Smad2/Smad3 (the anti-Smad antibody cross-reacted with Smad2 and Smad3). Expression of the TGF $\beta$  signaling components was compared between chronic POH-treated regressing carcinomas and chronic CON-treated carcinomas. Staining for TGF $\beta$ 1 was included in all the multiple-labeling IHC experiments as a common reference to determine cell type expression and colocalization of each of the TGF $\beta$  signaling molecules. Additionally, the fluorescence-IHC data are first presented as grayscale images, which reflect the staining intensity of each protein in its respective color channel, and second presented as a composite color image, which reflects relative localization of each of the tested proteins.

The first set of multi-labeling IHC experiment involved staining tissues for LAP-TGF $\beta$ 1 (green channel), active TGF $\beta$ 1 (red channel), and M6P/IGF2R (blue channel; Figure 6). Expression of each of these components was upregulated in the POH-treated carcinomas relative to CON-treated carcinomas. Expression of these proteins was restricted to the epithelium, as confirmed by positive staining with the mammary epithelial cell differentiation marker, cytokeratin 18 (data not shown). A comparison of Figure 6A through 6D reveals an area of intense LAP-TGF $\beta$ 1 staining (the green area in the composite panel) with a lack of active-TGF $\beta$ 1 and M6P/IGF2R staining, indicating the staining procedure itself did not activate TGF $\beta$ 1, and further supports the notion that the M6P/IGF2R facilitates activation of LAP-TGF $\beta$ 1 to TGF $\beta$ 1 (18). Therefore, other than select regions which have not yet processed LAP-TGF $\beta$ 1, LAP-TGF $\beta$ 1, TGF $\beta$ 1 and M6P/IGF2R expression was induced in POH-treated carcinomas, restricted to the parenchyma, and colocalized.

The second set of IHC studies addressed expression of TGF $\beta$ IIR (green channel) concurrently with TGF $\beta$ 1 (red channel; Figure 7) and expression of TGF $\beta$ IR (green channel) concurrently with TGF $\beta$ 1 (red channel; Figure 8). TGF $\beta$ IIR as well as TGF $\beta$ IR exhibited upregulated expression in POH-treated carcinomas (Figure 7A compared to 7D, and Figure 8A compared to 8D, respectively), which was restricted to the epithelium. Additionally, TGF $\beta$ IIR and TGF $\beta$ IR staining colocalized with TGF $\beta$ 1 staining (Figure 7C and 8C, respectively).

The third set of IHC studies examined expression of Smad2/Smad3 (Figure 10), termed such because the antibody cross-reacted with both Smad2 and Smad3. Pilot staining experiments for Smad2/Smad3 demonstrated some Smad2/Smad3 positive stained cells were present in areas consistent with cells undergoing apoptosis such as on the periphery of shrinking epithelial cords or being sloughed into pseudolumens. Therefore, tissue sections were triple-labeled for TUNEL nuclei (green channel), TGF $\beta$ 1 (red channel), and Smad2/Smad3 (blue channel). Smad2/Smad3 expression was induced and exhibited nuclear localization in POH-treated regressing carcinomas (Figure 10C compared to Figure 10D). Because activation of the TGF $\beta$  signaling pathway results in accumulation of Smad2 and Smad3 in the nucleus (25), Smad2/Smad3 nuclear staining in POH-treated regressing mammary carcinomas indicated the TGF $\beta$  signal transduction pathway was activated. Also, Smad2/Smad3 stained nuclei were primarily localized to regions of the epithelium expressing TGF $\beta$ 1. Notably, a subpopulation of Smad2/Smad3 positive nuclei colocalized with a subpopulation of TUNEL positive nuclei (compare Figures 10A, 10C, and 10D), thus suggesting a potential role of Smad2/Smad3 in apoptosis.

IHC studies of chronic POH and CON-treated normal mammary gland (never exposed to DMBA) on therapy for 4 weeks showed no alterations in the *in situ* protein expression of the tested TGF $\beta$ -related genes (data not shown).

## RNA Expression Analysis of Cell Cycle and Apoptosis Genes

Two potential downstream cellular effects due to activation of the TGF $\beta$  signal transduction pathway and consistent with carcinoma regression were induction of cytostasis and apoptosis. Therefore, RNA expression of many genes involved with regulation of the cell cycle and apoptosis, specifically, p21<sup>cip1</sup>/WAF1, p27<sup>Kip1</sup>, cyclin E, cyclin dependent kinase 2 (cdk2), annexin I, bad, bax, bcl-2, and p53, were quantified using another multiplexed-NPA and a panel of antisense oligodeoxynucleotide probes (sequences are given under the Experimental Procedures section). Expression of each gene was normalized to 18S rRNA expression.

The NPAs revealed the tested cell cycle- and apoptosis-related genes were differentially regulated by POH-treatment relative to CON treatment, as plotted in Figure 11.

Expression of the cyclin dependent kinase inhibitors (CDKIs) p21<sup>cip1</sup>/WAF1 and p27<sup>Kip1</sup> was induced 1.6-fold ( $p = 0.004$ ) and 1.5-fold ( $p = 0.008$ ), respectively, at 48 h of POH treatment. Expression of p21<sup>cip1</sup>/WAF1 and p27<sup>Kip1</sup> was further increased to 2.0-fold ( $p = 0.0001$ ) and 1.9-fold ( $p = 0.0008$ ), respectively, during active regression of chronic POH-treated carcinomas. In contrast, cyclin E and cdk2 were repressed to 67.5 % ( $p = 0.01$ ) and 68.8 % ( $p = 0.01$ ) of control levels at 48 h of POH treatment. Expression of cyclin E and cdk2 were further repressed to 51.7 % ( $p = 0.001$ ) and 53.1 % ( $p = 0.0009$ ), respectively, during active regression of chronic POH-treated carcinomas. Therefore, factors which inhibit the cell cycle, p21<sup>cip1</sup>/WAF1 and p27<sup>Kip1</sup>, were upregulated, while factors which promote the cell cycle, cyclinE and cdk2, were repressed in POH-treated tissue. Since these factors regulate the G1-S transition of the cell cycle [reviewed in (33)], it was likely that POH-treatment of mammary carcinomas resulted in a block of the cell cycle during G1, and possibly caused the carcinoma cells to enter G0.

RNA expression of annexin I, a marker of apoptosis in the mammary gland (23), was induced 2.6-fold ( $p = 0.0001$ ) at 48 h of POH treatment, and its induction was slightly potentiated to 2.9-fold in actively regressing POH-treated carcinomas over chronic CON-treated carcinomas ( $p = 0.0001$ ). The RNA expression of factors which mechanistically promote apoptosis, bad and bax, followed a similar pattern of regulation as annexin I. Bad and bax were induced 1.6-fold ( $p = 0.001$ ) and 1.6-fold ( $p = 0.008$ ), respectively at 48 h of POH treatment, and further increased their induction during active carcinoma regression to 2.2-fold ( $p = 0.00006$ ) and 2.3-fold ( $p = 0.0001$ ), respectively. The expression of bcl-2, which mechanistically blocks cells from proceeding through apoptosis, was not significantly altered in POH-treated carcinomas relative to CON-treated carcinomas (98.2 %,  $p = 0.7$ ; data not shown). Additionally, p53 expression was not significantly different in POH-treated versus CON-treated carcinomas (109.6 %,  $p = 0.5$ ; data not shown).

Figure 12 shows the expression profile of the cell cycle- and apoptosis-related genes during active regression of chronically treated mammary carcinomas as determined by the NPA.. Carcinomas treated chronically with POH, but which did not regress, were included in the analysis. These POH-treated non-responsive carcinomas showed no significant changes in expression of the cell cycle- and apoptosis-related genes compared to CON-treated carcinomas.

NPA's of chronic POH-treated normal mammary gland (never exposed to DMBA) and chronic CON-treated normal mammary gland on therapy for 4 weeks showed no change in RNA expression of the tested cell cycle- or apoptosis-related genes (data not shown).

Therefore, POH treatment resulted in a series of RNA differential expression events which promote a block in the cell cycle, probably at G1, and promote apoptosis, only in those carcinomas which responded to therapy, and specifically in carcinoma tissue and not normal tissue.

## Quantification of Cytostasis and Apoptosis

Cellular proliferation and apoptosis were simultaneously quantified using a combination of 5-bromo-2'-deoxy-uridine (BrdU) labeling of cells actively synthesizing cellular DNA, and terminal deoxytransferase (TdT)-mediated dUTP-end labeling (TUNEL) of cells exhibiting fragmented cellular DNA, respectively. Stained tissues were visualized using confocal microscopy. BrdU incorporation was detected using a 1° antibody directed against BrdU and a 2° antibody conjugated to Cy5, resulting in visualization of proliferating cells in the blue channel of the confocal microscope. TUNEL stained cells were detected using FITC-conjugated dUTP as the label, resulting in visualization of apoptotic nuclei in the green channel. Tissue sections were also counterstained with propidium iodide (PI), allowing visualization of all nuclei in the red channel. Quantification of BrdU and TUNEL indices involved summation of all respective labeled nuclei normalized to total PI stained nuclei in 6 randomly chosen fields per sample at 600X original magnification (Figure 12).

During the acute treatment protocol, rats were administered BrdU via intraperitoneal injection 1 h prior to tissue resection. During the chronic treatment protocol, rats were administered BrdU via a slow release pellet inserted into the rats' interscapular fat pad 2 days prior to tissue resection. Carcinomas in the chronic treatment groups were BrdU labeled for an extended period of 2 days versus the 1 h BrdU labeling period in the acute treatment groups in an effort to identify the potentially infrequent cycling cells of the POH-treated actively regressing carcinomas. Hence, the 48 h acute CON-treated carcinomas exhibited a much lower BrdU labeling index than the chronic CON-treated carcinomas (compare Figures 12A and 12C to Figures 12D and 12F). Interestingly, there was no significant change in the BrdU labeling indices between the 48 h POH-treated ( $4.1 \pm 1.6$  %) and the 48 h CON-treated carcinomas [ $(2.9 \pm 0.84$  %;  $p = 0.14$ ), (Figure 12C and compare Figures 12A to 12B)]. However, a comparison of the BrdU labeling indices in the chronic-POH treated actively regressing

carcinomas ( $12.9 \pm 1.7$  %) versus chronic CON-treated carcinomas ( $1.4 \pm 0.54$  %) revealed a 9.2-fold reduction [ $p = 5.6 \times 10^{-7}$ ], (Figure 12F and compare Figure 12D to 12E)].

Control carcinomas showed a low, basal level of apoptosis within 48 h or during chronic CON treatment (Figure 12A and 12C), as has been previously reported in DMBA-induced rat mammary carcinomas (34). The TUNEL indices of acute 48 h POH-treated carcinomas ( $2.0 \pm 0.50$  %) showed a 4.3-fold increase relative to 48 h CON-treated carcinomas [ $(0.47 \pm 0.13$  %,  $p = 2.0 \times 10^{-4}$ ), (Figure 12C and compare Figure 12A to 12B)]. The number of TUNEL stained cells further increased 14.1-fold in chronic POH-treated regressing tumors ( $3.9 \pm 1.3$  %) relative to chronic CON-treated carcinomas [ $(0.27 \pm 0.067$  %,  $p = 5.6 \times 10^{-5}$ ), (Figure 12F and compare Figure 12D to 12E)].

Comparison of chronic POH-treated normal mammary gland (never exposed to DMBA) to chronic CON-treated normal mammary gland on therapy for 4 weeks showed no change in the frequency of BrdU or TUNEL stained cells (data not shown).

Taken together, these data indicate POH-treatment induced both cytostasis and apoptosis, where the induction of cytostasis occurred subsequently to the induction of apoptosis. Furthermore, the POH-mediated cytostatic and apoptotic effects were specific for advanced mammary carcinomas compared to normal mammary gland.

## DISCUSSION

We have previously shown TGF $\beta$ , M6P/IGF2R, and TGF $\beta$ IIR were upregulated during regression of monoterpene-treated mammary carcinomas (19,22). Interestingly, in the rat liver tumor model, POH induced expression of the M6P/IGF2R, and the TGF $\beta$  type I, II, and III receptors (35). Here we expanded characterization of the potential role of the TGF $\beta$  signal transduction pathway and its downstream effects in POH-treated rat mammary carcinomas.

TGF $\beta$  related genes were analyzed for differential RNA expression after treatment of mammary carcinomas with POH. The NPAs showed both c-jun and c-fos were transiently induced at 12 h, followed by sustained induction of TGF $\beta$ 1 at 24 h, next by sustained induction of the M6P/IGF2R as well as the TGF $\beta$ IIR and TGF $\beta$ IR at 48 h, and lastly induction of smad3 only during active carcinoma regression.

*In situ* analysis of protein expression, as determined by fluorescence IHC in concert with confocal microscopy, confirmed upregulation and showed colocalization of TGF $\beta$ 1, M6P/IGF2R, TGF $\beta$ IIR, and TGF $\beta$ IR in epithelial cells but not in stromal cells of POH-treated carcinomas. IHC staining for Smad2/Smad3 exhibited upregulation and nuclear localization, indicating active TGF $\beta$  signaling, only during active regression of POH-treated mammary carcinomas. Additionally, a subpopulation of Smad2/Smad3 positive nuclei and apoptotic nuclei colocalized.

Potential downstream effects of TGF $\beta$  signaling, in particular inhibition of cellular proliferation and apoptosis, were characterized. NPAs using a panel of cell cycle related genes showed the cyclin dependent kinase (CDK) inhibitors (CDIs) p21<sup>waf1</sup> and p27<sup>kip1</sup> were both induced; likewise, cyclin E and cdk2 were repressed. NPAs of apoptosis related genes showed

annexin I, a marker of apoptosis in the mammary gland, as well as bax and bad, were upregulated. However, the RNA expression of bcl-2 or p53 was not changed. All tested cell cycle and apoptosis genes exhibited differential expression at 48 h after POH treatment of carcinomas, and the changes in expression were sustained during active regression.

Numerous studies have linked TGF $\beta$  to the regulation of cellular and morphogenic events in mammary derived tissues. For instance, TGF $\beta$  slow-release pellets implanted into the mammary gland reversibly inhibited mammary gland ductal growth due to the elimination of the proliferating stem cell layer (cap cells) and rapid involution of ductal end buds (36,37). Post-lactational mammary gland involution, a large scale tissue remodeling process characterized by readsorption of the bulk of epithelium by apoptosis (31), was associated with increased TGF $\beta$  expression (38,39). Additionally, treatment of mammary cell lines and carcinomas with anti-estrogen therapies (40-44), or other therapeutic agents (45-52) involved induction of apoptosis and association with increased levels of TGF $\beta$ . Furthermore, direct treatment of mammary cells with TGF $\beta$  will induce apoptosis (39,46), and the administration of agents which specifically block TGF $\beta$  signaling, such as antisense T $\beta$ IIIR oligomers, also block the induction of apoptosis in these cells (46). Other studies have shown that TGF $\beta$  regulation of morphogenic events may involve a complex interplay between TGF $\beta$  and the ECM. For example, using mammary cells, TGF $\beta$  has been shown to mediate induction of many ECM components such as fibronectin, collagen, and laminin (53,54). Additionally, the ECM of the mammary gland forms complexes with TGF $\beta$ , which serves as a reservoir to inhibit ductal bud growth since periductal focal loss of TGF $\beta$  immunostaining was observed in all areas of active ductal growth (55).

Observed gross and ultrastructural tissue remodeling events during active regression of POH-treated mammary carcinomas were consistent with known TGF $\beta$ -regulated cellular and morphogenic effects in mammary derived tissues. During active regression of POH-treated mammary carcinomas, the majority of the dense anaplastic epithelial compartment was



eliminated through an apoptotic process, whereby the epithelial cells were deleted from the periphery of epithelial cords so that the remaining epithelial cells could initially form pseudolumen structures, which resemble normal mammary gland architecture (Figure 3). It was previously suggested that apoptosis may be the process by which monoterpenes mediate tumor regression because of the identification of a marker for apoptosis, LC1, in a subtractive display screen (22). Additionally, POH induced apoptosis in a rat liver tumor model (35). Regression of POH-treated mammary carcinomas was also characterized by the partial replacement of the dense anaplastic epithelium with ECM (Fig. 3). The ECM expansion was not likely due to stromal cell growth since the *in vivo* BrdU labeling indicated a block in cellular proliferation (Fig. 12)

Quantification of cell growth and death revealed cellular proliferation was not inhibited but apoptosis was induced 4-fold 48 h after POH treatment, before carcinomas actively regress. However, during active regression of POH-treated mammary carcinomas, cellular proliferation was inhibited 9-fold and the apoptotic index increased 14-fold.

Notably, all of the above described molecular and cellular events were specific to carcinoma tissues and were not found in normal mammary gland treated with POH. Therefore, though the events are correlative, monoterpene therapy may selectively activate the TGF $\beta$  signal transduction pathway in carcinoma cells, leading to cytostasis and apoptosis, and thus account for the monoterpene's high therapeutic index *in vivo*.

## REFERENCES

1. Crowell, P. L., and Gould, M. N. (1994) *Crit Rev Oncog* **5**(1), 1-22
2. Gould, M. N. (1995) *J Cell Biochem Suppl* **22**, 139-44
3. Crowell, P. L., Siar Ayoubi, A., and Burke, Y. D. (1996) *Advances in Experimental Medicine & Biology* **401**, 131-6
4. Crowell, P. L., Kennan, W. S., Haag, J. D., Ahmad, S., Vedejs, E., and Gould, M. N. (1992) *Carcinogenesis* **13**(7), 1261-4
5. Elegbede, J. A., Elson, C. E., Qureshi, A., Tanner, M. A., and Gould, M. N. (1984) *Carcinogenesis* **5**(5), 661-4
6. Elegbede, J. A., Elson, C. E., Tanner, M. A., Qureshi, A., and Gould, M. N. (1986) *J Natl Cancer Inst* **76**(2), 323-5
7. Elson, C. E., Maltzman, T. H., Boston, J. L., Tanner, M. A., and Gould, M. N. (1988) *Carcinogenesis* **9**(2), 331-2
8. Haag, J. D., Lindstrom, M. J., and Gould, M. N. (1992) *Cancer Res* **52**(14), 4021-6
9. Haag, J. D., and Gould, M. N. (1994) *Cancer Chemother Pharmacol* **34**(6), 477-83
10. Maltzman, T. H., Hurt, L. M., Elson, C. E., Tanner, M. A., and Gould, M. N. (1989) *Carcinogenesis* **10**(4), 781-3
11. Vigushin, D. M., Poon, G., Boddy, A., Jarman, M., and Coombes, R. C. (1997) *Proc Annu Meet Am Assoc Cancer Res* **38**, A1490
12. Hohl, R., Ripple, G., Gould, M., Marnocha, R., Arzoomanian, R., Alberti, D., Tutsch, K., Feierabend, C., Simon, K., Morgan, K., Stewart, J., Wahamaki, A., Pomplun,

M., Lewis, K., Wilding, G., and Bailey, H. (1998) *PROC. AMER. ASSOC. CANCER RES.*

**39**

13. Ripple, G., Gould, M., Stewart, J., Tutsch, K., Alberti, D., Feierabend, C., Simon, K., Arzoomanian, R., Pomplun, M., Wilding, G., and Bailey, H. (1997) *Proc Annu Meet Am Assoc Cancer Res* **38**, A1490

14. Crowell, P. L., Chang, R. R., Ren, Z. B., Elson, C. E., and Gould, M. N. (1991) *J Biol Chem* **266**(26), 17679-85

15. Crowell, P. L., Ren, Z., Lin, S., Vedejs, E., and Gould, M. N. (1994) *Biochem Pharmacol* **47**(8), 1405-15

16. Ren, Z., Elson, C. E., and Gould, M. N. (1997) *Biochem Pharmacol* **54**(1), 113-20

17. Ren, Z., and Gould, M. N. (1994) *Cancer Lett* **76**(2-3), 185-90

18. Dennis, P. A., and Rifkin, D. B. (1991) *Proc. Natl. Acad. Sci. USA* **88**(2), 580-4

19. Jirtle, R. L., Haag, J. D., Ariazi, E. A., and Gould, M. N. (1993) *Cancer Res* **53**(17), 3849-52

20. Hankins, G. R., De Souza, A. T., Bentley, R. C., Patel, M. R., Marks, J. R., Iglehart, J. D., and Jirtle, R. L. (1996) *Oncogene* **12**(9), 2003-9

21. De Souza, A. T., Hankins, G. R., Washington, M. K., Orton, T. C., and Jirtle, R. L. (1995) *Nat Genet* **11**(4), 447-9

22. Ariazi, E. A., and Gould, M. N. (1996) *J Biol Chem* **271**(46), 29286-94

23. McKanna, J. A. (1995) *Anatomical Record* **242**(1), 1-10

24. Massague, J., and Weis-Garcia, F. (1996) *Cancer Surv* **27**, 41-64

25. Nakao, A., Imamura, T., Souchelnytskyi, S., Kawabata, M., Ishisaki, A., Oeda, E., Tamaki, K., Hanai, J., Heldin, C. H., Miyazono, K., and ten Dijke, P. (1997) *Embo J* **16**(17), 5353-62

26. Heldin, C. H., Miyazono, K., and ten Dijke, P. (1997) *Nature* **390**(6659), 465-71

27. Hartsough, M. T., and Mulder, K. M. (1997) *Pharmacol Ther* **75**(1), 21-41
28. Atfi, A., Djelloul, S., Chastre, E., Davis, R., and Gespach, C. (1997) *Journal of Biological Chemistry* **272**(3), 1429-32
29. Pertovaara, L., Sistonen, L., Bos, T. J., Vogt, P. K., Keski-Oja, J., and Alitalo, K. (1989) *Mol Cell Biol* **9**(3), 1255-62
30. Russo, J., Saby, J., Isenberg, W. M., and Russo, I. H. (1977) *J. Natl. Cancer Inst.* **59**(2), 435-445
31. Walker, N., I., Bennett, R., E., and Kerr, J. F. R. (1989) *Am. J. Anat.* **185**, 19-32
32. Kerr, J. F. R., and Searle, S. (1980) *Radiation Biology in Cancer Research* , 367-84
33. Ravitz, M. J., and Wenner, C. E. (1997) *Advances in Cancer Research* **71**, 165-207
34. Huovinen, R., Warri, A., and Collan, Y. (1993) *Int J Cancer* **55**(4), 685-91
35. Mills, J. J., Chari, R. S., Boyer, I. J., Gould, M. N., and Jirtle, R. L. (1995) *Cancer Res* **55**(5), 979-83
36. Silberstein, G. B., and Daniel, C. W. (1987) *Science* **237**(4812), 291-3
37. Robinson, S. D., Silberstein, G. B., Roberts, A. B., Flanders, K. C., and Daniel, C. W. (1991) *Development* **113**(3), 867-78
38. Strange, R., Li, F., Saurer, S., Burkhardt, A., and Friis, R. R. (1992) *Development* **115**(1), 49-58
39. Atwood, C. S., Ikeda, M., and Vonderhaar, B. K. (1995) *Biochem Biophys Res Commun* **207**(2), 860-7
40. Kyprianou, N., English, H. F., Davidson, N. E., and Isaacs, J. T. (1991) *Cancer Res* **51**(1), 162-6
41. Warri, A. M., Huovinen, R. L., Laine, A. M., Martikainen, P. M., and Harkonen, P. L. (1993) *J Natl Cancer Inst* **85**(17), 1412-8
42. Perry, R. R., Kang, Y., and Greaves, B. R. (1995) *Br J Cancer* **72**(6), 1441-6

43. Chen, H., Tritton, T. R., Kenny, N., Absher, M., and Chiu, J. F. (1996) *J Cell Biochem* **61**(1), 9-17
44. Benson, J. R., and Baum, M. (1996) *Br J Cancer* **74**(6), 993-4
45. Kakeji, Y., Maehara, Y., Ikebe, M., and Teicher, B. A. (1997) *Int J Radiat Oncol Biol Phys* **37**(5), 1115-23
46. Yu, W., Heim, K., Qian, M., Simmons-Menchaca, M., Sanders, B. G., and Kline, K. (1997) *Nutr Cancer* **27**(3), 267-78
47. Srivastava, P., Russo, J., and Russo, I. H. (1997) *Carcinogenesis* **18**(9), 1799-808
48. Armstrong, D. K., Kaufmann, S. H., Ottaviano, Y. L., Furuya, Y., Buckley, J. A., Isaacs, J. T., and Davidson, N. E. (1994) *Cancer Res* **54**(20), 5280-3
49. DeNardo, S. J., Gumerlock, P. H., Winthrop, M. D., Mack, P. C., Chi, S. G., Lamborn, K. R., Shen, S., Miers, L. A., deVere White, R. W., and DeNardo, G. L. (1995) *Cancer Res* **55**(23 Suppl), 5837s-5841s
50. Furuya, Y., and Shimazaki, J. (1996) *Anticancer Res* **16**(5A), 2613-8
51. Furuya, Y., Ohta, S., and Shimazaki, J. (1996) *Int J Cancer* **68**(1), 143-8
52. Nass, S. J., Li, M., Amundadottir, L. T., Furth, P. A., and Dickson, R. B. (1996) *Biochem Biophys Res Commun* **227**(1), 248-56
53. Stampfer, M. R., Yaswen, P., Alhadeff, M., and Hosoda, J. (1993) *J Cell Physiol* **155**(1), 210-21
54. Ignatz, R. A., and Massague, J. (1986) *J Biol Chem* **261**(9), 4337-45
55. Silberstein, G. B., Flanders, K. C., Roberts, A. B., and Daniel, C. W. (1992) *Developmental Biology* **152**(2), 354-62
56. Altschul, S. F., Gish, W., Miller, W., Myers, E. W., and Lipman, D. J. (1990) *Journal of Molecular Biology* **215**(3), 403-10

**Figure 1. Percentage of Actively Regressing Advanced Mammary Carcinomas.**

Advanced DMBA-induced mammary carcinomas were randomized to a 2% POH (chronic POH treatment) or a pair-fed control diet (chronic CON treatment). Carcinomas were followed by palpation for 10 weeks. Carcinomas that regressed to less than one-half of their maximum diameter were scored as actively regressing and resected.

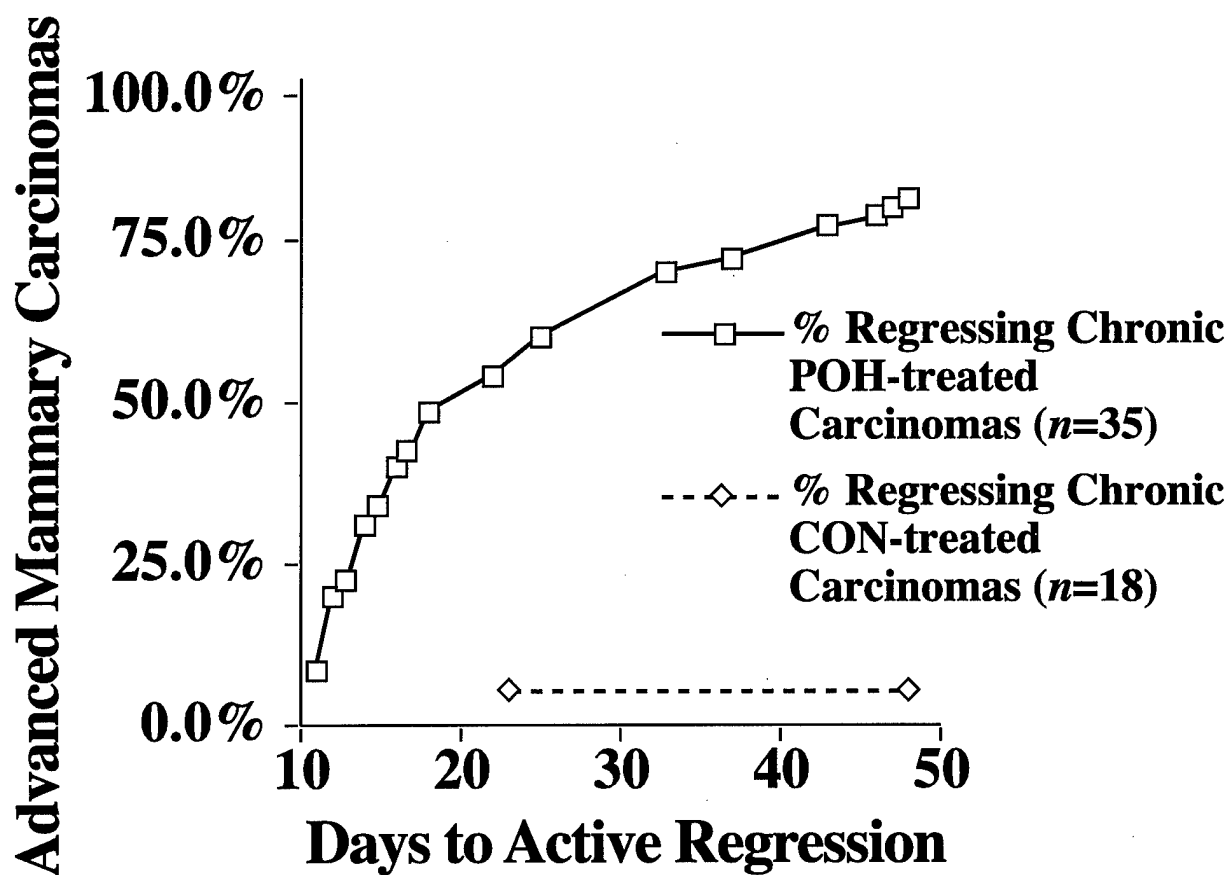
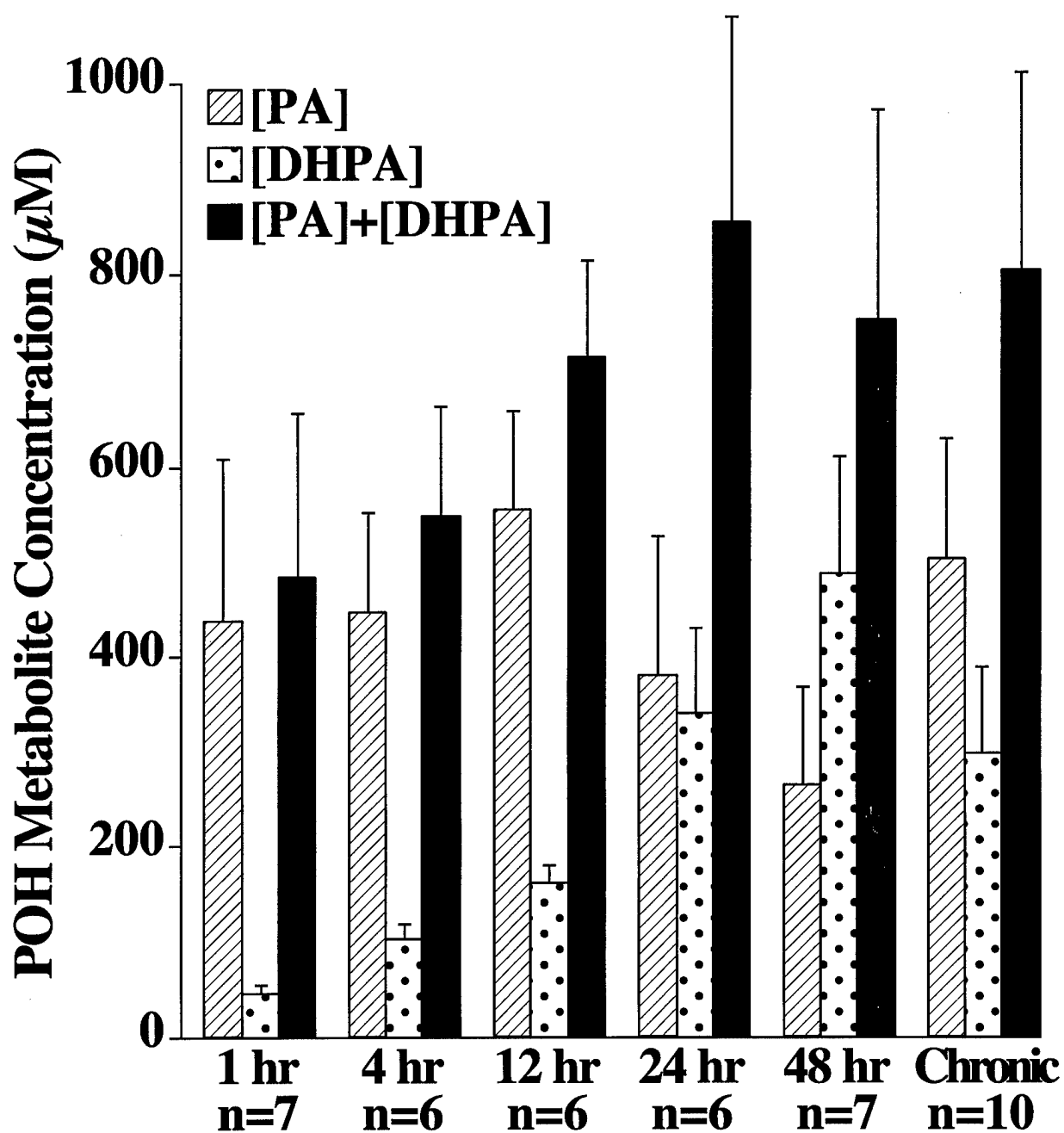


**Figure 2. Analysis of Plasma POH Metabolite Concentrations During the Acute and Chronic Treatment Protocol.**

Blood was collected at the indicated times after initial POH or CON treatment and centrifuged to generate plasma. Plasma was extracted with phosphate buffered t-butylmethylether and analyzed by GC-FID using a Supelco SPB-5 column.





**Plasma Collection Time After Initial Treatment**

**Figure 3. Morphology of Advanced Mammary Carcinoma Regression.**

(A-B) Gross morphology as visualized by H&E staining and light microscopy. (A) Chronic CON-treated mammary carcinoma. (B) Chronic POH-treated actively regressing mammary carcinoma.. (C-F) Ultrastructural morphology visualized by EM. (C) Chronic CON-treated mammary carcinoma. (D-F) Chronic POH-treated actively regressing mammary carcinomas. Arrows indicate apoptotic cells. Scalebars indicate microns.

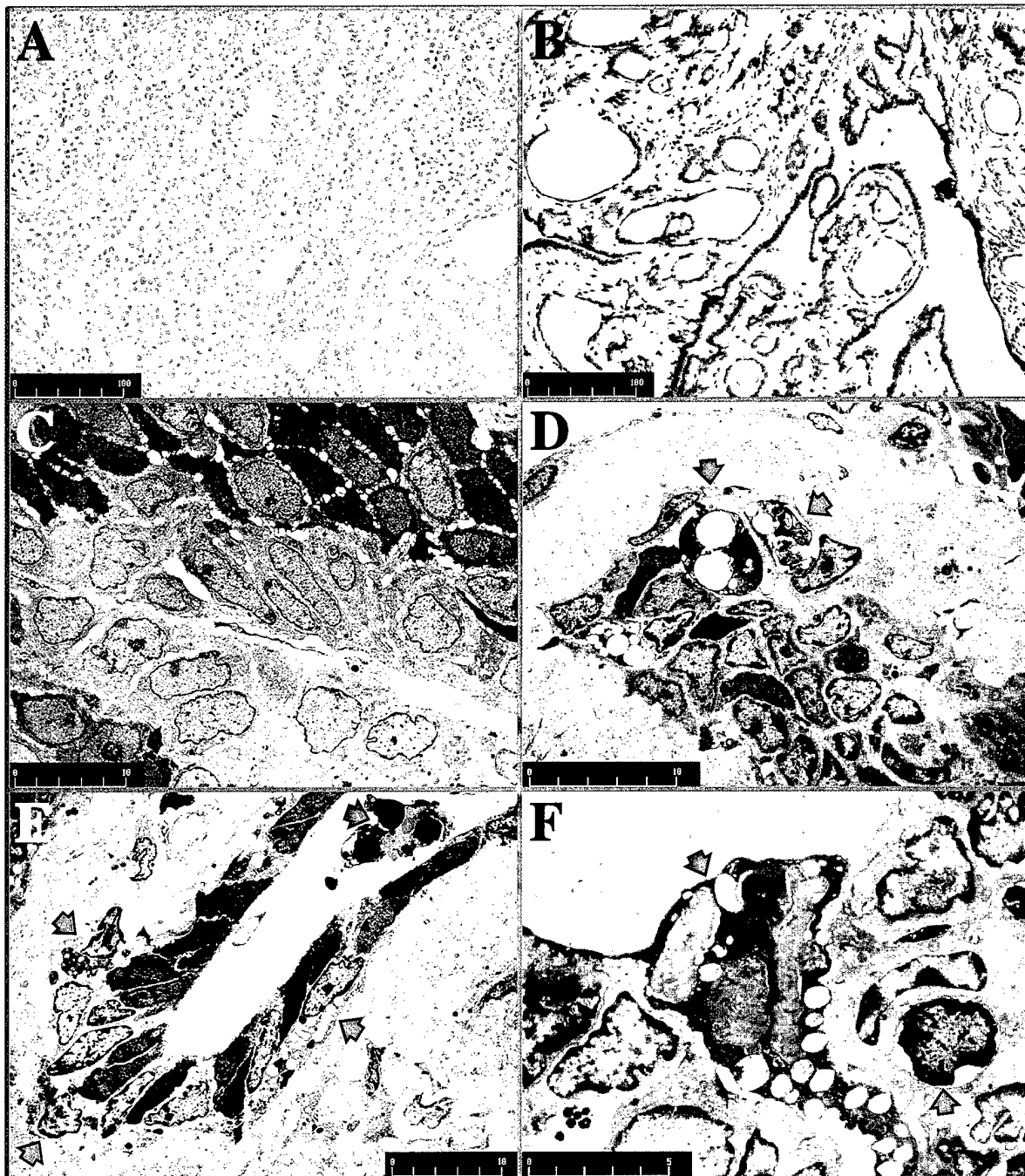


**Figure 4. Induction and Temporal Regulation of TGF $\beta$  Signal Transduction Genes' RNA Expression During the Acute and Chronic POH Treatment Protocols.**

Expression of the genes were quantitated using a multiplexed-NPA and a panel of oligodeoxynucleotide probes.

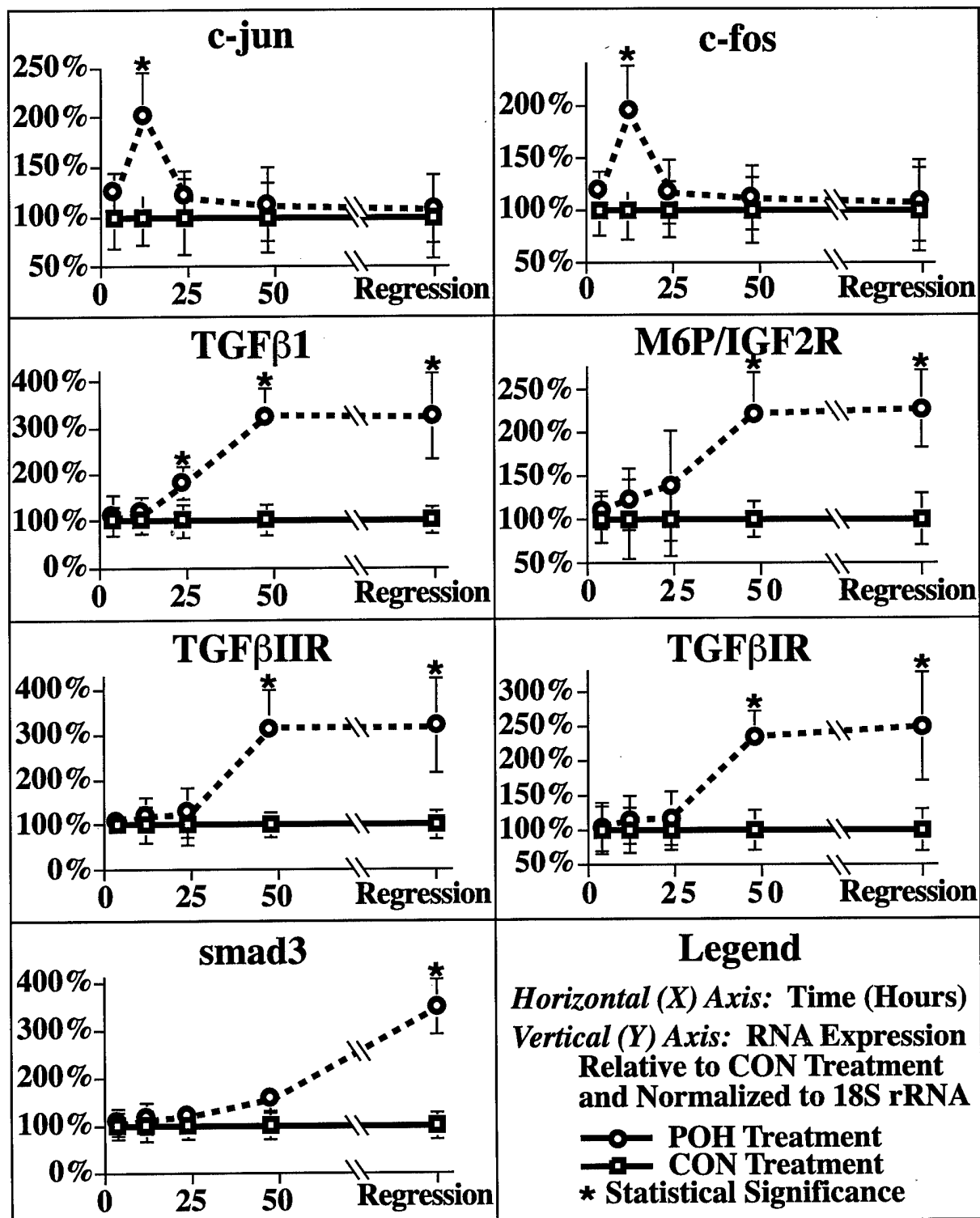


**Figure 5. Nuclease Protection Assay of TGF $\beta$  Signal Transduction Genes in Chronic POH-treated Regressing and Non-Responsive Mammary Carcinomas.**

Oligonucleotide probes were PAGE purified, 5'-end labeled with ( $\gamma$  -  $^{32}\text{P}$ ) ATP, hybridized to 50  $\mu\text{g}$  total RNA, digested with single-strand specific nucleases, and electrophoresed through a 12 % polyacrylamide/ 8 M urea gel. The gel was scanned using phosphor-imaging technology.

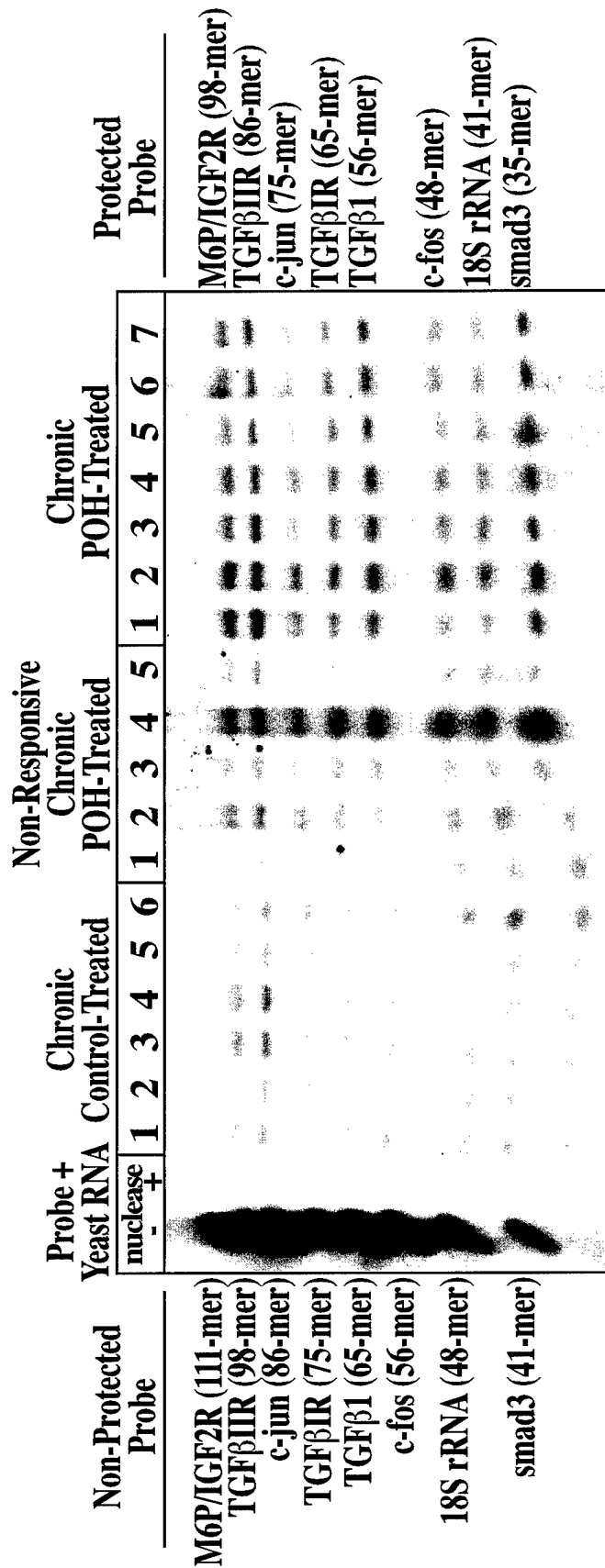


**Figure 6. LAP-TGF $\beta$ 1, TGF $\beta$ 1, and M6P/IGF2R IHC of Chronic POH-treated Mammary Carcinomas.**

Tissues visualized by confocal microscopy. LAP-TGF $\beta$ 1 staining (green channel) involved a 1° goat anti-LAP-TGF $\beta$ 1 antibody and a FITC-2° donkey anti-goat IgG antibody. Active TGF $\beta$ 1 staining (red channel) involved a 1° chicken anti-TGF $\beta$ 1 antibody and a LSRC-2° donkey anti-chicken IgY antibody. M6P/IGF2R staining (blue) involved a 1° rabbit anti-M6P/IGF2R antibody and a Cy5-2° donkey anti-goat IgG antibody. Scalebars indicate microns.



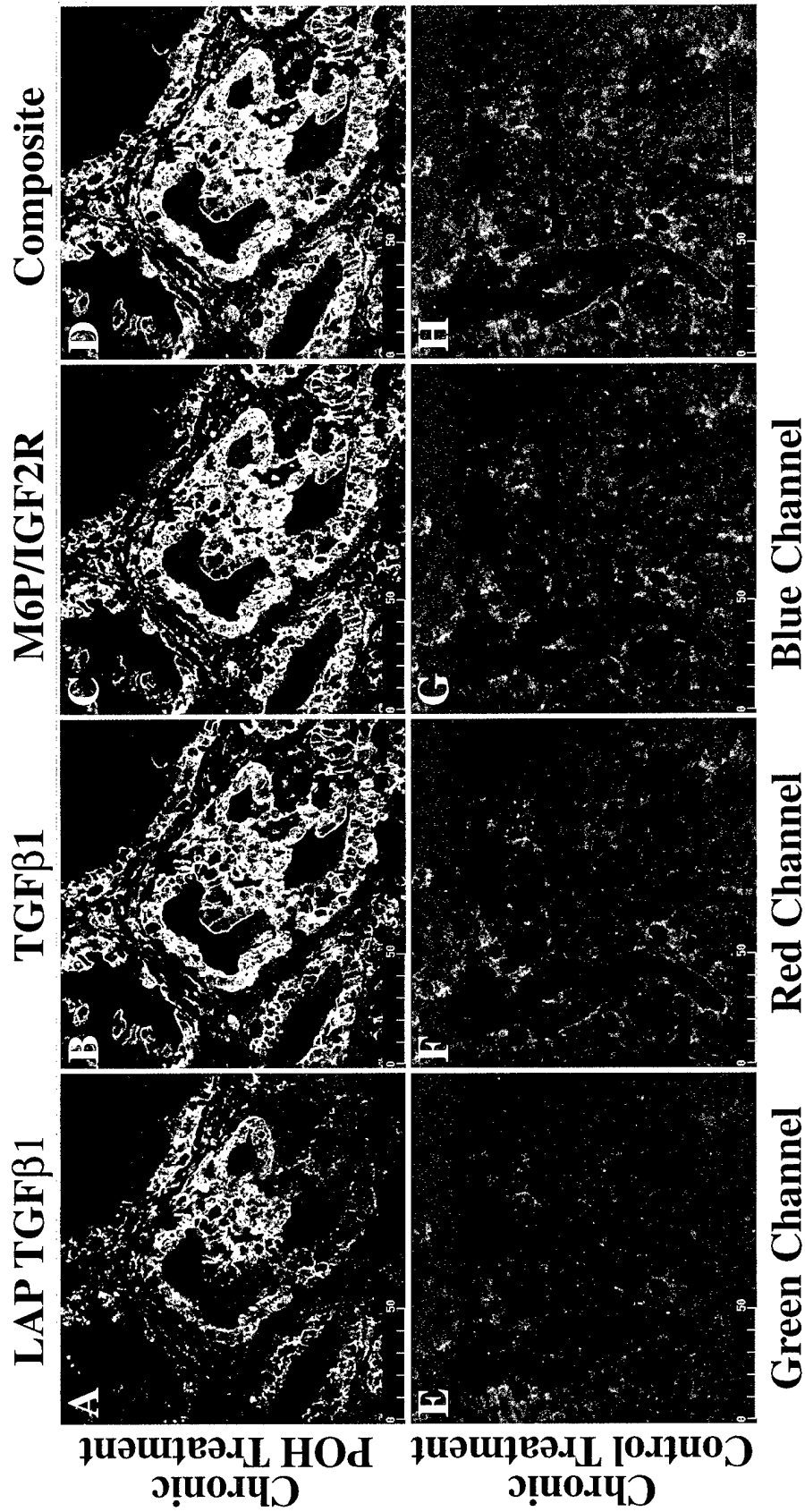


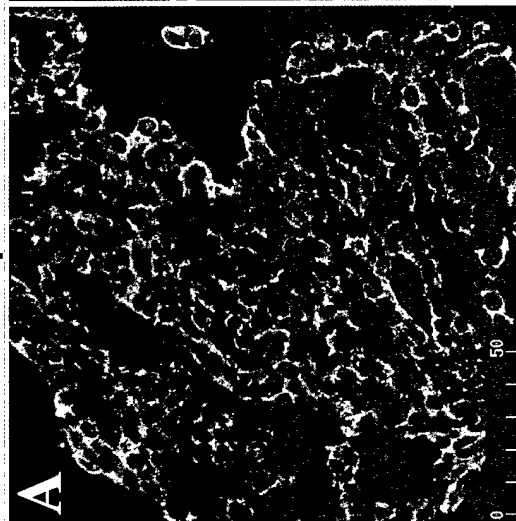
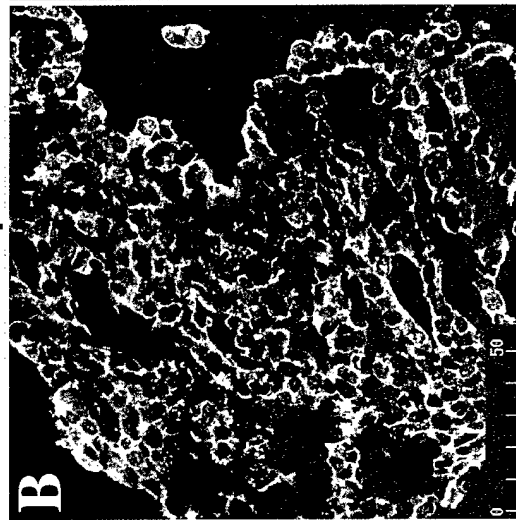
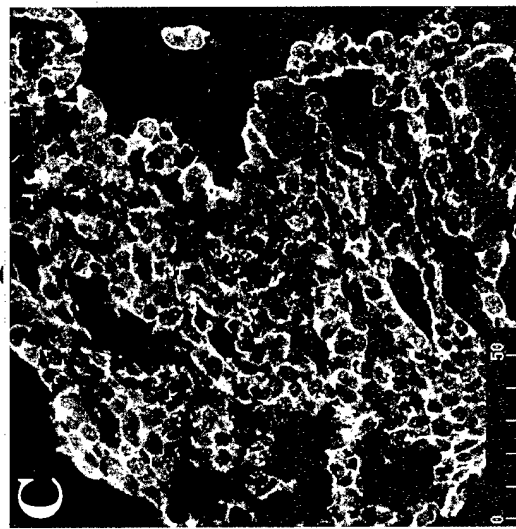
**Figure 7. TGF $\beta$ IIIR and TGF $\beta$ 1 IHC of Chronic POH-treated Mammary Carcinomas.**

Tissues visualized by confocal microscopy. TGF $\beta$ IIIR staining (green channel) involved a 1° rabbit anti-T $\beta$ IIIR antibody and a FITC-2° donkey anti-rabbit IgG antibody. TGF $\beta$ 1 staining (red channel) involved a 1° chicken anti-TGF $\beta$ 1 antibody and a LSRC-2° donkey anti-chicken IgY antibody. Scalebars indicate microns.

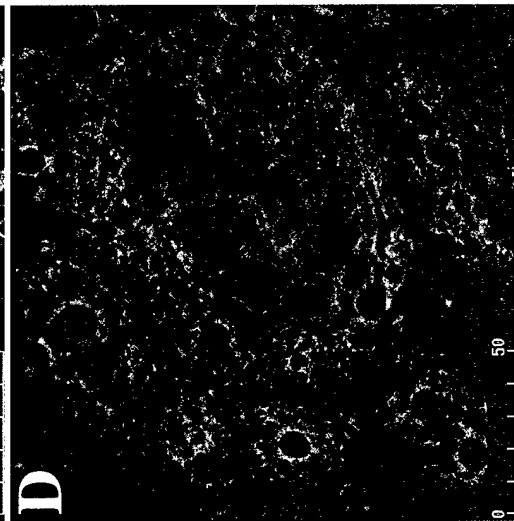
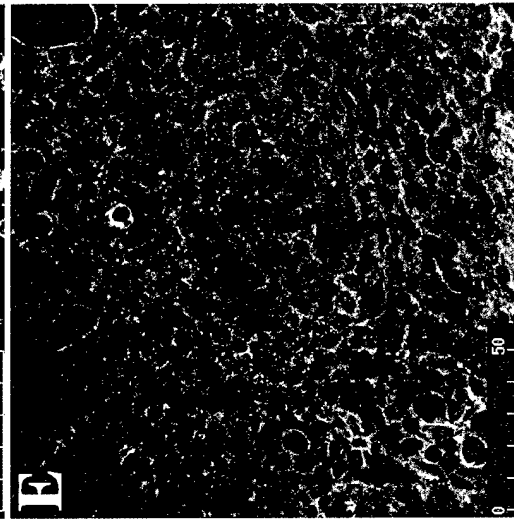
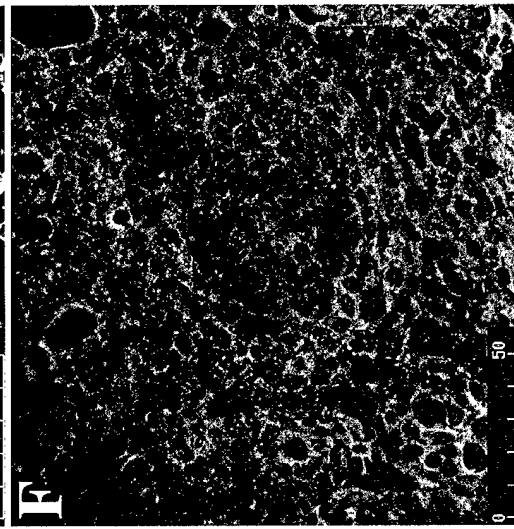
**Composite**

**TGFβ1**

**TGFβ1R**



**Chronic  
POH Treatment**



**Chronic  
Control Treatment**

**Red Channel**

**Green Channel**

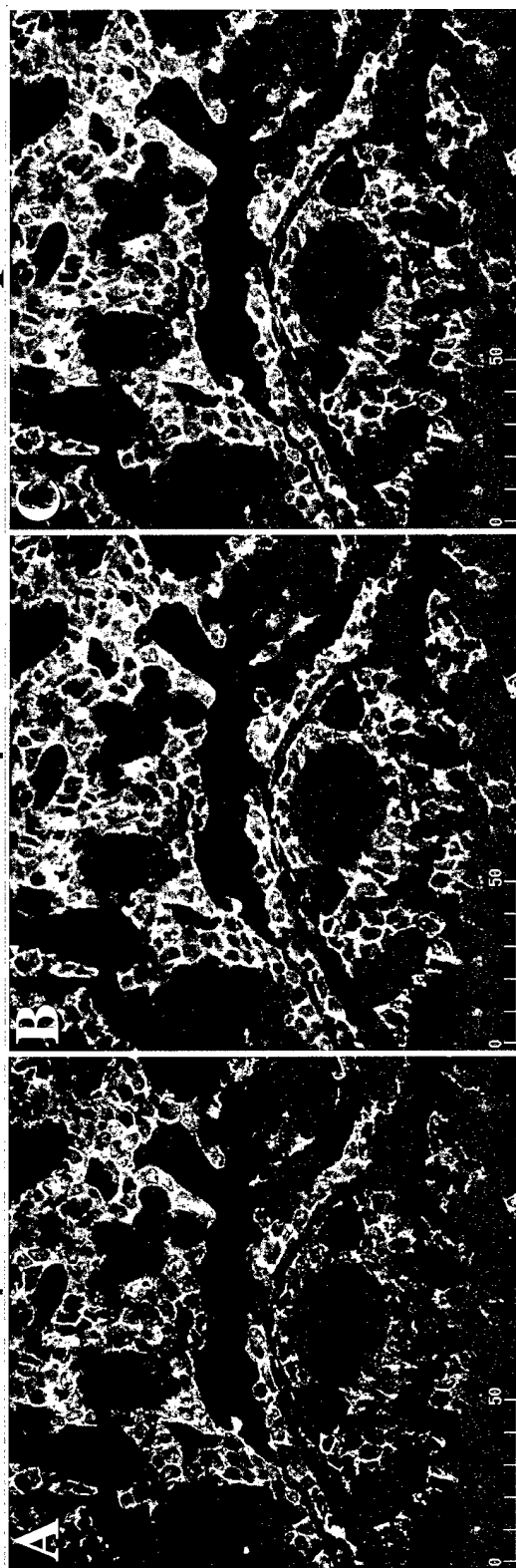
**Figure 8. TGF $\beta$ IR and TGF $\beta$ 1 IHC of Chronic POH-treated Mammary Carcinomas.**

Tissues visualized by confocal microscopy. TGF $\beta$ IR staining (green channel) involved a 1° rabbit anti-T $\beta$ IR antibody and a FITC-2° donkey anti-rabbit IgG antibody. TGF $\beta$ 1 staining (red channel) involved a 1° chicken anti-TGF $\beta$ 1 antibody and a LSRC-2° donkey anti-chicken IgY antibody. Scalebars indicate microns.

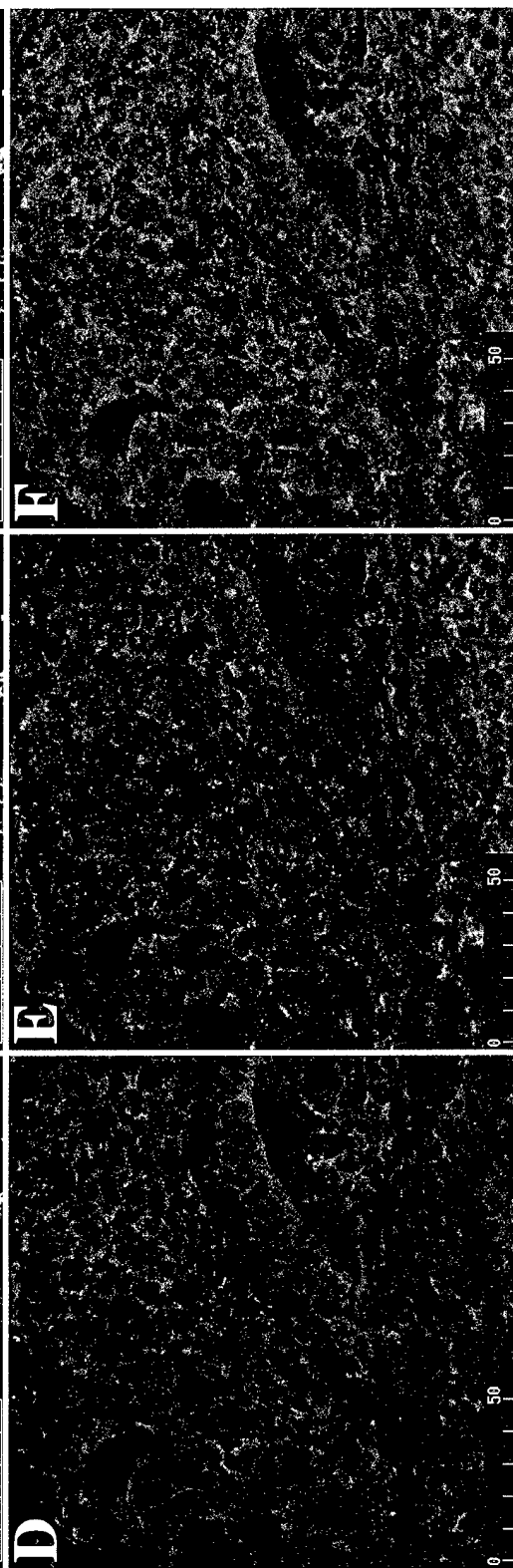
**TGFβ1R**

**TGFβ1**

**Composite**



**Chronic  
POH Treatment**



**Chronic  
Control Treatment**

**Green Channel      Red Channel**

**Figure 9. TUNEL, TGF $\beta$ 1, and Smad2/Smad3 IHC of Chronic POH-treated Mammary Carcinomas.**

Tissues visualized by confocal microscopy. TUNEL staining (green channel) involved FITC-dUTP. TGF $\beta$ 1 staining (red channel) involved a 1 $^{\circ}$  goat anti-TGF $\beta$ 1 antibody and a LSRC-2 $^{\circ}$  donkey anti-goat IgG antibody. Scalebars indicate microns. Scalebars indicate microns.

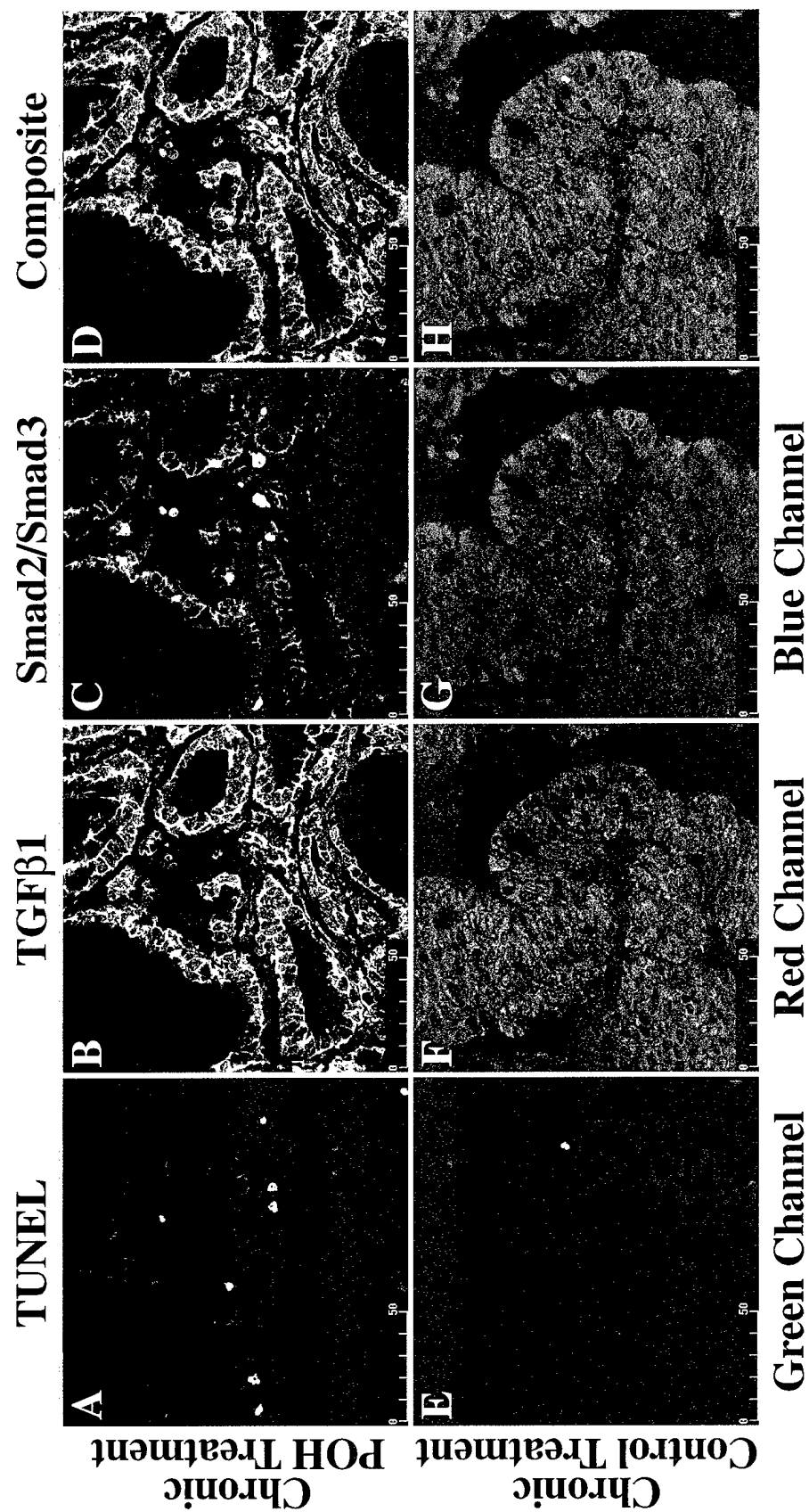


**Figure 10. Differential RNA Expression of Cell Cycle and Apoptosis Genes  
During the Acute and Chronic POH Treatment Protocols.**

Expression of the genes was quantitated using a multiplexed-NPA and a panel of oligodeoxynucleotide probes.



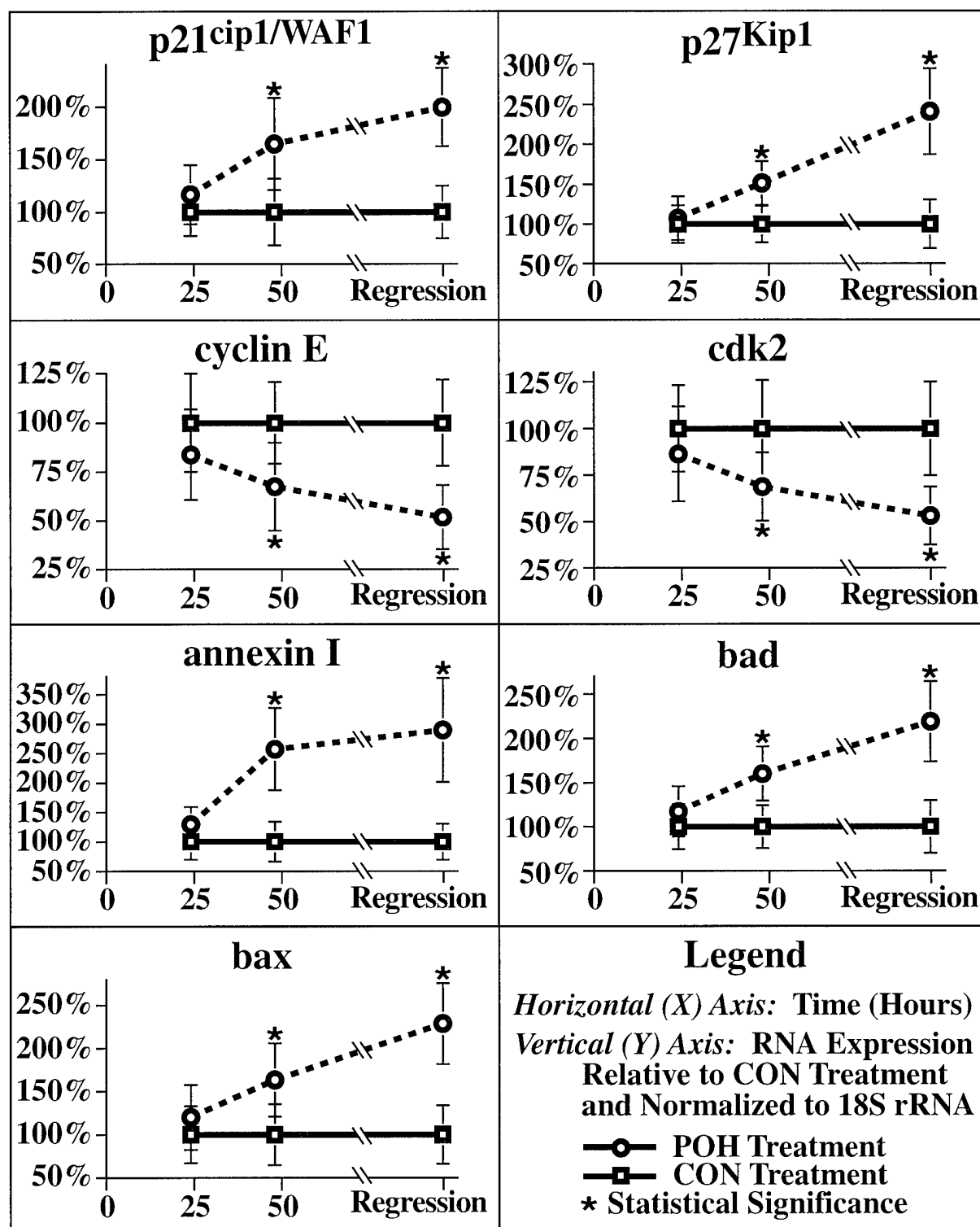


**Figure 11. Nuclease Protection Assay of Cell Cycle and Apoptosis-Related Genes in Chronic POH-treated Regressing and Non-Responsive Mammary Carcinomas.**

Oligonucleotide probes were PAGE purified, 5'-end labeled with ( $\gamma$ - $^{32}\text{P}$ ) ATP, hybridized to 50  $\mu\text{g}$  total RNA, digested with single-strand specific nucleases, and electrophoresed through a 12 % polyacrylamide/ 8 M urea gel. The gel was scanned using phosphor-imaging technology.

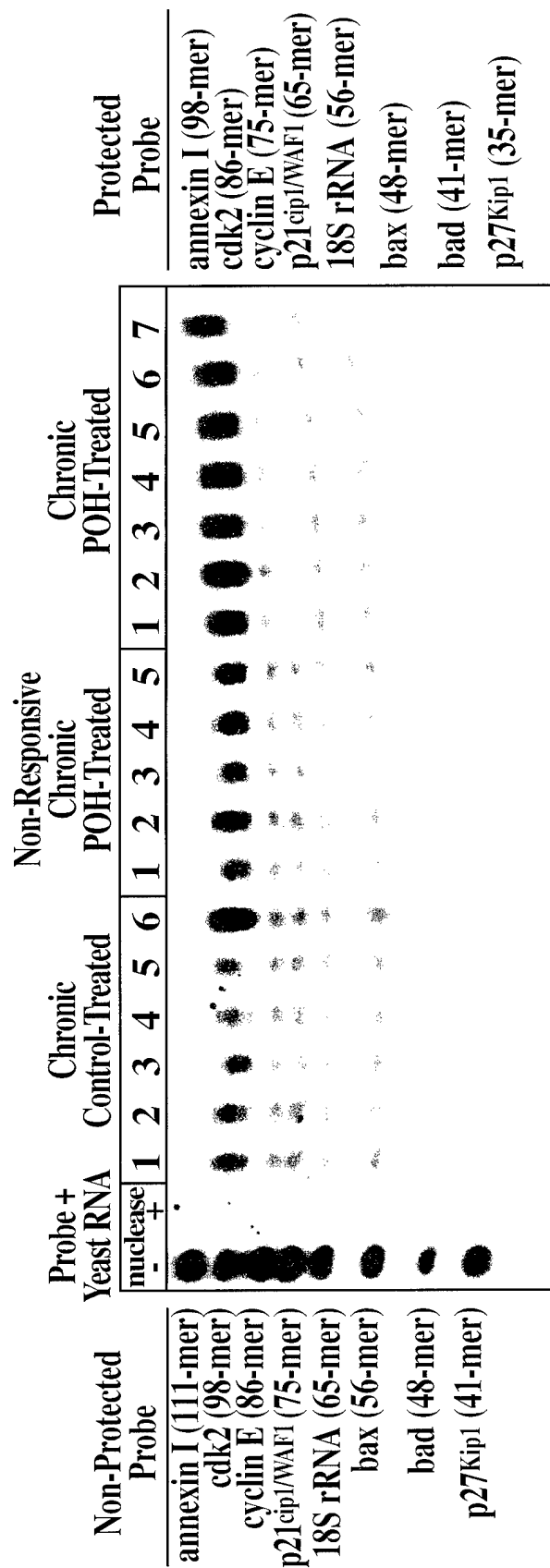
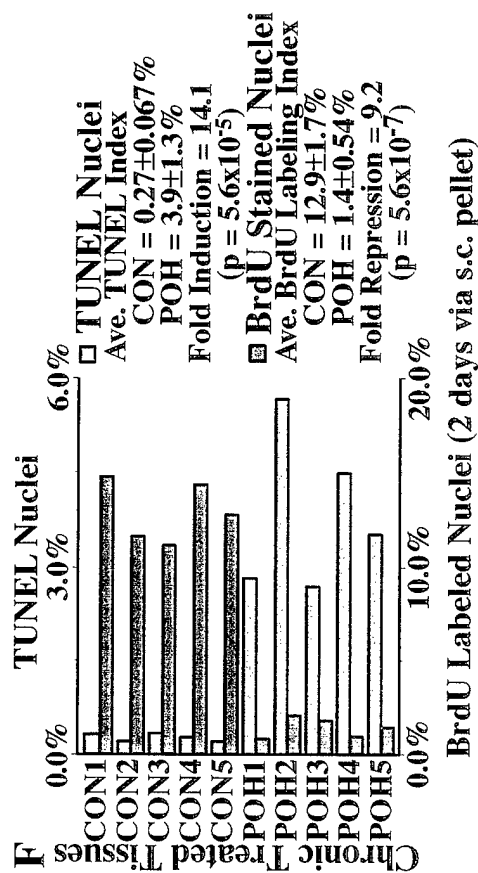
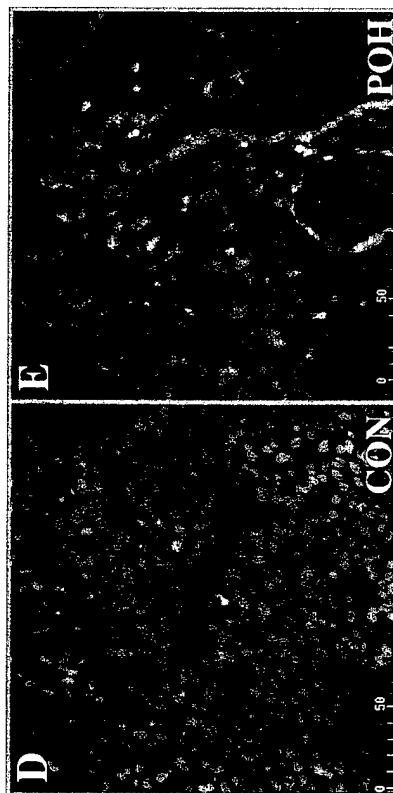
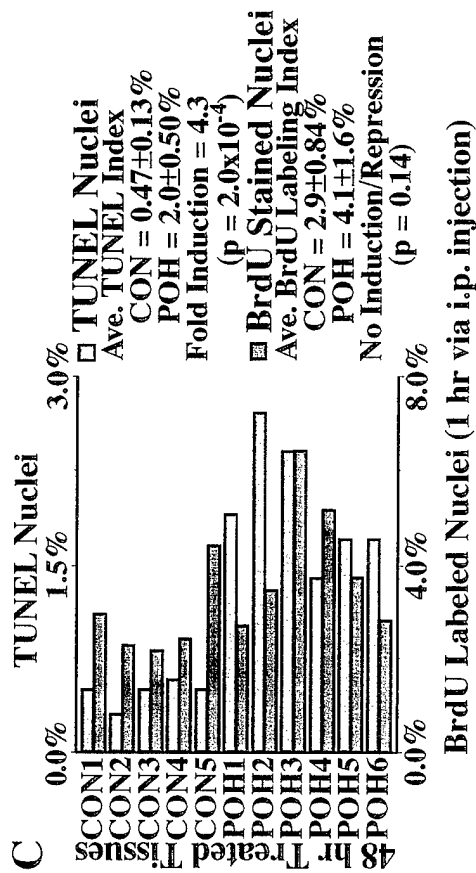
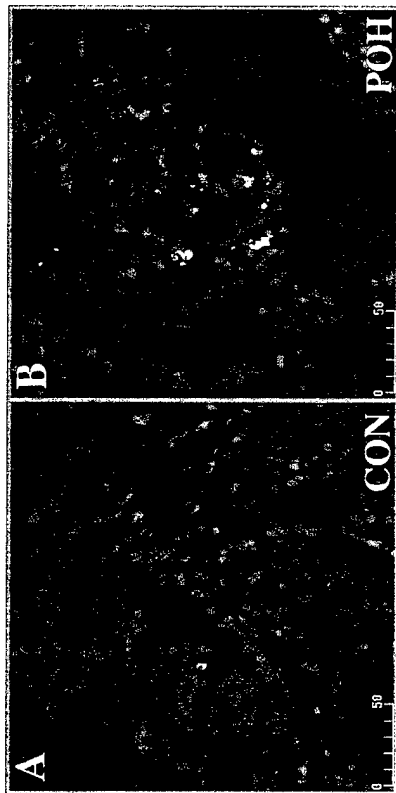


**Figure 12. Induction of Cytostasis and Apoptosis.**

Tissues visualized by confocal microscopy. (A) 48 h Acute CON-treated carcinoma. (B) 48 h Acute POH-treated carcinoma. (C) Quantitation of apoptosis and cytostasis at 48 h of the acute treatment protocol. (D) Chronic CON-treated carcinoma. (E) Chronic POH-treated regressing carcinoma. (F) Quantitation of cytostasis and apoptosis during the chronic treatment protocol. Tissues were triple-stained, first for TUNEL to identify apoptotic nuclei using FITC-dUTP (green nuclei), second for BrdU incorporation to identify proliferating cells using a 1° mouse monoclonal anti-BrdU antibody and a Cy5-2° anti-mouse IgG antibody (blue nuclei), and third with PI to identify all nuclei (red channel). Scalebars indicate microns.



## PUBLICATIONS SUPPORTED BY DAMD17-94-J-4041

### JOURNAL ARTICLES

1. Ariazi, E. A., and Gould, M. N. (1996) Identifying Differential Gene Expression in Monoterpene-treated Mammary Carcinomas Using Subtractive Display. *J Biol Chem* **271**(46), 29286-94
2. Ariazi, E. A., and Gould, M. N. (1996) Consecutive Cycles of Precise Unidirectional 14 bp Deletions Using a *Bse* RI/*Bsg* I Trimming Plasmid. *BioTechniques* **20**, 446-51
3. Ariazi, E. A., Satomi, Y., Ellis, M. J. C., Sattler, C., Haag, J., and Gould, M. N. (1998) Characterization and Downstream Effects of the TGF $\beta$  Signal Transduction Pathway in Mammary Carcinomas Treated with the Anticancer Agent Perillyl Alcohol. **In preparation**

### MEETING ABSTRACTS

4. Ariazi, E. A., and Gould, M. N. (1996) Identification of Induced/Repressed Genes in Monoterpene-treated Regressing Rat Mammary Carcinomas Using Subtractive Display. *Proc Annu Meet Am Assoc Cancer Res* **37**, A2720
5. Ariazi, E. A., and Gould, M. N. (1998) Apoptosis Induced by the Anticancer Agent Perillyl Alcohol Involves TGF-beta Signaling Components. *Proc Annu Meet Am Assoc Cancer Res* **39**, A461

**LIST OF PERSONNEL RECEIVING PAY FROM THIS EFFORT**

Eric A. Ariazi recieved a stipend.